THE FRACTIONAL FOURIER TRANSFORM

AND ITS APPLICATION TO FAULT SIGNAL ANALYSIS

A Thesis

by

XIAO DUAN

Submitted to the Office of Graduate Studies of
Texas A&M University
in partial fulfillment of the requirements for the degree of

MASTER OF SCIENCE

May 2012

Major Subject: Mechanical Engineering

THE FRACTIONAL FOURIER TRANSFORM

AND ITS APPLICATION TO FAULT SIGNAL ANALYSIS

A Thesis

by

XIAO DUAN

Submitted to the Office of Graduate Studies of
Texas A&M University
in partial fulfillment of the requirements for the degree of

MASTER OF SCIENCE

Approved by:

Chair of Committee,	Alexander G. Parlos
Committee Members,	Jim Ji
	Won-jong Kim
Head of Department,	Jerry Caton

May 2012

Major Subject: Mechanical Engineering

ABSTRACT

The Fractional Fourier Transform

and Its Application to Fault Signal Analysis. (May 2012)

Xiao Duan, B.S., Xi'an JiaoTong University, Xi'an, China

Chair of Advisory Committee: Dr. Alexander G. Parlos

To a large extent mathematical transforms are applied on a signal to uncover information that is concealed, and the capability of such transforms is valuable for signal processing. One such transforms widely used in this area, is the conventional Fourier Transform (FT), which decomposes a stationary signal into different frequency components. However, a major drawback of the conventional transform is that it does not easily render itself to the analysis of non-stationary signals such as a frequency modulated (FM) or amplitude modulated (AM) signal. The different frequency components of complex signals cannot be easily distinguished and separated from one another using the conventional FT. So in this thesis an innovative mathematical transform, Fractional Fourier Transform (FRFT), has been considered, which is more suitable to process non-stationary signals such as FM signals and has the capability not only of distinguishing different frequency components of a multi-component signal but also separating them in a proper domain, different than the traditional time or frequency domain.

The discrete-time FRFT (DFRFT) developed along with its derivatives, such as Multi-angle-DFRFT (MA-DFRFT), Slanted Spectrum and Spectrogram Based on Slanted

Spectrum (SBSS) are tools belonging to the same FRFT family, and they could provide an effective approach to identify unknown signals and distinguish the different frequency components contained therein. Both artificial stationary and FM signals have been researched using the DFRFT and some derivative tools from the same family. Moreover, to accomplish a contrast with the traditional tools such as FFT and STFT, performance comparisons are shown to support the DFRFT as an effective tool in multi-component chirp signal analysis. The DFRFT taken at the optimum transform order on a single-component FM signal has provided higher degree of signal energy concentration compared to FFT results; and the Slanted Spectrum taken along the slant line obtained from the MA-DFRFT demonstration has shown much better discrimination between different frequency components of a multi-component FM signal.

As a practical application of these tools, the motor current signal has been analyzed using the DFRFT and other tools from FRFT family to detect the presence of a motor bearing fault and obtain the fault signature frequency. The conclusion drawn about the applicability of DFRFT and other derivative tools on AM signals with very slowly varying FM phenomena was not encouraging. Tools from the FRFT family appear more effective on FM signals, whereas AM signals are more effectively analyzed using traditional methods like spectrogram or its derivatives. Such methods are able to identify the signature frequency of faults while using less computational time and memory.

Dedicated to my parents

ACKNOWLEDGEMENTS

I would like to thank my committee chair, Dr. Parlos, and my committee members, Dr. Kim, Dr. Ji, for their guidance during my research.

Thanks also to my friends in Texas A&M University: Xu Han, Xiaohua Zhang, Weesen Ng, Jianxi Fu, Gang Li, Yong Li and Chienhong Lin. You guys gave me a lot of support and showed me your wisdom on how to successfully pursue a degree in my stay in College Station.

Meanwhile, I would like to give my gratitude to Eason Chan from Hong Kong Showbiz, because you have made my life sounds good with beautiful auditory colors.

Finally, thanks to the inventor and maintenance staff of MATLAB, the incredible signal processing tool, which I would like to call: number chunk killer.

NOMENCLATURE

FRFT	Fractional Fourier Transform
FT	Fourier Transform
CFRFT	Continuous Fractional Fourier Transform
DFRFT	Discrete Fractional Fourier Transform
STFT	Short-Time Fourier Transform
FRFD	Fractional Fourier Domain
TFR	Time-Frequency Representation
LFM	Linear Frequency Modulation
AM	Amplitude Modulation
FM	Frequency Modulation
SBSS	Spectrogram Based on Slanted Spectrum

TABLE OF CONTENTS

Page

LIST OF TABLES

TABLE Page

LIST OF FIGURES

FIGURE Page

FIGURE Page

FIGURE Page

FIGURE Page

CHAPTER I

INTRODUCTION

A. Research Motivation

During the recent 3 decades, Fractional Fourier Transform (FRFT), which is an advanced innovation of the traditional Fourier Transform (FT), has gained more and more attention in engineering society. Due to the newly introduced degree of freedom – the transform order, FRFT is an ideal tool to process FM signals, and has distinguished itself from FT, one of the most basic tools applicable only to stationary signals.

The application of FRFT is tremendous, and its contribution is not simply confined to signal processing. Voluminous literature probing into the massive application could be found, with detailed discussion on its adoption in solving differential equations, quantum mechanics, quantum optics, optical diffraction, beam propagation, data compression, human emotional state recognition, moving targets detection and others.

Despite the extensive use, the focus of this research is in digital signal processing (DSP), or to be specific, the study in the discrete version of FRFT (DFRFT) is highly emphasized with a main motivation of unknown signal identification and fault analysis.

An FM signal is a very common type of both natural signal and industrial signal, and it could be modeled by an exponential function with a varying frequency. Modeling such signals is a good way of simulating real signals, which are ubiquitous in both nature

---

This thesis follows the style of *IEEE Transactions on Signal Processing*.

and project application field in industry. Moreover, this research direction will facilitate the subsequent study of some unknown signals, as well as provide researchers with the insight of comprehensive understanding of the signals. So the ultimate goal of identifying and distinguishing different components of sophisticated signals will be achieved with confidence and fidelity.

Fault analysis is the other essential motivation of this research. As for the case of all the other rotating machines, the safety and reliability of an induction motor will deteriorate after operation over some period of time. So in order to prevent the motor from posing grave threat to its operator and on-the-spot staff and eventually causing immense economic loss, effective motor maintenance is an absolutely necessary routine. Based on related statistics [1], a common failure of induction motors is related to bearing failures, so acquisition of real-time motor bearing signals is required. And then in the subsequent research, the signature frequency of the fault could be obtained with precision, reliability and promptness.

B. Literature Review

Even though “fractional” as a terminology emerged in the recent 30 years, the first reference dates back to 1695 when Bernoulli sent Leibniz a letter, questioning the meaning of a non-integer order derivative. And then Fractional Calculus (FC) had been gradually established over centuries until the 1920s, when there began relative systematic studies on FC in Applied Sciences [2]. In 1929 the concept of Fractional

Fourier Transform (FRFT) was presented into the Mathematics area, and in 1980 that this signal analysis tool was rediscovered by physicist Namias.

Basically, FRFT is an evolved version of the traditional Fourier Transform (FT); the most essential advantage of FRFT over FT is that it has introduced one more degree of freedom (DOF)—the fractional transform order a, normally varying in the range [0,2].

With the introduction of this transform order a, the Time-Frequency Representation (TFR) of a signal is not to be confined to the traditional "two degrees of freedom: time and frequency" mode, but instead, the representation can be realized in any range in between the Time-Frequency domain. This advanced property of FRFT has rendered itself one of the best approaches to analyze FM signals.

The Continuous FRFT (CFRFT) is well defined in many articles in journals and reports, but DFRFT, with a different kind of format, is more suitable for applications in digital signal processing. So the fact is that CFRFT is researched to help understand the essential meaning and properties of FRFT, whereas DFRFT is the real tool applied to the signal under research.

Among those researchers seeking a decent way to digitize the integral form of CFRFT, Ozakta et al. have done research on the DFRFT algorithm which uses Dickinson-Steigliz's Harper matrix S as the commuting matrix of the Discrete Fourier Transform (DFT) matrix, so the task of finding a complete and orthogonal set of eigenvectors of the DFT matrix has been converted to finding such a set of eigenvectors of the Harper matrix S [3]. And Pei et al. have also proposed a similar DFRFT algorithm [4].

Meanwhile, Vargas-Rubio and Santhanam mainly focused on the Centered Discrete Fractional Fourier Transform (CDFRFT) [5] and proposed an innovative method to calculate the spectrogram based on it, and then successfully demonstrated a great improvement in the resolution of TFR for a complicated signal [6].

As another approach to best simulate the Continuous Fractional Fourier Transform, which is expressed in a form of an integral, the CDFRFT algorithm shows great difference from DFRFT algorithm, because CDFRFT has adopted a different commuting matrix, Grunbaum's Tri-diagonal Commutor, to obtain a complete orthogonal set of eigenvectors for the DFT matrix [7].

In both literatures exploring into DFRFT and CDFRFT, the authors have explicitly pointed out that seeking for a decent way of expressing DFRFT is about furnishing orthogonal eigenvectors for the DFT, and these eigenvectors are actually the discrete versions of the Hermite-Gaussian functions which serve as the unique finite energy eigensolutions of differential equation structured by the Harper matrix S, also known as the Hamiltonian associated with the quantum-mechanical harmonic oscillator [8].

Generally speaking, both DFRFT and CDFRFT are able to perform higher resolution when processing signals with a chirp rate, or simply to say, Frequency Modulated (FM) signals, compared with the traditional tools, such as FFT and Short-Time Fourier Transform (STFT).

Two significant publications, [9] and [10] researching the CDFRFT algorithm have been found in the signal processing literature database in China. They have successfully

given a more concise and lucid CDFRFT algorithm than [5], so they should be given credit for their time-saving advantage.

It is worth mentioning that Vargas-Rubio and Santhanam's group has another contribution, which is the introduction of a method suitable for processing unknown signals [11]. This Multi-angle Centered Discrete Fractional Fourier Transform (MA-CDFRFT) provides an explicit demonstration of the concentrated signal components with both the *x*-axis and *y*-axis coordinates of acquired optimum transform orders a_{opt} as well as the indices in Fractional Fourier Domain (FRFD). This is a rotation from the traditional Frequency Domain (FD) [12], as shown in Fig. 1 below:

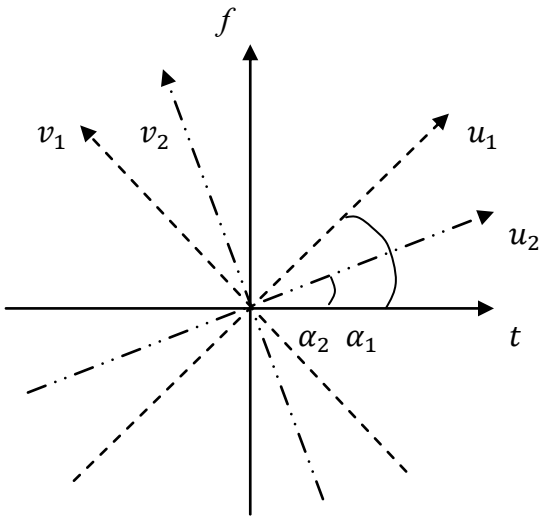

Fig. 1. Rotation of Fractional Fourier Domain from Time-Frequency Domain.

In Fig. 1, the new Fractional Time-Fractional Frequency plane ($u_1 - v_1$ plane) is a rotation by angle α_1 from the traditional Time-Frequency plane (*t*-*f* plane), with the

other $u_2 - v_2$ plane a rotation by angle α_2 from *t-f* plane. The rotation angle α has the following relationship with transform order *a*:

$$a = \frac{\alpha}{(\pi/2)} \tag{1.1}$$

And successive rotations of the Fractional Time-Fractional Frequency plane from Time-Frequency plane could be simply modeled by adding up the rotation angles α_i. This is the reason for the interpretation of FRFT as a rotation operator.

Since CDFRFT is similar to DFRFT, it also has the ability of concentrating the energy of different components of FM signal. The MA-CDFRFT, or MA-DFRFT, is actually a matrix, the plot of which illustrates the positions where the energy of different components of a complicated FM signal gets concentrated. The *x*-axis corresponds to the index *k*, which is shared by both time and frequency axes; meanwhile, the *y*-axis represents the index of transform order *a*, from which we determine whether the *x*-axis represents time or frequency.

So if the studied signal is merely a single-component sinusoid, the energy-concentration point with the brightest color in the MA-DFRFT 3D plot will have a *y*-axis coordinate of *a*=1; if the case is a little bit more complicated, where the studied signal is a multi-component sinusoid, the points where energy gets concentrated, or simply the peaks with the brightest color, will lie on the horizontal *a*=1 line; if the studied signal is a single-component FM signal with a certain chirp rate, the peak will appear elsewhere from *a*=1 line, and the specific position will depend on the specific signal property; if the studied signal is a multi-component FM signal with linearly related properties, the peaks

will be aligned along a slant line which passes the point with coordinates [N/2, 1], lying at the center point of the MA-DFRFT demonstration plot.

It should be noted that the case with the studied signal being a multi-component FM signal is the perfect material for research on Slanted Spectrum, which was firstly proposed on the basis of MA-CDFRFT by Vargas-Rubio and Santhanam. Slanted Spectrum is another derivative tool of CDFRFT, whose advent makes possible the high resolution for the different components of the complicated signal under research, which distinguishes itself from traditional tools like FFT.

Furthermore, there is another derivative belonging to the family of CDFRFT, and it could surpass the capability of the traditional spectrogram (STFT): Spectrogram Based on Slanted Spectrum (SBSS). This innovative tool is also mentioned and developed in [6]. With the demand for a better TFR, its generation is inevitable and favorable, because the performances of other different time-frequency representation tools are not very satisfactory in study of chirp signals.

For the real world applications, the simultaneous estimation of both time and frequency variables are highly expected for a precise measurement of signals. Classical tools for TFR which are more familiar to researchers include the Wigner-Ville distribution (WVD) and the traditional spectrogram based on STFT. However, WVD offers highly concentrated energy representation but suffers from cross-terms when analyzing multi-component signals; traditional spectrogram based on STFT is a good choice, but it often performs unsatisfactorily because of its failure to give highly concentrated energy representation [13].

So the generation of SBSS has eliminated this dilemma. This innovative spectrogram has the essential feature of being able to decompose a complicated signal into multiple components within the analysis frame with great distinguishability, and is highly suitable for TFR of FM signal. This spectrogram is not widely used for the time being, but its capability of decomposing complicated signals is on the top rank list, so it will surely gain more attention in the area of DSP.

So with all these tools from DFRFT family stated above, fault signal analysis is able to be realized in a way different from traditional methods. So the induction motor current signal including information of fault components could be processed with flexibility, due to the advantage of DFRFT.

C. Research Objectives

The objectives of this research are as follows:

- Develop an overall signal processing method comprised of DFRFT and its derivatives, MA-DFRFT, Slanted Spectrum and SBSS;
- Investigate whether or not DFRFT has an advantage over traditional tools, such as FFT, especially in FM signal processing; and
- Apply these developments to a real problem, motor electrical signal fault analysis.

D. Proposed Approach

As stated in Literature Review, there are a number of extant algorithms for both DFRFT and CDFRFT. They are both derived from the DFT matrix, but the commuting

matrices adopted are different. So the first big issue in this research is to select appropriate methods to calculate DFRFT and CDFRFT, and to decide which one has overwhelming advantages, such as higher resolution of the plots of their multi-angle versions, i.e. MA-DFRFT and MA-CDFRFT. Once a method is selected, the subsequent work will be mainly based upon it.

One important thing should be noted is that different components of a signal may have different a_{opt} values, so there are actually two cases: One is that both the healthy and faulty components of a signal require simply the same a_{opt} to adopt DFRFT to separate and distinguish different components in spectrum of the FRFD, which is a relatively simplified case. However, there exists another more complicated case when the healthy and faulty components within one data set require different values of a_{opt} to get concentrated to the best degree, so in this case, simply DFRFT will not successfully tackle the problem, but Slanted Spectrum could accomplish the components separation and distinguishing work. And then SBSS could be generated from Slanted Spectrum in succession.

A conclusion will be drawn from the results obtained using tools from DFRFT family and the counterparts obtained from traditional tools.

This methodology comprised of DFRFT, CDFRFT and their derivatives, MA-DFRFT, MA-CDFRFT, Slanted Spectrum and SBSS, is shown as a flowchart with sequential steps in Fig. 2:

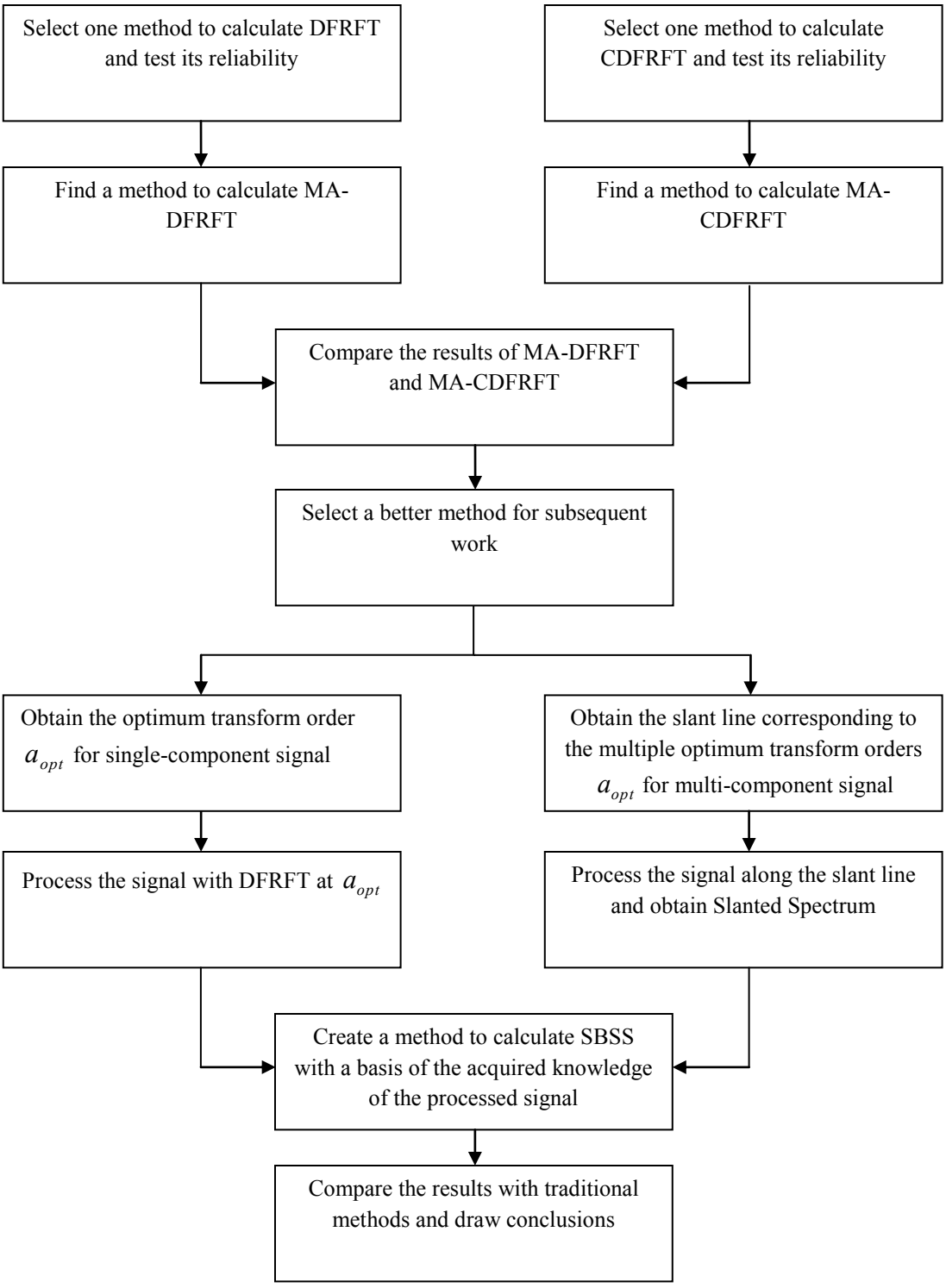

Fig. 2. Overall approach of proposed research.

E. Anticipated Contributions

The main contribution of this research is the development of a methodology for FM signal analysis with potential applications to the analysis of fault signals. The new method is different than traditional frequency domain analysis tools, such as FFT, or traditional TFR tools, such as STFT. By acquiring information of the extra DOF, the frequencies, chirp rates and other essential information of unknown signals could be obtained. Simultaneously, the multiple components of FM signals will be distinguished by applying this method, which could provide significantly higher resolution once the energy of the different components has been compared with traditional FFT.

F. Thesis Organization

This thesis is expected to give a thorough overlook on the current advancement of the research of FRFT and its applications to practical problems. The remaining parts of this thesis are organized as follows. Chapter II presents the proposed method of DFRFT and CDFRFT, and there are comparisons between their algorithms based upon which the digital computations have been carried out and between their performances when applied to some basic signals. And then there begins to be an emphasis in DFRFT, due to its higher development than its homogeneous tool: CDFRFT. In Chapter III, other derivative tools of DFRFT are introduced. Finally whether to adopt DFRFT or CDFRFT in the subsequent research will be decided from generating the MA-DFRFT and MA-CDFRFT demonstrations of some chirp signal. And then all the other related tools in the DFRFT family, such as Slanted Spectrum and SBSS are elaborated with their

performances when applied to complicated chirp signals. And then Chapter IV mainly deals with the proposed method applying to the real world problem: DFRFT and its derivatives applied to motor current signal, and the results are presented. Successively, in Chapter V, a summary and conclusions of this research, and the directions for future work are briefly discussed.

CHAPTER II

PROPOSED METHODS OF DFRFT AND CDFRFT

A. From the Traditional Fourier Transform to Fractional Fourier Transform

Interestingly enough, the appearance of the Fractional Calculus could be dated back to the time period between the two world wars [14]. And the Fractional Fourier Transform (FRFT) was firstly employed by a Physicist named Namias to solve both differential and partial differential equations in 1980 [15] with a specific academic field of quantum mechanics. And then McBride et al. carried out a more meticulous analysis of this mathematical technique [16], which forms the basis for majority of the subsequent works. And then a great number of research papers were published in 1990s, and most of them are aiming at relating the Fractional Fourier operator to other fields, i.e. differential equations, optical systems, time-variant filtering, multiplexing, neural networks, machine diagnosis, and digital signal processing.

In the field of signal processing, FRFT can be applied without a-priori knowledge of the transmitted signal. So it is a favorable tool for efficaciously extracting useful information from a signal in FRFD. Moreover, FRFT can recover a signal from noises using a filtering technique [17]. For linear frequency modulated (LFM) signals, the power of the signal spans the entire of the frequency and time axes, and an ordinary filter cannot separate the signal from the noise [18]. However, it has been shown that by selecting a proper transform domain other than the traditional ones, noise separation can

be realized: FRFT can be used to separate signals which cannot be separated in traditional domains as demonstrated in the Fig. 3:

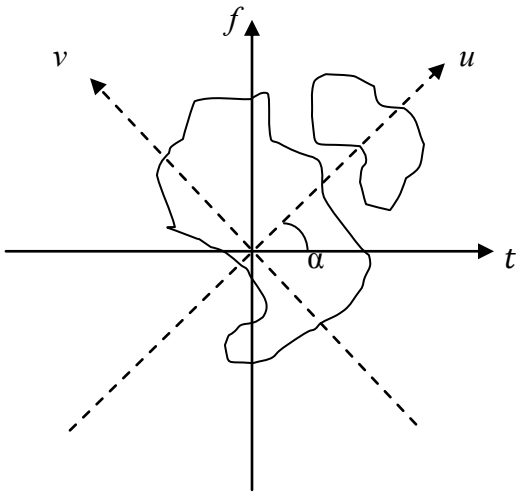

Fig. 3. Separation of a signal from noise in an appropriate Fractional Fourier Domain.

Both the signal and noise components are shown in Fig. 3, and their projections on both time and frequency axes have inevitably overlapped, thus it is difficult to separate the signal from the noise background either in time domain or in frequency domain. However, their projections on the axis corresponding to the *a*-th FRFD (the *u* domain in Fig. 3) have not overlapped with each other. So FRFT is suitable to be exploited to decouple the energy overlap between the signal and noise. Depending upon the concept that the energy of an LFM signal is concentrated on the straight line illustrated as dashed on the time-frequency plane, therefore the signal can be reduced to a stationary sinusoid by rotating the signal by the angle of α as shown. As a result, there would be the least spectrum overlap between the signal and noise in FRFD, and a narrowband filter needs

to be exploited to extract the signal from the noise background. And then the elimination of noise could be achieved effectively. Finally, using inverse FRFT, the filtered LFM signal can be rotated back to the time domain and get recovered [19].

The orthogonal relationship between the time and frequency domains under the conventional FT is mirrored in a similar relationship between any two fractional domains spaced infinitesimally. Moreover, it should be noted that the conventional time and frequency domains are a part of the continuum of the FRFD. Also as an important fact, the signal representation in the u domain is a combination of the representations in time and frequency domains.

The conventional FT has only the ability of removing time-invariant type of noises. However, certain types of noise are fairly intractable due to their high frequencies. For an instance, noise with a chirp rate and it will be discussed in details in the next Chapter. On the contrary, the fact that FRFT has better control over the time variance/invariance of the system, has expanded the applications that used to be only associated with the conventional FT.

Besides, FRFT has greatly broadened the conventional Fourier theory for both the analysis and synthesis of LFM signal, which is also referred to as chirp signal.

Nevertheless, FRFT has not gained the attention and exploration that it should have in the signal processing community, only due to the fact that there was a deficiency of proper physical illumination and an algorithm for fast digital computation of this new physics tool.

It was not until the discovery of feasible interpretation of FRFT as a rotation operator [6] and the publication on the efficient digital computational algorithms of FRFT [13], that FRFT began to interest more scholars and researchers for its flexibility and suitability for processing FM signals with one extra DOF. Fractional order signal processing has become an active research area during recent years, due to the FM and non-Gaussian model it has employed.

And a number of researches have been focused on the development of the algorithms for digitized FRFT. Among these, algorithms for fast computation of discrete FRFT have been proposed in [4] and [14], hence finally the door to wider application of FRFT was opened to the DSP community.

It should be noted that in order to distinguish the two different forms of FRFT, CFRFT is used to denote the continuous-time FRFT, and DFRFT is for the discrete-time version. Even though they have different mathematical expressions, DFRFT is still derived from CFRFT, as explained in the following sections.

1. Standard Form of Continuous-time Fractional Fourier Transform

Briefly, CFRFT is a generalization of the conventional continuous FT. Signals are processed with CFRFT in the FRFD, and the most significant parameter which differentiates CFRFT from the conventional continuous FT is the transform order a, the new DOF. The other parameter in correspondence with it is the rotation angle α, and (1.1) has given a physical illustration between α and the transform order a which helps with understanding the essential meaning of CFRFT:

Normally, if a CFRFT calculation is noted as *a*-th order, it means that the projection of the original signal has been rotated by an angle of $\alpha = (\pi/2)a$ from the conventional time domain to a brand new FRFD. It is by conventions that the time-frequency plane is defined such that time and frequency are mutually orthogonal coordinates. The representations of a signal in these two domains, time and frequency, are related by the conventional FT. And here we consider a continuum of "fractional" domains making arbitrary angles with the two traditional domains. The representations in these domains are related by the FRFT. A perspicuous geometric interpretation for the FRFD and the two traditional domains could be derived like demonstrated in Fig. 3 in the previous section.

It's been well-known to the signal processing community that the continuous FT of a finite energy signal $x(t)$ is defined via the equation in (2.1):

$$X(\omega) = F(x(t)) = \frac{1}{\sqrt{2\pi}} \int_{-\infty}^{+\infty} x(t) e^{-j\omega t} dt \tag{2.1}$$

And the continuous FRFT of the same finite energy signal $x(t)$ is defined in a similar integral form as below, and it can be clearly seen from (2.2) that CFRFT is a one-dimension linear operator, totally different from other bilinear or nonlinear time-frequency analysis tools:

$$X_a(u) = F_a(x(t)) = \int_{-\infty}^{+\infty} x(t) K_a(u,t) dt \tag{2.2}$$

where *t* is the variable in the traditional time domain, and *u* denotes the variable in the *a*-th order FRFD. Throughout this thesis, F_a is used to denote the FRFT operator, whereas

F denotes the traditional FT. And $K_a(u,t)$ is the kernel function in the integral, shown as below:

$$K_a(u,t)=\begin{cases}\sqrt{\dfrac{(1-j\cot\alpha)}{2\pi}}\cdot e^{j\frac{t^2+u^2}{2}\cot\alpha-jut\csc\alpha}, & \alpha\neq n\pi, a\neq 2n \quad (2.3)\\ \delta(t-u), & \alpha=2n\pi, a=4n \quad (2.4)\\ \delta(t+u), & \alpha=2n\pi\pm\pi, a=4n\pm 2 \quad (2.5)\end{cases}$$

where the subscript of the Left Hand Side (LHS) of (2.3)-(2.5) and the integral kernel of (2.3) is the transform order *a* of CFRFT, which could take arbitrary real values. And the angle α and the notation *n* which has also appeared in (2.3)-(2.5) are respectively the rotation angle and an arbitrary integer. It should be noted that there are often confusions about the transform order *a* with the rotation angle α in some literatures, but they are totally different two parameters both frequently used in the FRFT research. They hold an explicit relationship as in (1.1). To remove any unwanted ambiguity, the Greek letters are assigned to denote the rotation angles in the time-frequency plane, and the English letters are referring to the transform order of FRFT, which is also the power value of the traditional FT kernel. And it should also be mentioned that $\delta(t)$ represents the Dirac function.

By careful observation of (2.3), if set $\alpha=\pi/2$, there will be $\cot\alpha=0$ and $\csc\alpha=1$. And if replace *u* with ω, then (2.3) will be reduced to the form of the conventional FT. This is actually one of the most essential properties of FRFT, as mentioned in Chapter I, and now it has been proved mathematically.

The kernel $K_a(u,t)$ in (2.2)-(2.5) can be interpreted as the basis in the FRFD, or simply *u* domain. And it has the following properties:

$$K_{-a}(u,t) = K_a^*(u,t) \tag{2.6}$$

$$\int_{-\infty}^{+\infty} K_a(t,u)K_a^*(t,u')dt = \delta(u-u') \tag{2.7}$$

where K_a^* is the complex conjugate of K_a, and u' is the variable in the (-*a*)-th FRFD.

The kernel $K_a(u,t)$ is a chirp function, which allows the transformation in (2.2) to be interpreted as a coordinate transformation where the chirp function plays the role of a basis function.

In addition, there is another expression of the kernel denoted as the spectral expansion given by (2.8):

$$K_a(u,t) = \sum_{k=0}^{\infty} H_k(u)e^{-j\frac{\pi}{2}ka}H_k(t) \tag{2.8}$$

where $H_k(t)$ is denoted as the *k*-th Hermite-Gaussian function and has the following mathematical definition:

$$H_k(t) = \frac{1}{\pi^{1/4}\sqrt{2^k k!}}h_k(t)e^{-\frac{t^2}{2}} \tag{2.9}$$

where $h_k(t)$ are the Hermite polynomials, which are the solutions of the second-order Hermite differential equation given by (2.10):

$$\frac{d^2x(t)}{dt^2} - (t^2+\lambda)x(t) = 0 \tag{2.10}$$

And simultaneously the eigenfunction of the Hermite differential operator is shown in (2.11):

$$H(x(t)) = (D^2 - t^2 I)x(t) = -(2n+1)x(t) \tag{2.11}$$

with a corresponding eigenvalue of $\lambda_k = e^{-j\frac{\pi}{2}k}$.

From (2.9) it is clear that the Hermite-Gaussian function is a chirp function.

It needs to be pointed out that these Hermite-Gaussian functions are the eigenfunctions of both the FT and FRFT, and (2.2) could also be written as (2.12):

$$X_a(u) = \int_{-\infty}^{+\infty} x(t) \sum_{k=-\infty}^{+\infty} e^{-j\frac{\pi}{2}ka} H_k(t) H_k(u) dt \tag{2.12}$$

Equation (2.12) is seen to be a multiplication by a chirp in the time domain, followed by FT, subsequently followed by another multiplication by a chirp in the transformed domain. And importantly, $e^{-j\frac{\pi}{2}ka}$ is the *a*-th fractional power of the eigenvalue $\lambda_k = e^{-j\frac{\pi}{2}k}$ of the traditional continuous FT. So it could be easily understood why there is an interpretation of FRFT as a one-parameter generalization of FT. In this fashion, FRFT suggests a potential amelioration in any application where the traditional FT originally has been exploited since it provides this extra DOF corresponding to the careful selection of transform order *a*.

For the integrity of this thesis, the inverse transform of FRFT is defined accordingly:

$$x(t) = \int_{-\infty}^{+\infty} X_a(u) K_{-a}(u,t) du \tag{2.13}$$

This expression in (2.13) provides a different interpretation for any signal $x(t)$ in time domain: it is decomposed in the function space formed by the basis function $K_{-a}(u,t)$, which serves as the kernel function of the inverse FRFT. Just like the kernel of CFRFT, $K_{-a}(u,t)$ is also a chirp signal and at different values of u, they form a group of orthogonal base.

Meanwhile, it could also be deduced from (2.13) that any signal can be expressed by a linear combination of a group of orthogonal base on the u domain.

As the last part of this section, it is worth mentioning that FRFT is a member of a more general class of transforms that are sometimes called linear canonical transformations or quadratic phase transforms. All members of this class of transformations can be broken down into a succession of simpler operations, such as chirp multiplication, chirp convolution, scaling, and ordinary FT as stated in the previous pages.

2. Properties of Fractional Fourier Transform

The FRFT transform order a is defined within the range of $0<|a|<2$, so the definition range of the rotation angle α is $0<|\alpha|<\pi$, due to its essential property of periodicity (with F_4 being the identity operator, which will be elaborated in the following section) and the need to avoid redundancy of calculation. However, normally the researchers are more interested in the range of $0<|a|<1$, which only covers the

region of first quadrant of the time-frequency plane. And this artificial setting of the range of transform order has greatly simplified the following research.

Referring back to (2.3)-(2.5), it is seen that the kernel $K_a(u,t)$ is defined separately for $a = 4n$ and $a = 4n \pm 2$ (n is an arbitrary integer here) as $K_{4n}(u,t) = \delta(u-t)$ and $K_{4n\pm2}(u,t) = \delta(u+t)$. The definition can be easily extended outside the interval [-2, 2] by noting that $F_{4l+a}(x(t)) = F_a(x(t))$ with l being an arbitrary integer.

FRFT also has other properties which are used to simplify calculations, and they will be more thoroughly discussed in Section B, Properties of DFRFT, since this thesis puts more emphasis in DFRFT, but not CFRFT.

3. Main Applications of Fractional Fourier Transform and the Need of a Digitized Version of FRFT

FRFT is mainly applied in two main fields: optics and signal processing.

For optics, beam forming with FRFT, Fourier optics and optical information processing are the main research interests of practitioners. But those are not the main research topics for this thesis. Rather, signal processing has the priority.

As to the area of signal processing, there are applications like optimal filtering in FRFD, cost-efficient linear system synthesis and filtering, time-frequency analysis, and biomedical imaging. Whereas the specific applications of FRFT in several specialized areas will be discussed in the following paragraphs.

Some medical engineering practitioners have used FRFT for medical ultrasound imaging, with the aim of improving the axial resolution and imaging depth of an

ultrasound system through the use of FM chirp waveforms. The technique associated with FRFT has allowed the relationship between the maximum achievable spatial resolution and the pulse length to be changed. So a compromise for the tradeoff between axial resolution and the maximum imaging depth, posed on medical ultrasound systems can be achieved [20].

Another interesting application is that FRFT could be utilized in language identification (LID), a developing branch of speech signal processing. By implementing FRFT and properly selecting the FRFT transform order, more discriminative information for language identification may be extracted from the speech signal. It is known that young people are familiar with Nintendo, the most famous handheld game console company in Japan. Some of the RPG games developed for Nintendo Dual Screen (NDS) are specializing in the research of LID techniques. So FRFT could be exploited to develop the LID system for speaking to Mario and directly sending him commands for jumping.

Besides the two interesting applications related above, FRFT has also been increasingly applied to music processing, watermarking, communications, pattern recognition, cryptography, Fractal signal processing, and mechanical vibrations analysis.

As depicted in the previous sections, CFRFT is a subclass of integral transformations characterized by quadratic complex exponential kernels. These complex exponential kernels often introduce in very fast oscillations. Therefore, it is not possible to evaluate these transforms by direct numerical integration since the fast oscillations require excessively large sampling rates higher than Nyquist rate, depending on the order and

particular decomposition employed. This returns in great computational cost, large numerical inaccuracies, and the need for more computer memory.

So talking about the computer memory, almost all these applications of FRFT in signal processing have to be carried out on digital devices with the digitized version of FRFT installed.

Therefore finding decent ways of digitizing CFRFT has been one of the most essential issues discussed widely in the research community. Among those research papers, the most straightforward approach for obtaining the discrete counterpart of CFRFT is to sample it directly, since the sampling criteria for CFRFT of band-limited and time-limited signals has utterly complied with the Shannon sampling theorem [21]. But quite the opposite, the resultant form of DFRFT will have a chance of losing many important properties, i.e. unitarity and reversibility. In addition, DFRFT obtained by direct sampling of CFRFT lacks closed-form properties and is not additive, so its applications are very limited [22]. Worse still, since the basis functions of the CFRFT are not bandlimited, directly sampling of the kernel will result in aliasing.

Then probing into the existent literatures, the most reliable approach to digitize CFRFT and generate a proper DFRFT algorithm which preserves all the properties of FRFT is based upon the notion of generating the discrete time counterparts of the continuous time Hermite-Gaussian functions in (2.9). And this approach has conclusively shown better approximations than the other proposed approaches in [8].

And there are actually two different main branches of study following the proposed approach above to accomplish the digitization process: Discrete Fractional Fourier

Transform (DFRFT) and Centered Discrete Fractional Fourier Transform (CDFRFT), and the differences of them will be elaborated in the following section.

B. Discrete Fractional Fourier Transform

A satisfactory definition of DFRFT which is fully consistent with CFRFT has been the research objective of scholars who have been striving to find a resemblance for CFRFT and finally applying it to real problems.

There are several algorithms which digitize CFRFT into a discrete mode in literatures, and each of the algorithms has a particular way of processing signals, so different algorithms would have yielded different accuracies.

1. Specific Introduction of DFRFT

As elucidated in Chapter I, a restriction for CFRFT is that it cannot be directly applied on DSP, so there is a high demand for a digitized form of it. To approximate CFRFT to a best degree, the DFRFT algorithm should exhibit high internal consistency and analytical elegance which the conventional DFT has already shown successfully. And the DFRFT algorithm is finally established by seeking for an exceptional set of eigenvectors of the DFT matrix, and this set of eigenvectors is the discrete counterpart of Hermite-Gaussian functions (the eigenfunctions of CFRFT), and then a resemblance of CFRFT will be achieved.

A good resemblance requires that DFRFT also have the main properties that CFRFT has: unitarity, index additivity, and reduction to the ordinary FT when a=1. It's been

shown that these 3 requirements will be spontaneously fulfilled when DFRFT is specified by a spectral expansion with the form of (2.8) [8]. Assuming $\psi_k[n]$ to be an arbitrary orthonormal eigenvector set of the $N \times N$ DFT matrix and λ_k to be the associated eigenvalues, then the discrete analog of (2.8) is:

$$F_a[m,n] = \sum_{k=0}^{N-1} \psi_k[m](\lambda_k)^a \psi_k[n] \tag{2.14}$$

which constitutes a definition of the DFRFT matrix.

There are two ambiguities to be eliminated in (2.14). The first is in regard to the eigenstructure of DFT. Since the number of the distinct eigenvalues that the DFT matrix F has is only four: $\{1,-1,j,-j\}$ as shown in Table I:

TABLE I
EIGENVALUE MULTIPLICITY OF THE DFT MATRIX

N	1	$-j$	-1	j
$4m$	m+1	m	m	m-1
$4m$+1	m+1	m	m	m
$4m$+2	m+1	m	m+1	m
$4m$+3	m+1	m+1	m+1	m

Where the eigenvalues are degenerate, hence there is no unique eigenvector set. Consequently, there is a high necessity to specifically determine a particular eigenvector set for (2.14). In the continuous case, this ambiguity has been removed by picking the

Hermite-Gaussian functions as the eigenfunctions or, comparably, by selecting that eigenfunction set of the continuous FT which are also eigenfunctions of the Harper matrix *S*. And that is to say, based upon the fact that the operators *S* and *F* commute with each other, the common eigenfunction set of them should be picked. Thus with the motivation of obtaining an appropriate definition of DFRFT, in the same way by selecting the common eigenvector set of the DFT matrix and the discrete analogue of the matrix *S*, which we define to be the discrete counterpart of the Hermite-Gaussian functions, this first ambiguity will be eliminated.

The second ambiguity will appear when there is a need to take the fractional power of the eigenvalues, for the reason that the fractional power operation is not single valued. This ambiguity should be removed by analogy with the continuous case again: taking the fractional power of the DFT eigenvalue: $\lambda_k^a = e^{-j\frac{\pi}{2}ka}$. There are a number of distinct methods of choosing the eigenvector set, but in the development process of the DFRFT algorithm for this research, one particular method is concentrated on to develop an accurate definition.

Then the discrete counterpart of Hermite-Gaussian functions is able to be defined explicitly.

2. Discrete Hermite-Gaussian Functions

The discrete Hermite-Gaussains are defined in [3] as the solutions of a difference equation which is analogous to the defining differential (2.10) of the continuous

Hermite-Gaussian functions. This second-order difference equation analogous to the defining differential equation of the continuous Hermite-Gaussians is:

$$x[n+1]-2x[n]+x[n-1]+2(\cos(\frac{2\pi}{N}n)-1)x[n]=\lambda x[n] \tag{2.15}$$

where $x[n]=x(nh)$, and $h=1/\sqrt{N}$. It could be observed from (2.15) that the coefficients are periodic with *N*, implying the existence of periodic solutions with the same period. If (2.15) is written explicitly by concentrating on a single period, say, $0\le n\le N-1$, (2.16) will be obtained as shown below:

$$\begin{bmatrix} -2 & 1 & 0 & \cdots & 0 & 1 \\ 1 & 2\cos(\frac{2\pi}{N})-4 & 1 & \cdots & 0 & 0 \\ 0 & 1 & 2\cos(\frac{2\pi}{N}2)-4 & \cdots & 0 & 0 \\ \vdots & \vdots & \vdots & \ddots & \vdots & \vdots \\ 1 & 0 & 0 & \cdots & 1 & 2\cos(\frac{2\pi}{N}(N-1))-4 \end{bmatrix} \times \begin{bmatrix} x[0] \\ x[1] \\ x[2] \\ \vdots \\ x[N-2] \\ x[N-1] \end{bmatrix} \tag{2.16}$$
$$= \lambda \begin{bmatrix} x[0] \\ x[1] \\ x[2] \\ \vdots \\ x[N-2] \\ x[N-1] \end{bmatrix}$$

where the rows of the matrices in both LHS and RHS are derived from the substitution of $n=0,1,2,...,N-1$ in (2.15) and the utilization of the periodicity relation $x[n+N]=x[n]$. This step has completed the derivation of the discrete analogue of *S*, which has been referred to as the Harper matrix in the preceding part. As previously

explained, *S* commutes with the DFT matrix, hence the common eigenvector set of *S* and the DFT matrix is unique and orthogonal.

This unique orthogonal eigenvector set, which is denoted as u_k, will be taken as the discrete counterpart of the continuous Hermite-Gaussians to be used in defining (2.14), and in the following part, the uniqueness of this eigenvector set will be discussed in details.

3. Uniqueness of the Common Eigenvector Set of *S* and DFT

The parity of the eigenvectors of the DFT matrix is a factor that needs to be taken into consideration. There are either even or odd eigenvectors, thus it follows from this fact that the common eigenvector set of *S* and the DFT matrix, which is confirmed as existent since the two matrices commute, should be also composed of even or odd vectors.

It has been discussed in the previous parts that the kernel of CFRFT has a periodicity of 4, and this has led to the following discussion on the multiplicity of *N*:

It's been validated by researchers that when *N* is not a multiple of 4, all of the eigenvalues of *S* will be distinct. And the main reason why all of its eigenvectors of *S* is orthogonal and unique (within multiplicative constants) is that *S* is a real symmetric matrix. Since it's already been shown that *S* has a common eigenvector set with the DFT matrix, it is the same logic that this unique set of eigenvectors of *S* must also be a set of eigenvectors of the DFT matrix *F*. Then the discrete Hermite-Gaussian functions will be defined as the normalized version of this eigenvector set.

However, it does not necessarily mean that when N is a multiple of 4, the eigenvalues of S will take on absolutely the same values. There will still be distinct eigenvalues, but with the exception of only one eigenvalue: the one with the value of 0 and a degeneracy of 2. The eigenvectors corresponding to all the other eigenvalues except for 0 are guaranteed orthogonal to each other. But the two eigenvectors corresponding to the eigenvalue 0 can be selected to be orthogonal, again because S is a real symmetric matrix. A great number of means of selecting these two eigenvectors such that they are orthogonal are available; however, there is only one way to pick them such that one is even and the other is odd. Since the common set of eigenvectors between S and F should be sought for, and since all the eigenvectors of F are either even or odd vectors, then both the even and odd eigenvectors corresponding to the eigenvalue 0 should be selected.

Therefore, the search for the common set of S and F will be confined on the even and the odd spaces, and a matrix P that decomposes an arbitrary vector $x[n]$ into its even and odd components needs to be introduced here. The P matrix, as in (2.17), has the capability of mapping the even part of the N-dimensional vector $x[n]$ to the first $\lfloor (N/2+1) \rfloor$ components and the odd part to the remaining components of a new matrix $f[n]$. This new matrix should be understood as a sorting process of the even and odd elements of $x[n]$. For example, the P matrix of dimension 5 is defined as in (2.17) [3]:

$$P = \frac{1}{\sqrt{2}} \begin{bmatrix} \sqrt{2} & 0 & 0 & 0 & 0 \\ 0 & 1 & 0 & 0 & 1 \\ 0 & 0 & 1 & 1 & 0 \\ 0 & 0 & 1 & -1 & 0 \\ 0 & 1 & 0 & 0 & -1 \end{bmatrix} \tag{2.17}$$

The even part of $x[n]$ is represented by the first three components of $f = Px$ as shown in (2.18):

$$\begin{aligned} [f[0], f[1], f[2]] &= \frac{1}{\sqrt{2}} [\sqrt{2}x[0], x[1] + x[-1], x[2] + x[-2]] \\ &= \frac{1}{\sqrt{2}} [\sqrt{2}x[0], x[1] + x[4], x[2] + x[3]] \end{aligned} \tag{2.18}$$

As a matter of course, the remaining two components represent the odd part of $x[n]$ as in (2.19):

$$\begin{aligned} [f[3], f[4]] &= \frac{1}{\sqrt{2}} [x[2] - x[-2], x[1] - x[-1]] \\ &= \frac{1}{\sqrt{2}} [x[2] - x[3], x[1] - x[4]] \end{aligned} \tag{2.19}$$

The arguments of P are interpreted modulo N, the same as the ordinary DFT. What merits the researchers' attention is that the P matrix is both symmetric and unitary, to be expressed mathematically, there is a relation as in (2.20):

$$P = P^T = P^{-1} \tag{2.20}$$

and this important property of P has been effectively exploited in the digital calculation of DFRFT, where the Harper matrix has to go through a similarity transformation as PSP^{-1}, so the resultant matrix will be in a block diagonal form as shown in (2.21):

$$PSP^{-1} = PSP = \begin{bmatrix} Ev & 0 \\ 0 & Od \end{bmatrix} \tag{2.21}$$

Only by taking this similarity transformation could all the even/odd eigenvector set of the S matrix be obtained. It is clearly seen that eigenvectors of PSP^{-1} can be determined separately from the Ev and Od matrices, so the corresponding eigenvectors of S will be acquired simply from the even/odd extension of the eigenvectors of PSP^{-1}. Therefore, looking for the common eigenvector set of S and F is no longer an intractable issue, because this procedure could be reduced to obtaining the eigenvectors of the Ev and Od matrices.

Referring back to (2.16), it could be observed that the configuration of the S matrix is tridiagonal, except for the two entries at the upper-right and lower-left corners. But after going through a similarity transformation PSP^{-1}, S will become strictly tridiagonal, and its submatrices Ev and Od will consequently be tridiagonal. Based on the research of [23], it is guaranteed that tridiagonal matrices have distinct eigenvalues, and this result has successfully implied the uniqueness of the eigenvectors of the Ev and Od matrices, so as to having completed the proof of the uniqueness of the common eigenvector set of S and the DFT matrix F. So in a word, the common set of eigenvectors of the Harper matrix S and the DFT matrix F can be determined uniquely, despite the dimension of S.

4. Ordering the Eigenvectors of *S*

It has been demonstrated in the last part that the common eigenvector set of *S* and *F* not only exists but also is unique, then the determination of which eigenvector of this set and which Hermite-Gaussian function correspond with each other will be the subsequent procedure of the DFRFT calculation. The approach selected for ordering eigenvectors of Hermite-Gaussians will be dependent on the number of zero-crossings of the discrete Hermite-Gaussians, in correspondence with the number of zeros of the continuous Hermite-Gaussians.

The definition of zero crossing of a discrete vector has already been discussed in lots of textbooks. The vector $x[n]$ has a zero crossing at n if $x[n]x[n+1]<0$. There is a convention that the number of zeros in merely one period $0 \le n \le N-1$ shall be counted, when counting the number of zero crossings of the periodic sequence $x[n]$ with a period of *N*. Besides, the zero crossing at the boundary points of a period such as when $x[N-1]x[N]=x[N-1]x[0]<0$ will also be included. So regardless of the shift, any shifted periodic sequences will have exactly the same number of zero crossings. This interesting property of zero crossings belongs to the whole periodic sequence, but not just a specific segment of the sequence with the length of the period *N*.

And then before applying this property to the eigenvector issue, the following task should be made clear: since it is already known that each of the eigenvectors has a distinct number of zero crossings, so there is a need to find an appropriate approach to efficiently count the zero crossings for each eigenvector.

It has been elaborated in the last part that the common eigenvectors of the *S* and *F* matrices need to be obtained from the tridiagonal *Ev* and *Od* matrices. It has been shown in [3] that the *Ev* matrix has eigenvectors with a number of zero crossings ranging from 0 to $\lfloor N/2 \rfloor$, and the eigenvector of *Ev* with *k* zero crossings yields the even eigenvector of *S* with 2*k* ($0 \le k \le \lfloor N/2 \rfloor$) zero crossings; While the *Od* matrix has eigenvectors whose number of zero crossings is within the range from 0 to $\lfloor (N-3)/2 \rfloor$, and the eigenvector of *Od* with *k* zero crossings yields the odd eigenvector of *S* with 2k+1 ($0 \le k \le \lfloor (N-3)/2 \rfloor$) zero crossings. So now precisely determining the number of zero crossings of an eigenvector of *S* avoiding any ponderous means of counting is possible.

It will be shown in the following that an even eigenvector of *S* can be formed complying with the convention mentioned above

$$e = P[\hat{e}_k{}^T : 0,...,0]^T \tag{2.22}$$

where $\hat{e}_k$ is the eigenvector of *Ev* with *k* zero-crossings ($0 \le k \le \lfloor N/2 \rfloor$), which is already reflected by the subscript. And the vector *e*, which denotes the eigenvector of *S*, is given by

$$e = \frac{1}{\sqrt{2}}[\sqrt{2}\hat{e}_k[0], \hat{e}_k[1],...,\hat{e}_k[r] : \hat{e}_k[r],...,\hat{e}_k[1]] \tag{2.23}$$

And *e* has 2*k* zero crossings, according to the convention of zero counting above

$$[\text{e e}[0]] = \frac{1}{\sqrt{2}}[\underbrace{\sqrt{2}\hat{e}_k[0], \hat{e}_k[1],...,\hat{e}_k[r]}_{k \text{ zero crossings}} : \underbrace{\hat{e}_k[r],...,\hat{e}_k[1], \sqrt{2}\hat{e}_k[0]}_{k \text{ zero crossings}}] \tag{2.24}$$

where N, the dimension of S, satisfies this relationship with r: $N=2r+1$.

Similarly, odd eigenvectors of S will also be acquired from the eigenvectors of Od through the same zero padding and transformation process as the derivation of even eigenvectors: $o = P[0,\ldots,0 \vdots \hat{o}_k^T]^T$. Based on that convention of zero crossing counting, the odd eigenvector o derived from the eigenvector $\hat{o}_k^T$ of the Od matrix with k zero crossings yields an eigenvector of S with $2k+1$ zero crossings $(0 \le k \le \lfloor (N-3)/2 \rfloor)$.

It should be noted that by the convention introduced in this part, each of the eigenvectors of S comes with a unique number of zero crossings hence an index equal to its number of zero crossing can be allocated to each vector. And for a stringent definition of DFRFT, it should also be mentioned that the index k spans different ranges of discrete time for different parity of N, to be specific, $k=\{0,\ldots,N-1\}$ for odd N and $k=\{0,\ldots,N-2,N\}$ for even N.

So up to this point, an approach has been explicitly established for finding and ordering the common eigenvector set of the matrices S and F. Thereby the k-th element of this eigenvector set must have k zero crossings and its parity is dependent on the parity of k.

5. Final Definition of the Discrete Fractional Fourier Transform

The final version of definition for DFRFT is given by

$$F_a[m,n] = \sum_{k=0, k \neq (N-1+(N)_2)}^{N} u_k[m] e^{-j\frac{\pi}{2}ka} u_k[n] \tag{2.25}$$

where $u_k[n]$ is the k-th discrete Hermite-Gaussian function (the eigenvector of S with k zero crossings) and $(N)_2 \equiv N \bmod 2$. It might be noticed that the range of the summation is unusual, because there is no such an eigenvector with N-1 zero crossings when N is even, nor is there an eigenvector with N zero crossings when N is an odd number.

This index skipping law is related to the eigenvalue multiplicity of the DFT matrix which is as well unusual, as already demonstrated in Table I.

6. Properties of DFRFT

Mostly inherited from DFT and FRFT, the properties of DFRFT are presented in Table II, with new properties of DFRFT covered. And it could be observed that DFRFT has all the essential properties that CFRFT has:

TABLE II
PROPERTIES OF DFRFT

Name of Properties	Mathematical Expressions
Unitarity	$F_a^* = F_a^{-1} = F_{-a}$
Index additivity	$F_{a_1} F_{a_2} = F_{a_1+a_2}$
Reduction to the DFT when the order equals unity	$F_1(x[n]) = F(x[n])$
Linearity	$F_a(\sum_k c_k x_k[n]) = \sum_k c_k F_a(x_k[n])$

TABLE II, Cont.

Time inversion	$F_a(x[-n]) = X_a[-m]$
Periodicity	$F_{4l+a} = F_{4l}$
Repetitiveness	$F_a = F_{2-a}$
Symmetricity	$F_a(i,j) = F_a(j,i)$
Parity	$\begin{cases} X_a[m] & \text{is even, if x[n] is even} \\ X_a[m] & \text{is odd, if x[n] is odd} \end{cases}$
Commutativity	$F_{a_1} F_{a_2} = F_{a_2} F_{a_1}$
Associativity	$(F_{a_1} F_{a_2}) F_{a_3} = F_{a_1} (F_{a_2} F_{a_3})$
Parseval theorem	$\sum_{n=0}^{N-1} \lvert x[n] \rvert^2 = \sum_{n=0}^{N-1} \lvert X_a[n] \rvert^2$

For the property of Unitarity, the asterisk denotes Hermitian conjugation. The DFRFT operator F_a has inherited the unitarity of the DFT kernel. In other words, this property enables this transform to preserve the signal energy:

$$\left\| F_a(x[n]) \right\| = \left\| x[n] \right\| \tag{2.26}$$

For the Index additivity property, DFRFT at transform order a_1 followed by another DFRFT at transform order a_2 is equivalent to the DFRFT at a transform order of their addition: $a_1 + a_2$.

Besides, a satisfactory DFRFT algorithm should have as many operational properties as possible to be a well-founded counterpart of CFRFT.

7. DFRFT of Some Basic Types of Signals

a. Sinusoidal signal

This part is the DFRFT applied on a sinusoidal signal $x(t) = \sin(2\pi ft)$ with a fundamental frequency f=2000Hz. And the sampling frequency is $F_s = 8000Hz$.

Its plot in time-domain as in Fig.4:

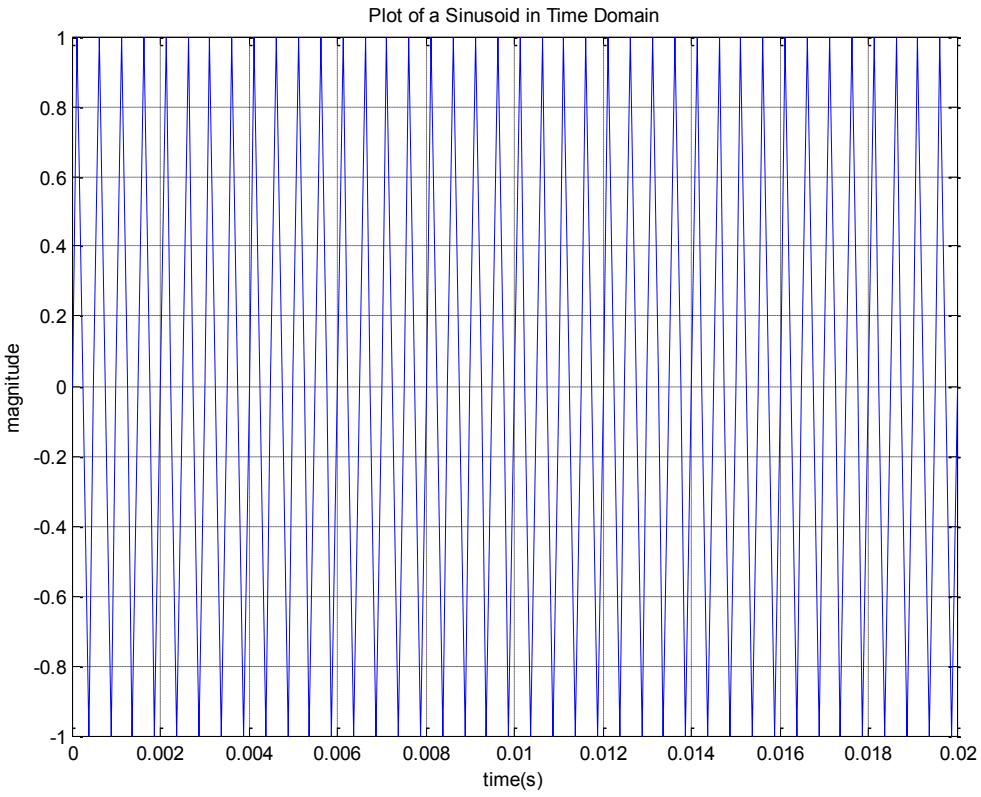

Fig. 4. A sinusoid in time domain.

Analysis with the traditional FFT in frequency domain is shown in Fig. 5:

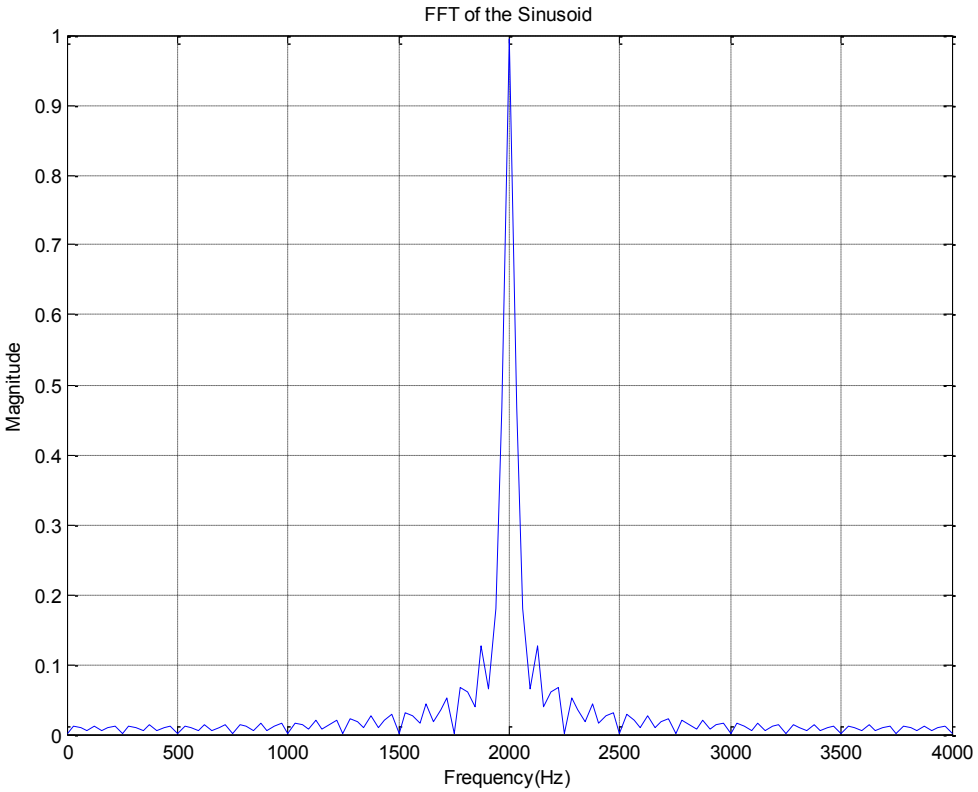

Fig. 5. FFT of the sinusoid.

It could be seen that the inherent frequency of 2000*Hz* is picked out by FFT.

And the DFRFT at a=1 is shown in Fig. 6:

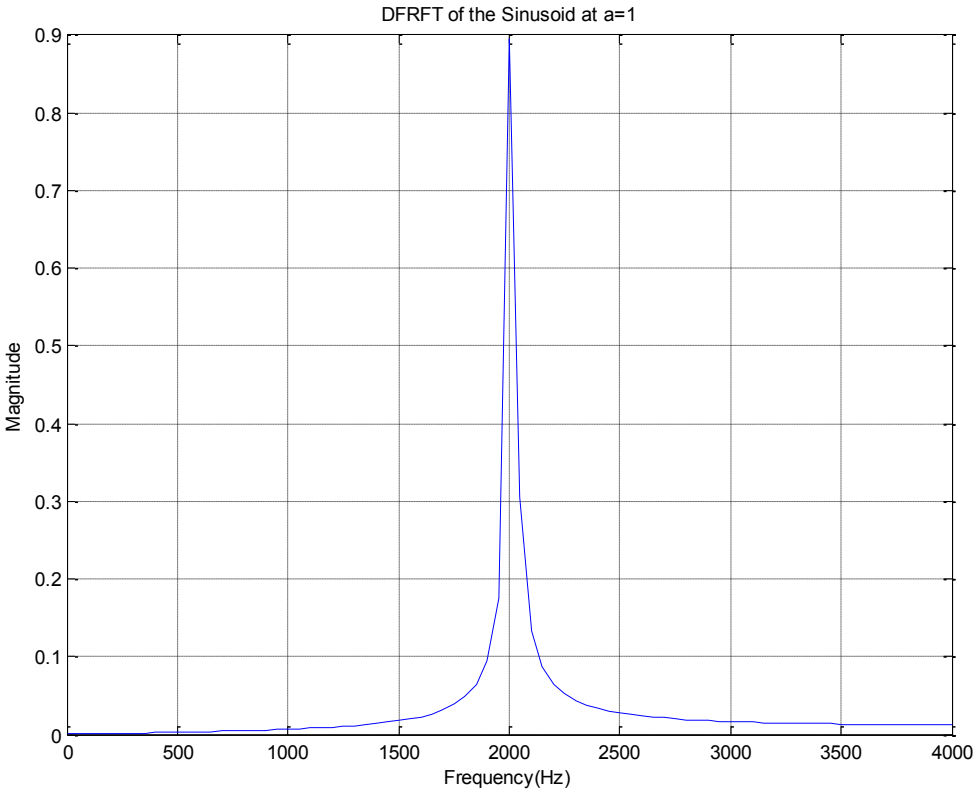

Fig. 6. DFRFT at a=1 of the sinusoid.

It could be observed that in both FFT and DFRFT, the peak is located at f=2000Hz. The magnitude of DFRFT is slightly different from FFT due to its higher energy leakage to other frequency band which is caused by the imperfection of the approximation with CFRFT. At different transform orders, the energy leakages are even more severe than at a=1, which is shown in Fig. 7:

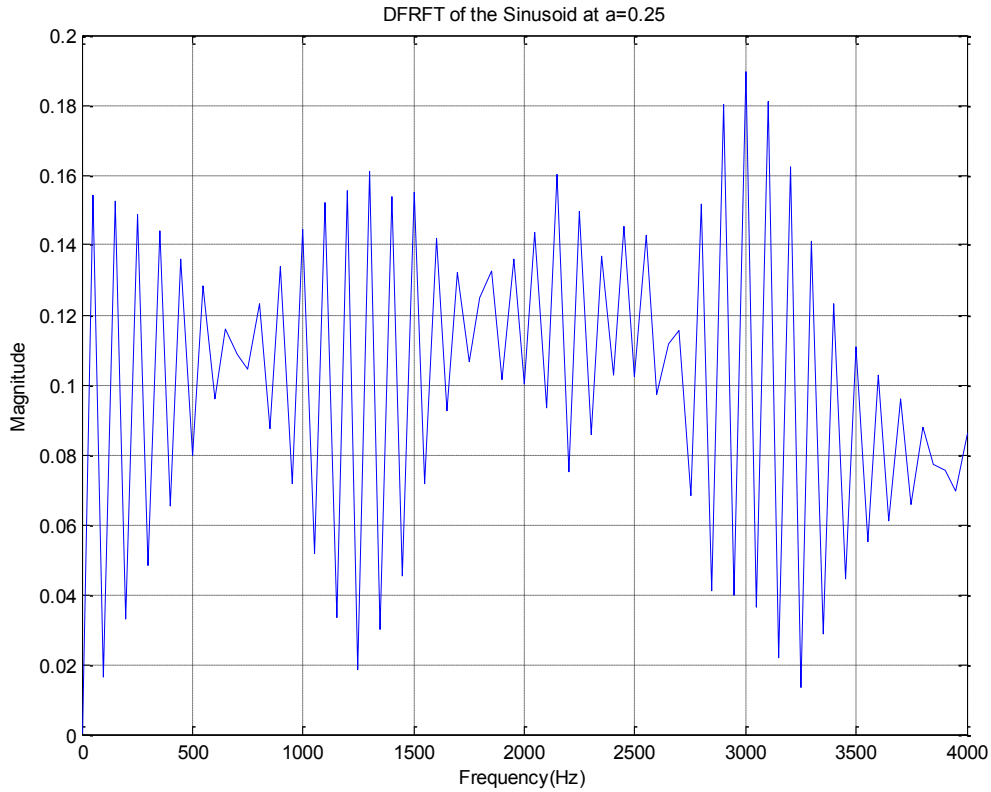

Fig. 7. DFRFT at a=0.25 of the sinusoid.

The following Fig. 8 shows the DFRFT plot at a=0.5:

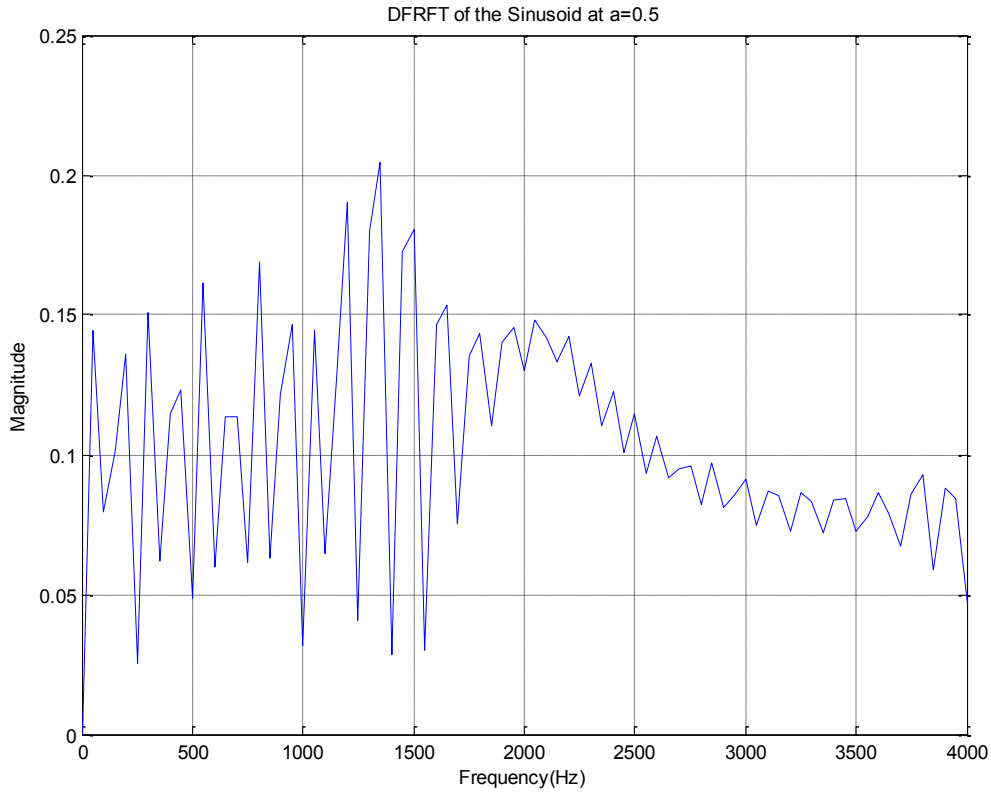

Fig. 8. DFRFT at a=0.5 of the sinusoid.

Fig. 9 gives the DFRFT result at a=0.75 of the sinusoid signal:

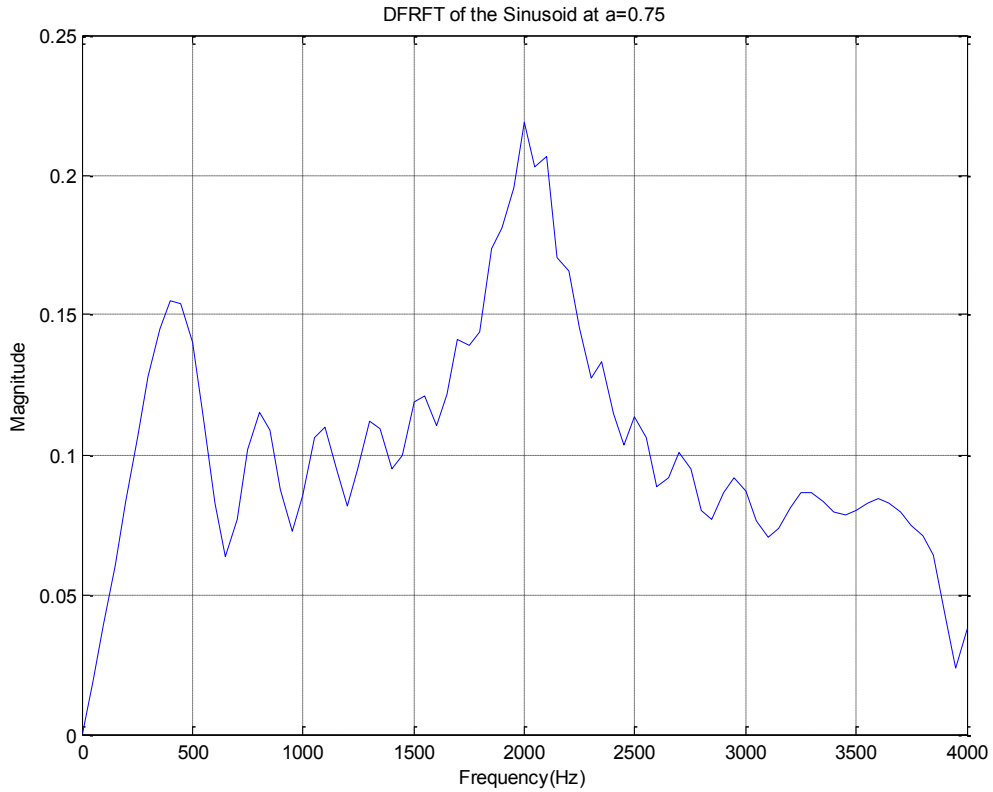

Fig. 9. DFRFT at a=0.75 of the sinusoid.

All these plots of DFRFT at a transform order other than 1 fail to give a pulse signal, but Fig. 10 shows that DFRFT at a transform order much closer to 1 can provide relatively satisfactory energy-concentration performance:

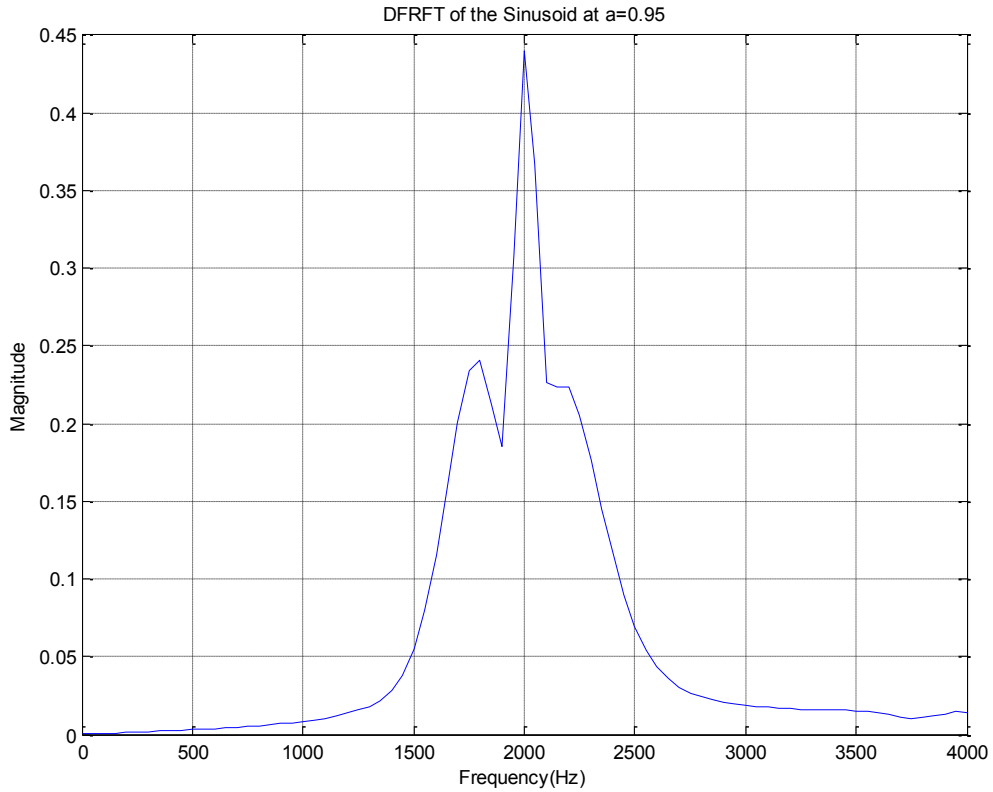

Fig. 10. DFRFT at a=0.95 of the sinusoid.

By careful observation, it could be discovered that as a approaches to 1, the DFRFT plot will be approximating FFT to a better degree.

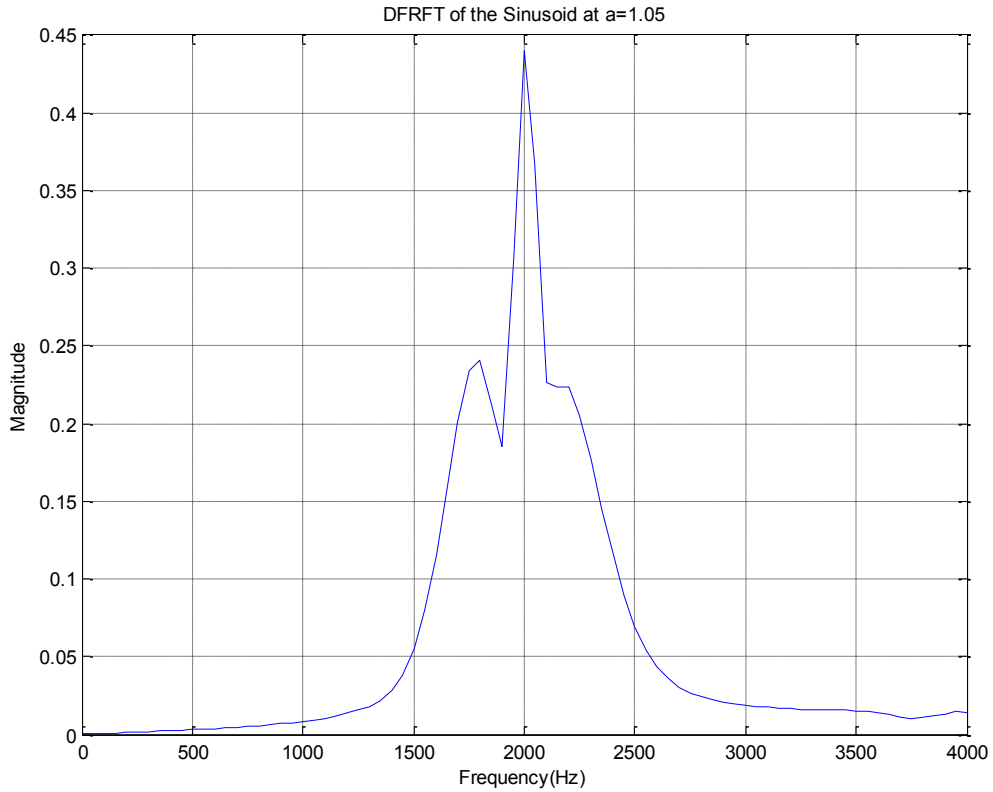

Fig. 11. DFRFT at a=1.05 of the sinusoid.

From Fig. 11, it is obvious that when a=1.05, the DFRFT plot is the same with the plot when a=0.95.

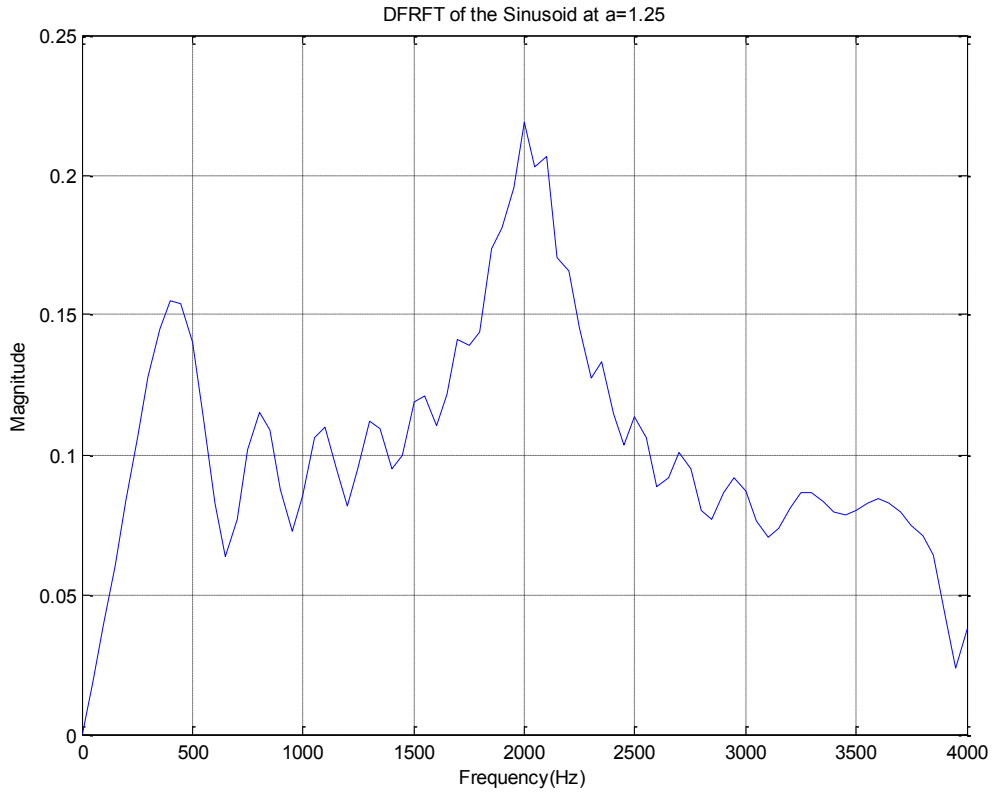

Fig. 12. DFRFT at a=1.25 of the sinusoid.

From Fig. 12, it is similarly evident that with the transform order a=1.25, the DFRFT plot is the same with the plot at a=0.75.

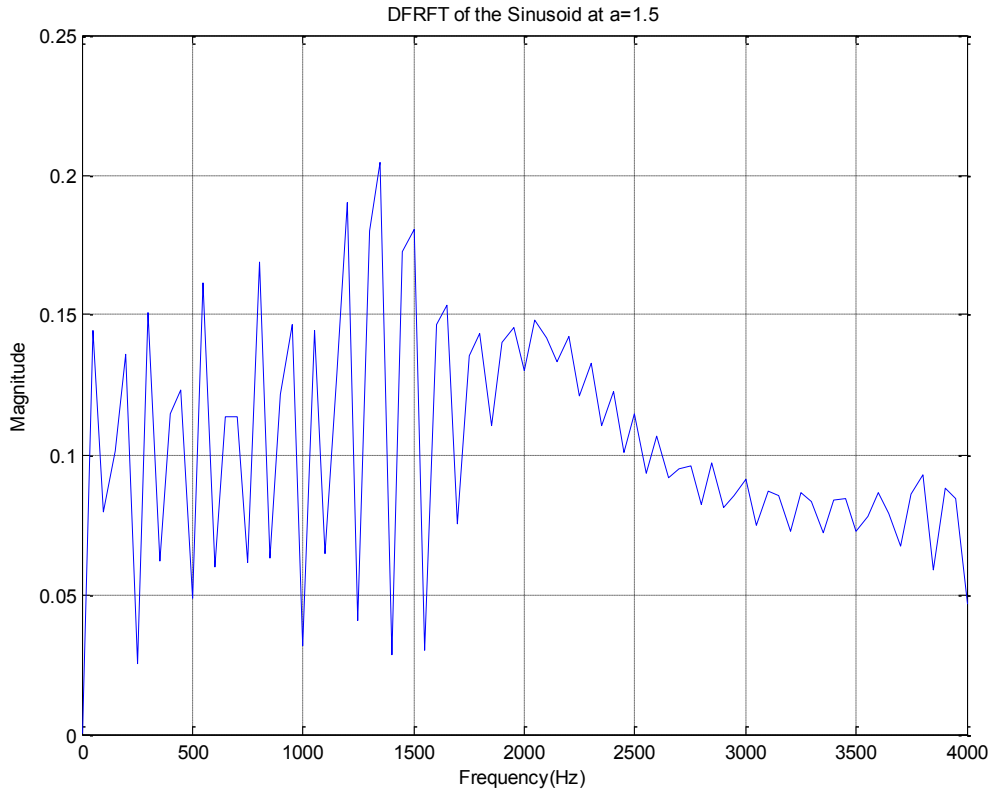

Fig. 13. DFRFT at a=1.5 of the sinusoid.

In a same way, it shows in Fig. 13 that when a=1.5, the DFRFT plot matches with the plot when a=0.5.

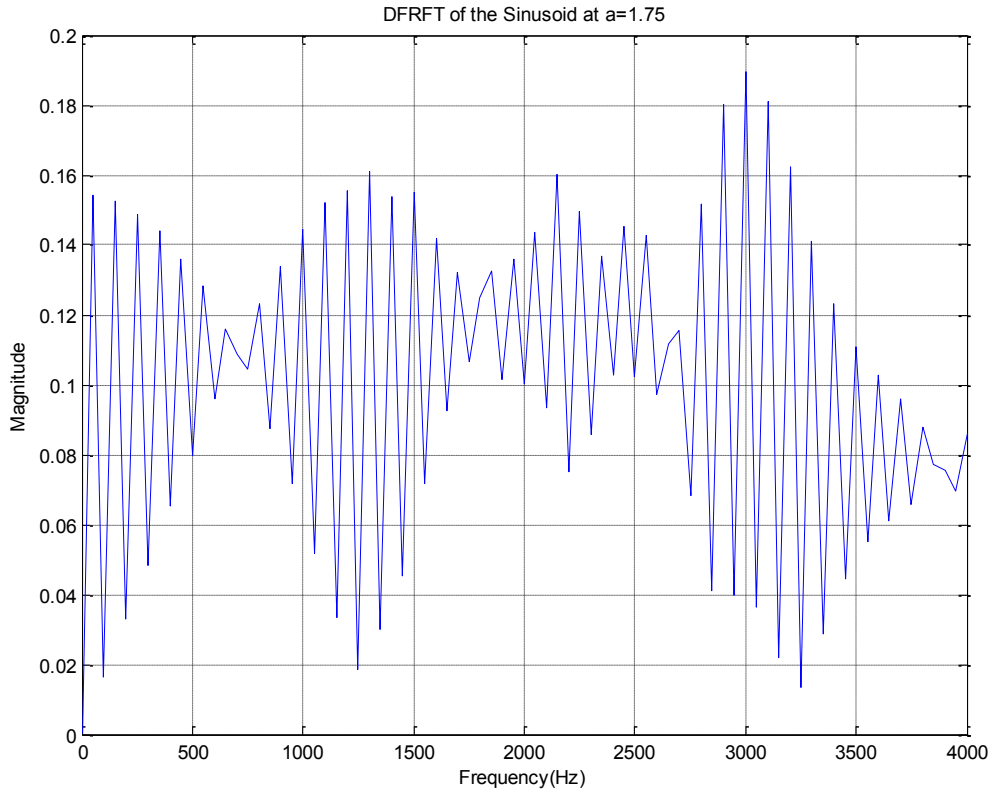

Fig. 14. DFRFT at a=1.75 of the sinusoid.

Likewise, it is obvious as shown in Fig. 14 that the DFRFT plot at a=1.75 is the same with the plot at a=0.25.

As a contrast, the DFRFT of the sinusoid at different transform orders are plotted in this section. It is easily concluded that the DFRFT of a sinusoid resembles FFT furthest when a=1 is selected to carry out the transformation, and the results of the DFRFT at transform orders other than 1 have proved the property of Repetitiveness: $F_a = F_{2-a}$.

b. Harmonic signal comprised of 12 components

$$x(t) = \cos(2\pi ft) + 2\cos(2\pi 2ft) + 3\cos(2\pi 3ft) + 4\cos(2\pi 4ft) + 5\cos(2\pi 5ft) + 6\cos(2\pi 6ft)$$
$$+ 7\cos(2\pi 7ft) + 8\cos(2\pi 8ft) + 9\cos(2\pi 9ft) + 10\cos(2\pi 10ft) + 11\cos(2\pi 11ft) + 12\cos(2\pi 12ft)$$

where f is the fundamental frequency, and f=200Hz. The sampling frequency is also F_s, and $F_s = 8000Hz$.

The time domain plot of this harmonic signal is shown in Fig.15:

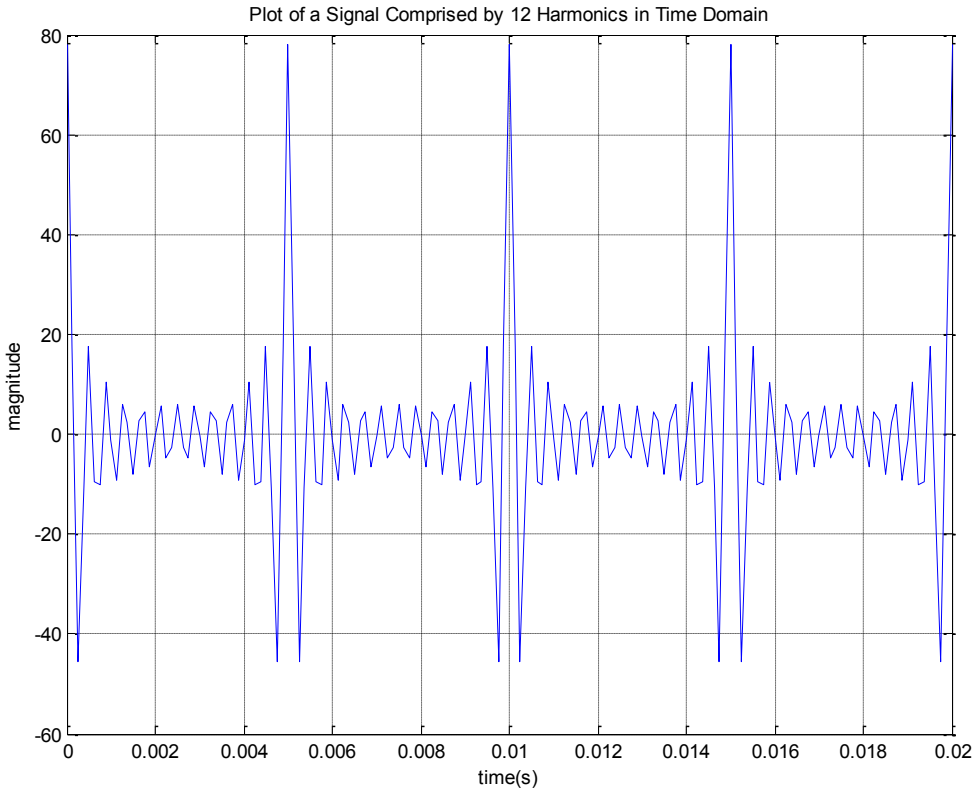

Fig. 15. Signal comprised by 12 harmonics in time domain.

Being such a complicated signal, it is difficult to distinguish the information contained separately in each of the frequency component. But FFT, as a conventional

frequency domain analysis tool, has the capability of effectively separating the different frequency information. The FFT plot of the harmonic signal is given by Fig. 16:

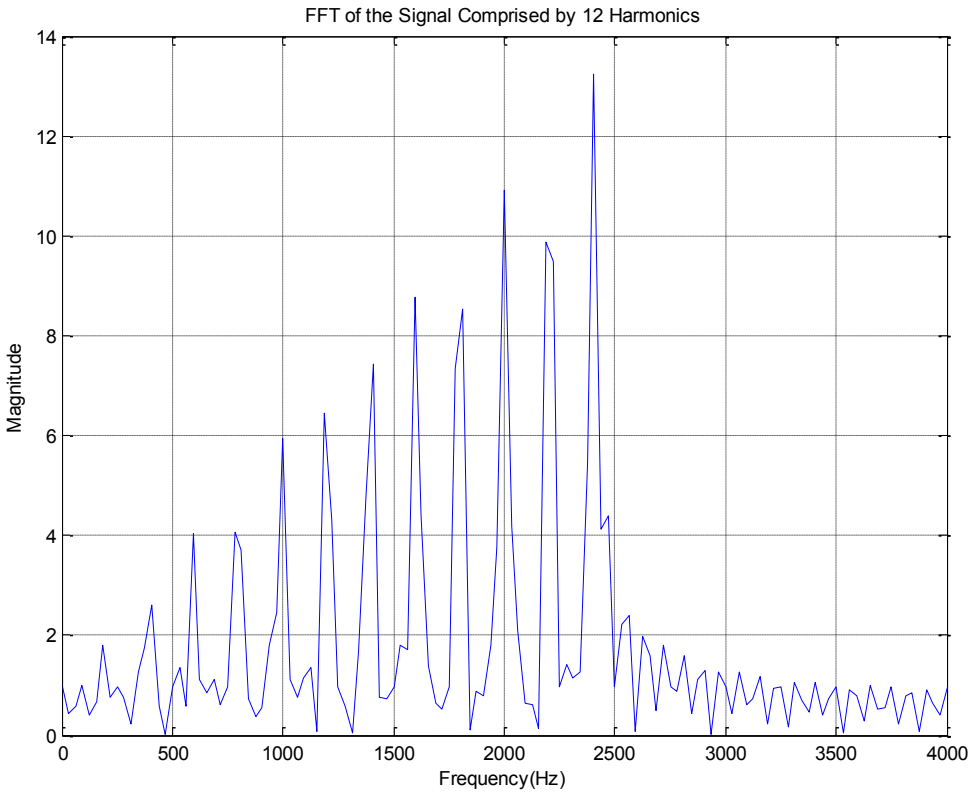

Fig. 16. FFT of the signal comprised by 12 harmonics in frequency domain.

There are clearly 12 spikes in Fig. 16, and each one corresponds with the different multiples of the fundamental frequency f=200 Hz. So the highest peak has a frequency of 2400Hz which lies near the location of f=2500Hz.

The following Fig. 17 is the DFRFT plot of the harmonic signal:

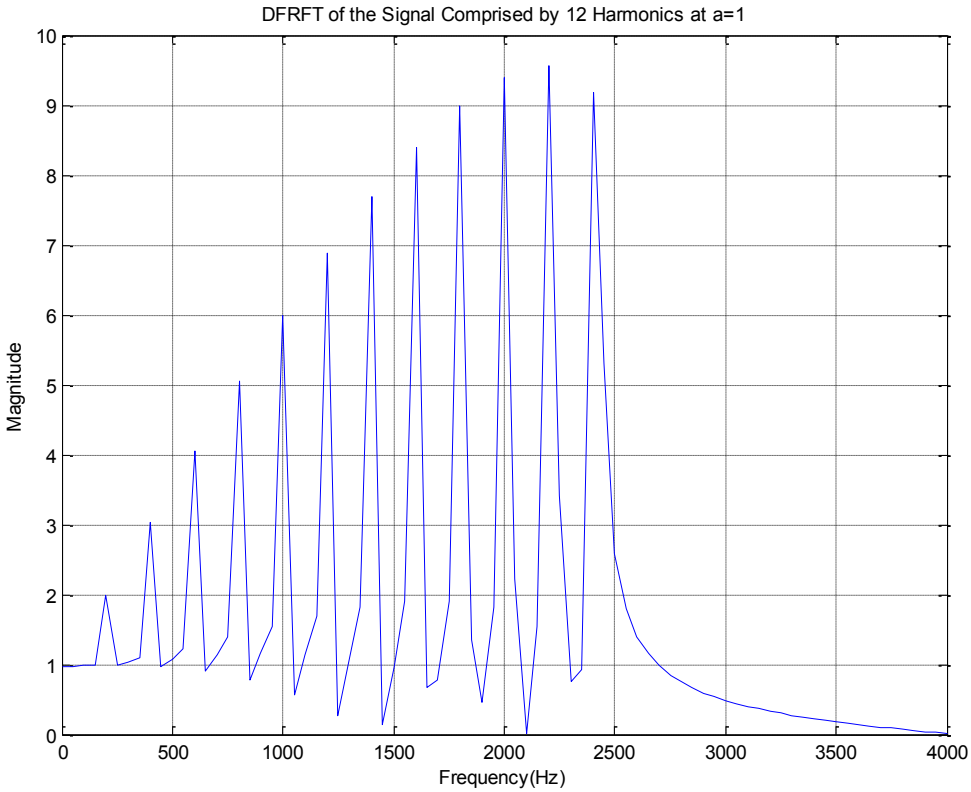

Fig. 17. DFRFT at a=1 of the signal comprised by 12 harmonics.

Where we could see the curve is more smooth compared with the FFT result in Fig. 16. And all the 12 harmonics are shown at all the harmonic frequencies ranging from 200Hz to 2400Hz with an interval of 200Hz.

c. Rectangular signal

A rectangular signal with a mathematical expression is given by

$$x(t)=\begin{cases}1, & -0.01\le t\le 0.01\\ 0, & \text{elsewhere}\end{cases}$$

with a sampling frequency of $F_s = 8000Hz$.

The time domain plot of the rectangular signal is shown as in Fig. 18:

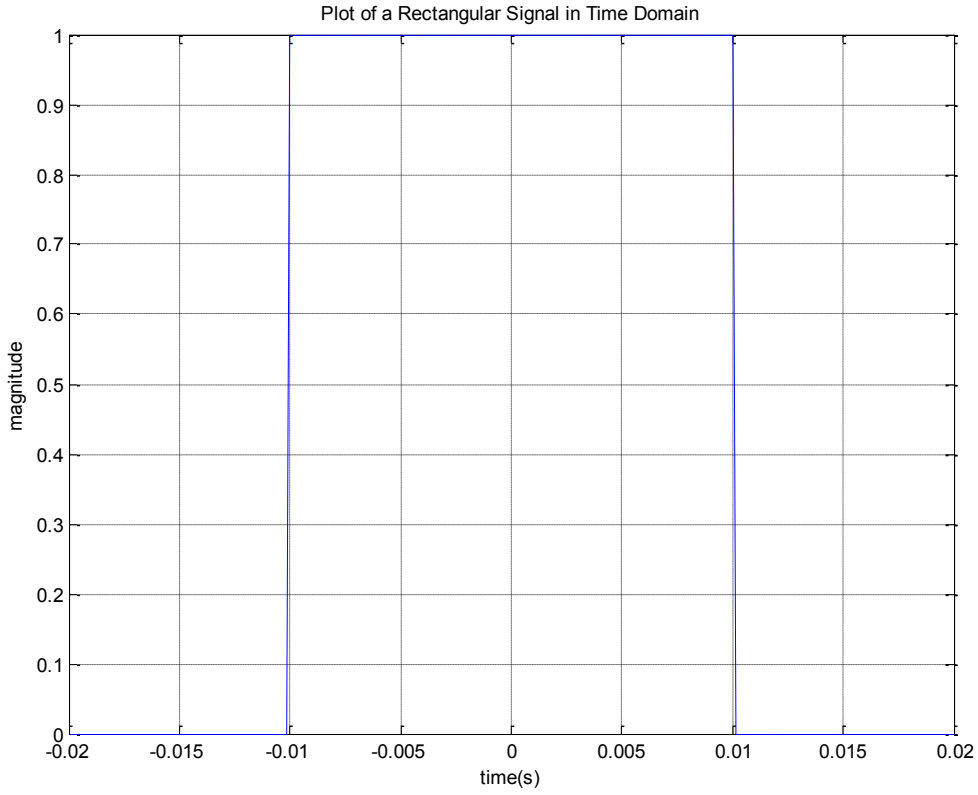

Fig. 18. Rectangular signal in time domain.

And then Fig. 19 gives the FFT result of the rectangular signal:

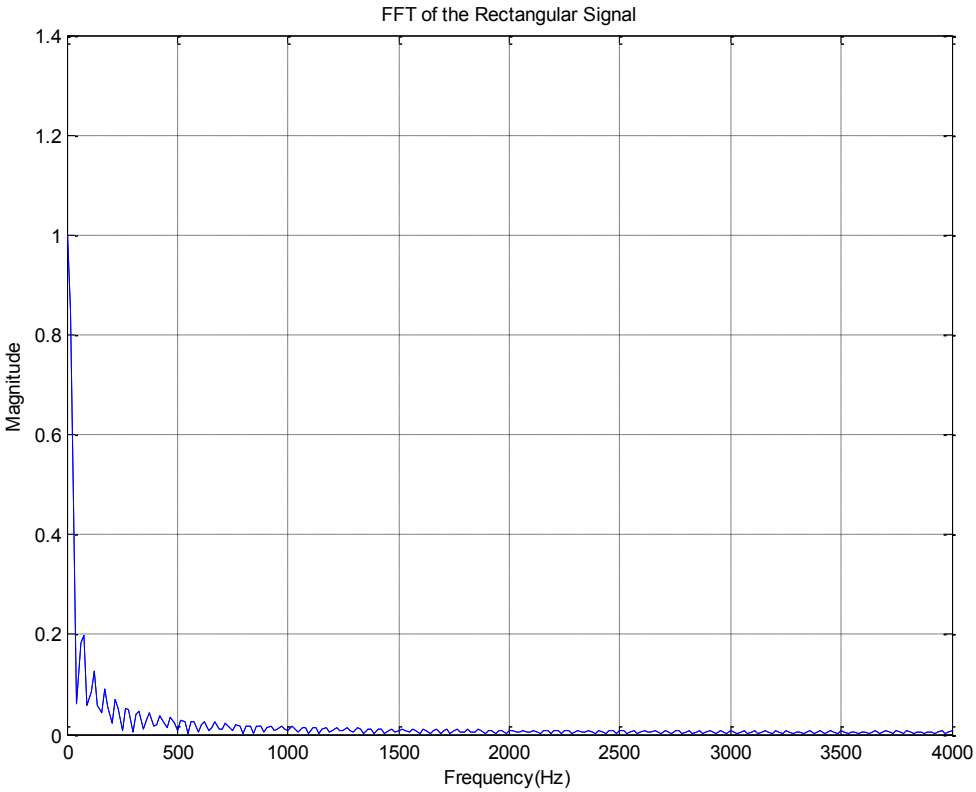

Fig. 19. FFT of the rectangular signal in frequency domain.

Where a peak at 0 Hz is easy to be spot. And Fig. 20 shows the DFRFT at a=1 for the rectangular signal:

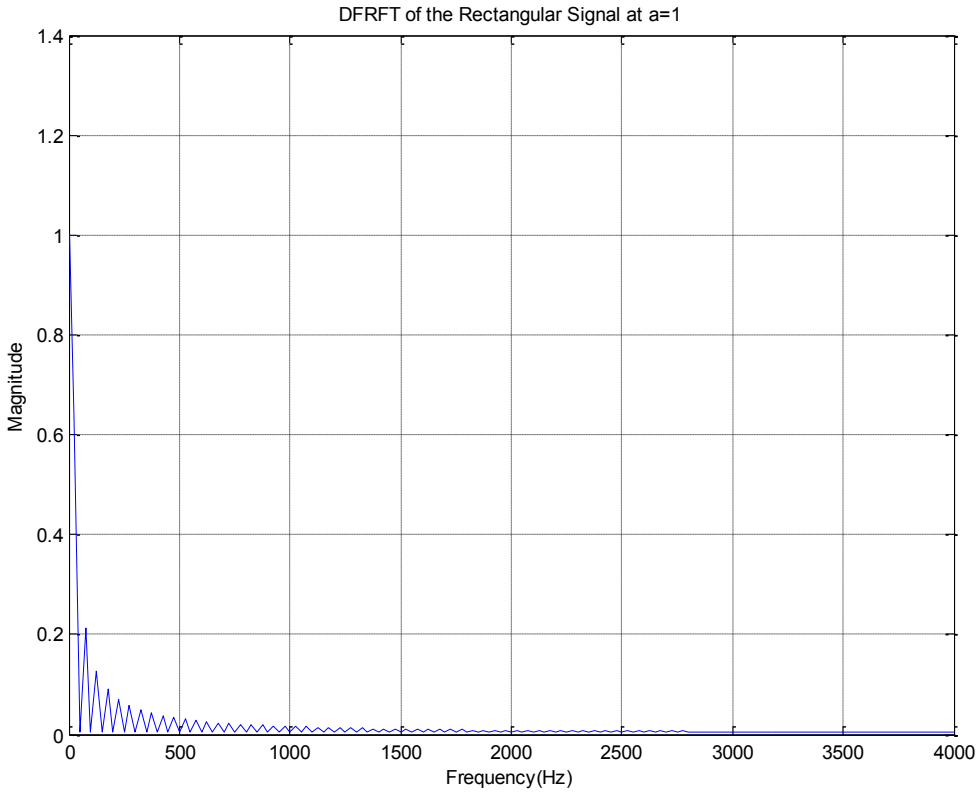

Fig. 20. DFRFT at *a*=1 of the rectangular signal.

So it could be concluded that even for the side lobes, FFT and DFRFT at *a*=1 have yielded almost 100% similar results. It is possible that one particular transformation algorithm works especially well on a particular type of signal.

C. Centered Discrete Fractional Fourier Transform, a Centered Version of DFRFT

1. Definition of CDFRFT

As DFRFT is based on the DFT, the centered version of DFRFT is based on a centered version of DFT in the same manner. But a bit different from DFRFT,

CDFRFT has adopted the eigenvectors of the Grünbaum tridiagonal commuter which has been testified to be superior discrete approximations to the continuous Hermite-Gaussian functions. This Grünbaum commuting matrix has basis functions that have a sigmoidal instantaneous frequency and produces a transform that is approximately and impulse for discrete chirps. And it has been shown in [5] that the basis functions of the CDFRFT contain both amplitude and frequency modulation for the sake of preserving orthogonality and those functions have a sigmoidal instantaneous frequency (IF), compared with DFRFT whose basis functions only contain frequency modulation.

As an alternative of Harper matrix S, the Grünbaum commuting matrix is exploited because it could also successfully furnish a complete basis for the DFT matrix of any dimension N, and could also serve as the solution of the second-order differential Hermite-Gaussian function.

The feasibility of this type of approach, which is based upon a commuter to obtain the DFT eigenvectors, rests with the Linear Algebraic theorem that two unitary-symmetric matrices A and B share a basis of eigenvectors as long as they commute with each other. As a supplementary theorem, it needs to be mentioned as well that if the eigenvalues of the commuter B are distinct, the eigenvectors of B without degeneracy will provide with the sought basis of eigenvectors.

The Grünbaum tridiagonal commuting matrix is defined as in (2.27):

$$T = \begin{bmatrix} a_1 & b_1 & \cdots & 0 & 0 \\ b_1 & a_2 & \cdots & 0 & 0 \\ \vdots & \vdots & \ddots & \vdots & \vdots \\ 0 & 0 & \cdots & a_{N-1} & b_{N-1} \\ 0 & 0 & \cdots & b_{N-1} & a_N \end{bmatrix} \tag{2.27}$$

where its diagonal, off-diagonal elements are defined as below:

$$a_m = \cos(\pi / N) - \cos(2\pi(m + \frac{1}{2}) / N), \quad 1 \le m \le N \ ; \ b_m = \sin^2(\pi m / N), \quad 1 \le m \le N-1 \ .$$

And $T(N)$ has $\lambda = 1$ as its only repeated eigenvalue.

We define CDFRFT with parameter *a* (should be distinguished from the diagonal elements of *T*) in a similar spectral expansion form as DFRFT in (2.28):

$$A_a = V \, \Lambda^a V^T \tag{2.28}$$

where V is the matrix of orthogonal eigenvectors derived from the Grünbaum tridiagonal 56ommuter T. The eigenvectors are in a descending order with respect to their corresponding eigenvalues of T, or put it in a simple way, the first column of V corresponds with the eigenvector with the largest eigenvalue. And all these columns together serve as the discrete counterparts of the continuous Hermite-Gaussian functions. While Λ^a is a diagonal matrix with elements $\lambda_k^a = e^{-j\frac{\pi}{2}ka}$, $0 \le k \le N-1$. With this substitution, the definition becomes:

$$A_a = \sum_{k=0}^{N-1} V \, e^{-j\frac{\pi}{2}ka} V^T \tag{2.29}$$

This definition orders the eigenvalues of the Grünbaum matrix T and assigns the eigenvector with m sign changes to the eigenvalue $\lambda_k = e^{-j\frac{\pi}{2}ka}$ and this is the same resemblance between the CFRFT and Hermite-Gaussian functions.

CDFRFT will become an identity matrix at a=0, where the basis functions are merely shifted delta functions as the case of DFRFT. At a=1, it will be reduced to CDFT, whose basis functions are complex exponentials of constant frequency and amplitude.

The elements of the CDFRFT matrix A_a have the following mathematical expression:

$$\{A_a\}_{kn} = \sum_{p=0}^{N-1} v_{kp} v_{np} e^{-j\frac{\pi}{2}pa} \tag{2.30}$$

where v_{kp} is the k-th element of the p-th eigenvector of T, and v_{np} is the n-th element of the p-th eigenvector. And then Multiplied by the transformation matrix A_α, the transform from the discrete time domain to the Centered Fractional Fourier Domain for the untreated signal $x[n]$ will be achieved:

$$X_a[k] = \sum_{n=0}^{N-1} x[n] \sum_{p=0}^{N-1} v_{kp} v_{np} e^{-j\frac{\pi}{2}pa} \tag{2.31}$$

And then the two summations need to be rearranged:

$$X_a[k] = \sum_{p=0}^{N-1} v_{kp} \sum_{n=0}^{N-1} x[n] v_{np} e^{-j\frac{\pi}{2}pa} \tag{2.32}$$

CDFRFT is actually another version of DFRFT, which is also a generalization of the Centered Discrete Fourier Transform (CDFT). The transform matrix of the N-point CDFT is given by:

$$\{A\}_{m,n} = \frac{1}{\sqrt{N}} e^{j\frac{2\pi}{N}(m-\frac{N-1}{2})(n-\frac{N-1}{2})} \tag{2.33}$$

where m, n=0, …, N-1. And there is an offset of (N-1)/2 for both m and n in this definition.

The reason why CDFT has been selected to define a fractional transform is that the multiplicities of its eigenvalues have shown great distinction from those of the conventional DFT, and this distinguished feature of CDFT can be employed to simplify the computations. Observed from Table I, when N is a multiple of 4, DFT has totally distinct multiplicities for the 4 eigenvalues, while the CDFT has a multiplicity of N/4 for each one of the eigenvalues, as it can be observed in Table III:

TABLE III
EIGENVALUE MULTIPLICITY OF THE CDFT

N	1	$-j$	-1	j
$4m$	m	m	m	m
$4m$+1	m+1	m	m	m
$4m$+2	m+1	m+1	m	m
$4m$+3	m+1	m+1	m+1	m

The fact that when (2.28) is utilized the DFT eigenvalues will have different multiplicities exerts an immediate influence that Λ^a requires a different effectuation for the cases of N being even and odd, as already discussed in the DFRFT section. However, when using the CDFT to define a fractional transform, there is a single definition of CDFRFT for all values of N as in (2.29).

Eigenvectors of the Grünbaum matrix being able to be exploited in generating CDFRFT is based on the following facts:

a) As another commuter of Hermite-Gaussian functions like Harper matrix, this tridiagonal matrix can also be viewed as the discrete analogue of the Hermite-Gaussian operator showing up in Schroedinger's equation for the harmonic oscillator, and it has been shown to converge to the Hermite-Gaussian differential operator asymptotically;

b) They furnish a full set of eigenvectors for any matrix size N. And for each N, there is a tridiagonal matrix $T(N)$ commuting with the N-point CDFT matrix, hence the eigenvectors of $T(N)$ give a "natural" basis for the eigenvectors of the CDFT matrix.

2. CDFRFT of Some Basic Types of Signal

a. Sinusoidal signal

For this part, CDFRFT is applied on a sinusoidal signal $x(t) = \sin(2\pi ft)$ with a fundamental frequency $f = 2000Hz$. And the sampling frequency is $F_s = 8000Hz$.

Its plot in the Fractional Domain as in Fig.21, r=N/4 resembles the result of DFRFT at a=1.

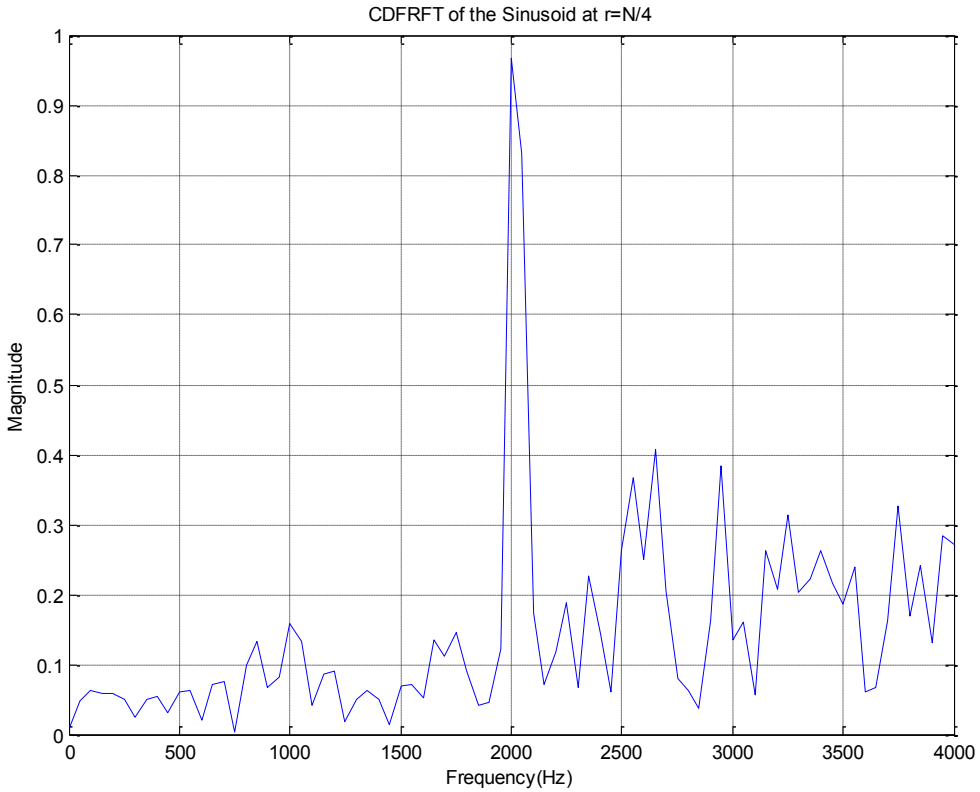

Fig. 21. CDFRFT at r=N/4 of the sinusoid.

Compared with the result of DFRFT when a=1 in Fig.6, it could be seen that the curve generated by CDFRFT is not as smooth as DFRFT.

b. Harmonic signal comprised of 12 components

$$x(t) = \cos(2\pi ft) + 2\cos(2\pi 2ft) + 3\cos(2\pi 3ft) + 4\cos(2\pi 4ft) + 5\cos(2\pi 5ft) + 6\cos(2\pi 6ft)$$
$$+ 7\cos(2\pi 7ft) + 8\cos(2\pi 8ft) + 9\cos(2\pi 9ft) + 10\cos(2\pi 10ft) + 11\cos(2\pi 11ft) + 12\cos(2\pi 12ft)$$

where f is the fundamental frequency, and f=200Hz. The sampling frequency is also F_s, and $F_s = 8000Hz$.

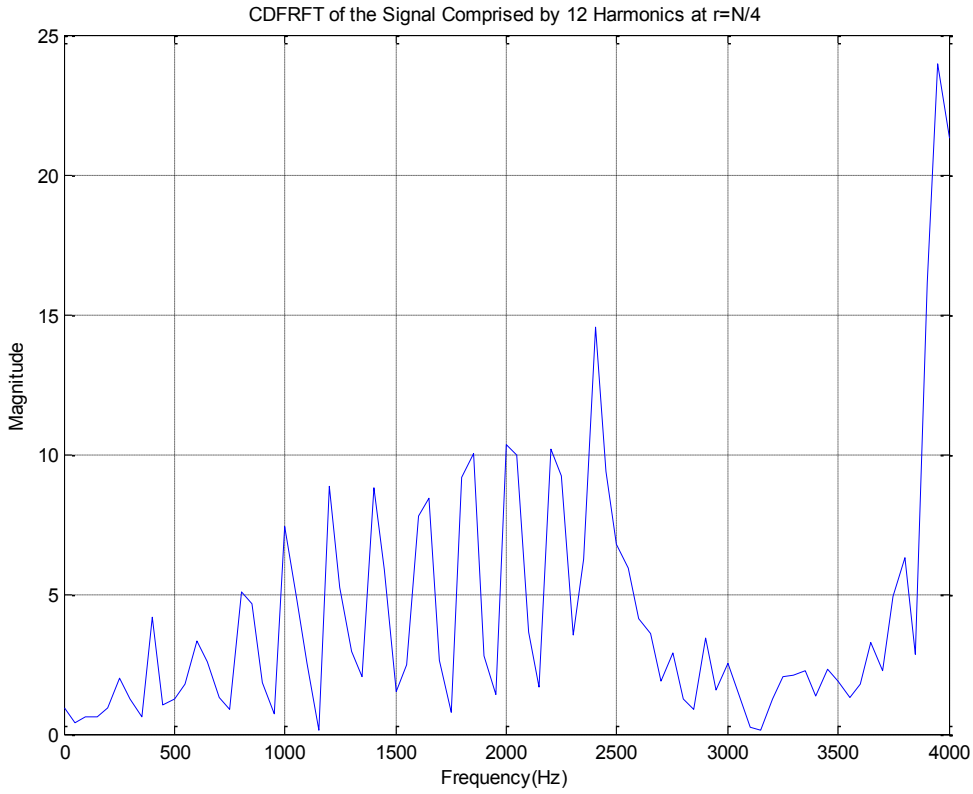

Fig. 22. CDFRFT at r=N/4 of the signal comprised by 12 harmonics.

The CDFRFT result of the signal comprised by 12 harmonics shown in Fig. 22 has introduced in great errors, especially at around f=4000Hz. And the 12 spikes are not as distinguished as the DFRFT result in Fig. 17.

c. Rectangular signal

The rectangular signal with a mathematical expression is given by

$$x(t)=\begin{cases}1, & \text{-0.01≤t≤0.01}\\ 0, & \text{elsewhere}\end{cases}$$ still with a sampling frequency of $F_s = 8000Hz$.

The CDFRFT plot at *r*=*N*/4 is shown in Fig. 23:

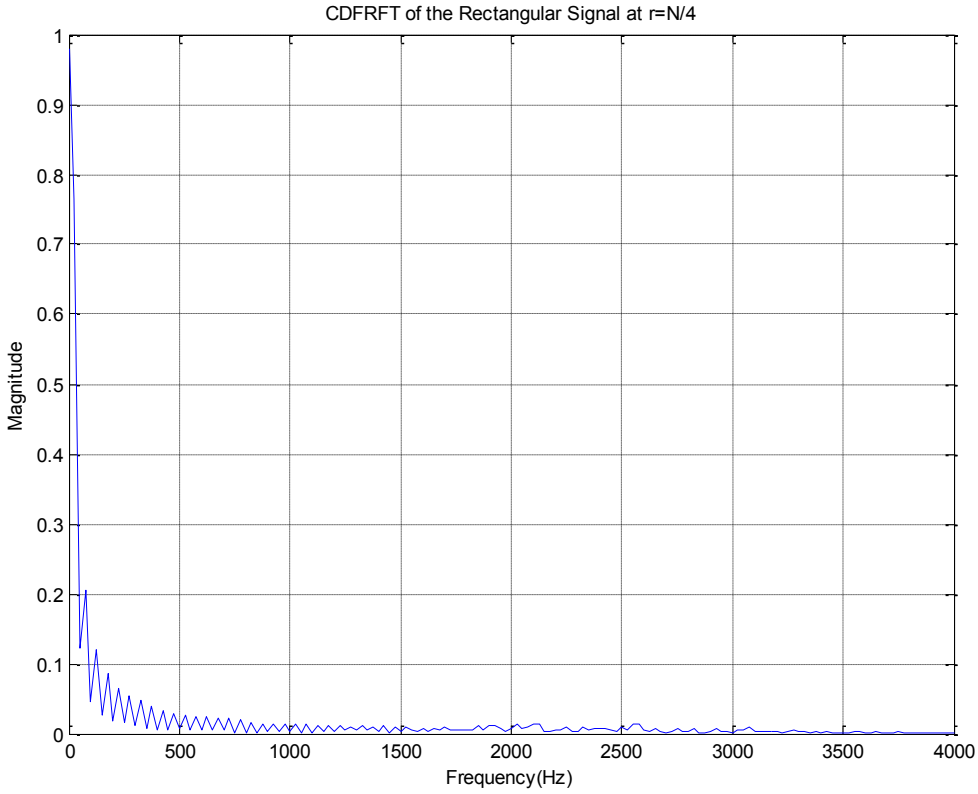

Fig. 23. CDFRFT at *r*=*N*/4 of the rectangular signal.

This time, CDFRFT has yielded better result than it has been applied on other basic signals. But the question that which algorithm should be exploited in the subsequent research, will be decided in the successive section.

So based on the processing results of these basic types of signals, there is a primary observation that CDFRFT cannot give a highly precise performance, if compared with that of DFRFT.

D. Comparison between DFRFT and CDFRFT

DFRFT uses the eigenvectors of the Hermite-Gaussians as its eigenvectors and have a similar eigen-decomposition form with the CFRFT kernel. And this eigen-decompostion method has been proved and justified in [8]. CDFRFT also holds this similar eigen-decomposition form, which makes it easier to understand the similarities of DFRFT and CDFRFT.

Both of DFRFT and CDFRFT have two main facets to be considered in the computation process:

a) Computation of the eigenvectors, which is a one-time task for a given matrix size N, and

b) Computation of the transform itself.

The origins of the generation of the DFRFT and CDFRFT algorithms are the same, but still, they also have some differences from each other, and the most important one is that CDFRFT is based on the Grünbaum's tridiagonal matrix T as a commuting matrix, while DFRFT exploits the Harper matrix S which is not strictly tridiagonal but could be

transformed into a tridiagonal matrix with employment of the matrix P, as the commuting matrix. Both T and S commute with the DFT matrix F, but their mathematical expressions are totally different. It is amazing that 64ommuters in totally distinct forms can yield similar computation results.

E. Comparison between FRFT and FT

In very simple terms, FRFT is a generalization of the ordinary FT. But further, the ordinary FT decomposes signals by sinusoids, whereas the FRFT is a decomposition of signals by chirps. Hence this essential principle makes FT the ideal tool for processing sinusoids and signals comprised by harmonics, while FRFT a favorable option when it comes to processing chirp signals, which will be defined and elaborated in the next chapter.

To be more specific, FRFT has implemented the so-called parameter a which acts on the FT operator as the transform order of FRFT. Or put differently, the a-th order FRFT stands for the a-th power of FT operator. As stated in previous sections, for a=0, the initial input signal will be obtained; It has also been proved that FRFT will be reduced to traditional FT when a=1 in the former section of CFRFT; And any intermediate value of a ($0 < a < 1$) will develop a new representation which is actually the rotated TFR of the initial signal.

What is more is that FRFT is not a time-invariant transformation as a comparison with the conventional FT, which means that the transformed signal still contains time information, or rather, FRFT contains both information of time and frequency. This

feature offers the advantage of extracting time information directly from the transformed domain without having to invert the transform result back to the initial domain. And this is also why the inversed FRFT is not a research interest in this thesis.

It has been testified in lots of cases, FRFT exceeds the regular FFT method in signal detection and time-frequency analysis, especially on the occasions when tremendous variations occur in the signal's frequency content and the chirp rate.

CHAPTER III

MULTI-COMPONENT FM SIGNAL PROCESSING WITH MA-DFRFT, MA-CDFRFT, SLANTED SPECTRUM AND SBSS

A. Introduction to the FM signals

It's been discussed in previous chapters that FRFT has been greatly exploited in FM signal processing.

FM signal processing is frequently confronted with in the DSP area and has incurred appreciable interest in the community. The chirp signal, as a special kind of FM signals, should be regarded as a natural physical phenomenon which exists in many areas, for example, gravity waves, seismography, and bats navigation systems, but it is mostly renowned from its use in signal processing fields like radar and sonar.

As already mentioned in the previous chapter, chirp signal is also referred to as linear frequency modulation (LFM) signal, which denotes the signal with linearly varying frequency.

B. Introduction to the Multi-component Chirp Signal

A multi-component chirp signal, or multi-component LFM signal could be modeled as:

$$x(t) = \sum_{i=1}^{N} A_i e^{j\phi} = \sum_{i=1}^{N} A_i e^{j2\pi(\frac{1}{2}\mu_i t^2 + f_i t + c_i)} \tag{3.1}$$

where N is the number of the components which comprise the chirp signal, and A_i is the signal component amplitude. Most interestingly, μ_i is the chirp rate (or variation rate of frequency) corresponding to the acceleration of a moving target which this chirp signal expression models, and different values of μ_i (i=1, 2,…, N) will introduce in distinct line spectra in different FRFD. f_i is the initial frequency (or center frequency) corresponding to the velocity of the moving target, and c_i is only a constant of the phase angle. By taking derivative of the phase angle ϕ (3.1), the instantaneous frequency of the chirp signal will be obtained as in (3.2):

$$\phi' = 2\pi(\mu_i t + f_i) \tag{3.2}$$

from which it could be seen that μ_i is indeed the variation rate of frequency.

C. Multi-angle Discrete Fractional Fourier Transform (MA-DFRFT)

The multi-angle version of DFRFT is the best approach to directly demonstrate the points at which the energy of different components of a complicated signal would get concentrated to the highest degree.

1. Introduction to MA-DFRFT

The reason that MA-DFRFT has been researched on is that when the different components of a complicated signal overlap spectrally or when one or two components are stronger than the others, the job of signal components separation and demodulation cannot be achieved with the existing algorithms.

However, as a 2D mapping of the 3D plot of a multi-angle version of DFRFT, with the *x*-axis representing a combination of the information in both time and frequency domains, *y*-axis representing the multi-values of transform order *a*, and *z*-axis representing the magnitudes of different DFRFT results at various values of *a*, MA-DFRFT is a proper tool for the component separation and demodulation of complicated signals.

Most importantly, the information of the optimum transform order a_{opt} could be obtained from the MA-DFRFT matrix, and based on the formula of the relationship between the optimum transform order and the chirp rate of the analyzed signal shown in (3.2), the intrinsic property of the signal, the corresponding optimum transform order of one component of the chirp signal, will be acquired with precision:

$$a = 2 - \frac{2}{\pi}\tan^{-1}\left(\frac{F_s^2 / N}{\mu}\right) \tag{3.3}$$

where F_s is the frequency at which the chirp signal gets sampled, and N is the total number of the samples.

So MA-DFRFT is the better tool to be adopted if the researched object is a signal with unknown chirp rates. By calculating the MA-DFRFT, even though the researched signal is a complicated one with several different components, the optimum transform order for each of them will be clearly shown in the MA-DFRFT plot, so there will be no need for trial-and-error procedures by using merely DFRFT to find the proper parameter *a* to concentrate the signal energy.

2. Chirp Signal Processed with MA-DFRFT

a. Single-component chirp

Given a single-component chirp (FM signal) $x(t) = e^{j(\omega t + c_r t^2)}$ where the initial angular frequency $\omega = 1000 rad/s$, and the angular chirp rate $c_r = 15000 rad/s^2$, and the sampling frequency is *Fs*=8000Hz.

Compared with (3.1) and (3.2), the initial frequency $f = \omega/(2\pi) \approx 159.15 Hz$, and the chirp rate $\mu = 2c_r/(2\pi) = c_r/\pi \approx 4774.65 Hz/s$.

The time-domain plot of this single-component chirp signal is shown in Fig. 24：

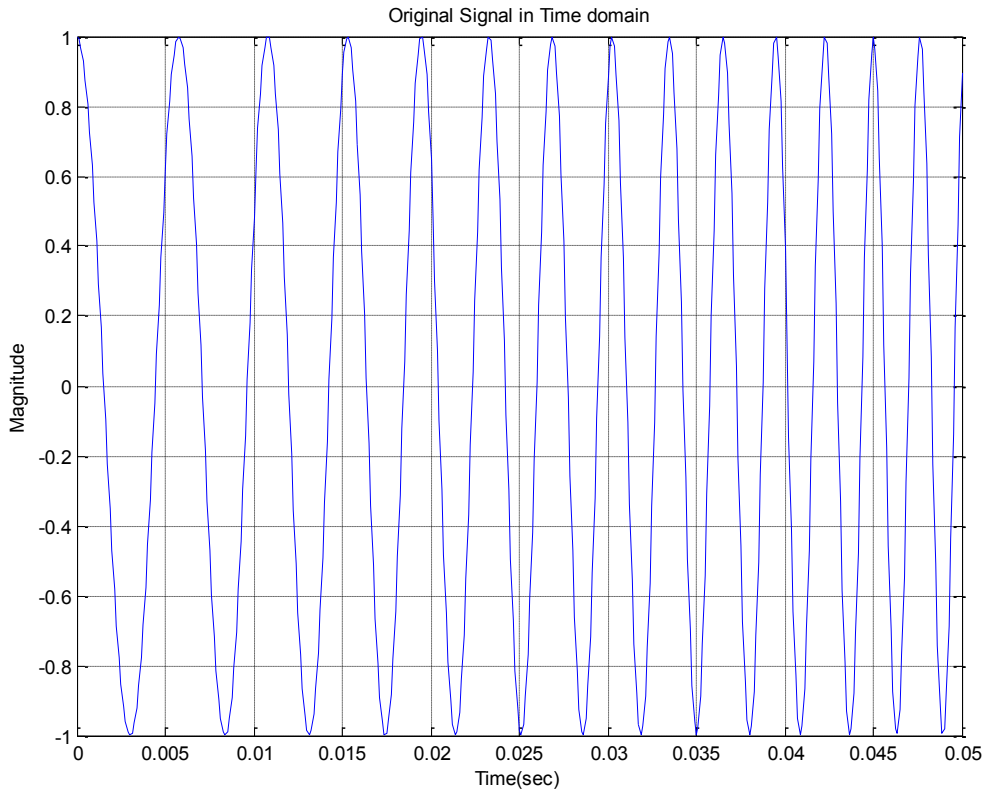

Fig. 24. Plot of a single-component chirp in time domain.

And then the MA-DFRFT result follows as in Fig. 25:

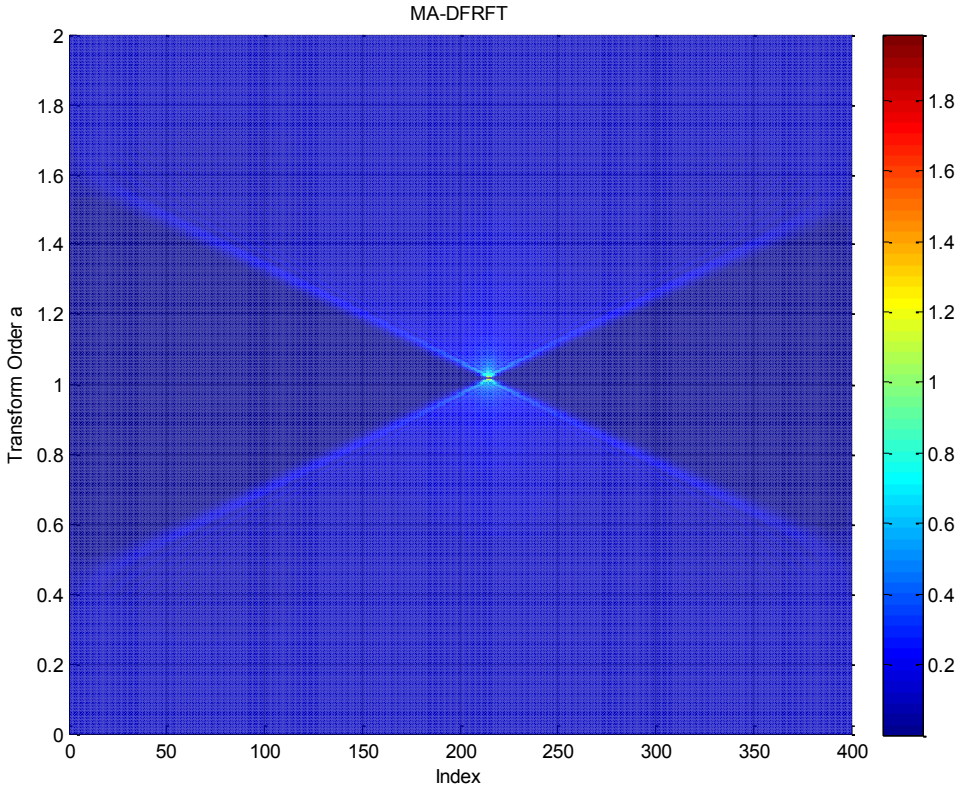

Fig. 25. MA-DFRFT plot of a single-component chirp.

Just by observation, it is difficult to determine the position of the energy-concentration point from Fig. 25, so the horizontal a=1 line is added in Fig. 26:

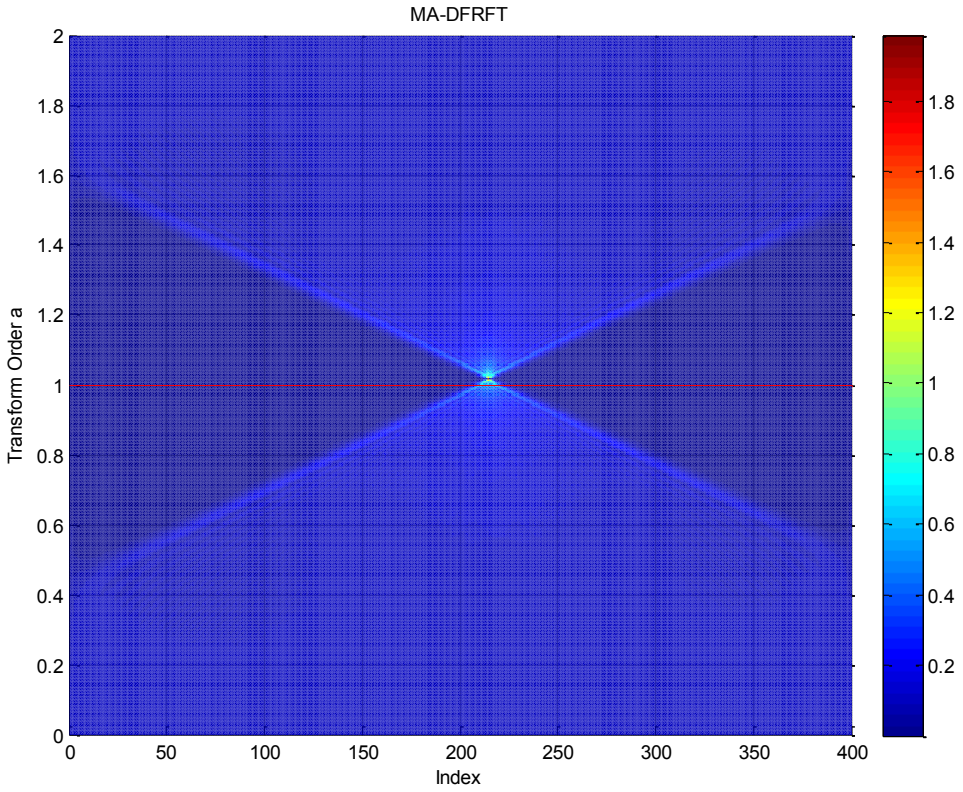

Fig. 26. MA-DFRFT of a single-component chirp with the a=1 line.

So from Fig. 26 above, it is obvious that the energy-concentration point lies above the a=1 line, which is because the chirp rate has a positive value.

Calculated directly from the MA-DFRFT matrix already obtained from the algorithms of MA-DFRFT, the energy-concentration point above the a=1 line has a corresponding transform order a=1.020. If calculated from the formula given by (3.3), the optimum transform order for this single-component chirp signal can also be obtained: a=1.019. So it could be seen that the simulation result almost matches with the empirical formula in (3.3), and the absolute error is only 0.001.

On the contrary, if the chirp rate has a negative value, the energy-concentration point will move to the position beneath the a=1 line, as shown in Fig. 27 below:

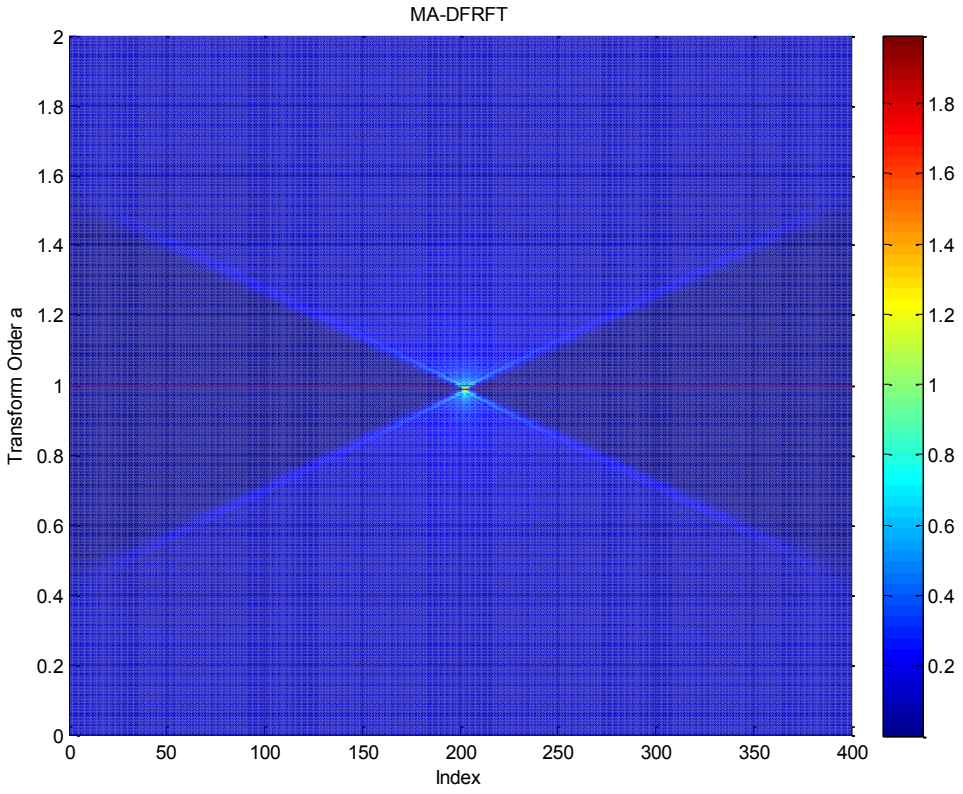

Fig. 27. MA-DFRFT of a single-component chirp with negative chirp rate.

The relative positions of the energy-concentration point and the a=1 line is dependent on the chirp rate itself, because any component of a chirp signal with a given chirp rate has its corresponding optimum transform order a_{opt}, which can be calculated

from (3.3). And it should be noted that if the chirp rate has a negative value, then (3.4) should replace (3.3):

$$a = \frac{2}{\pi}\tan^{-1}\left(\frac{F_s^2 / N}{\mu}\right) \tag{3.4}$$

Another issue which is worth noticing is the *x*-coordinate of the energy-concentration point. The label for the *x*-axis of the MA-DFRFT plot has been set to be "Index" as in Fig. 25-27, and whether it refers to time or frequency should be assessed according to the following map which shows the criterion aiding with the interpretation of the *x*-axis of MA-DFRFT:

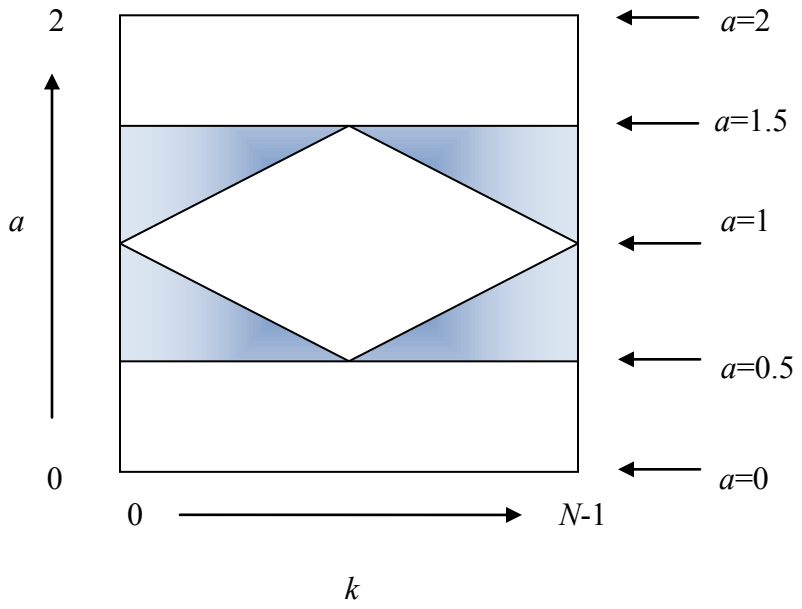

Fig. 28. Map of the *a*=[0,2] region where index *k* should be interpreted as time or frequency in the MA-DFRFT matrix $X_a[k]$.

In Fig. 28, within all the white regions, including the white diamond region in the middle, the upper and the lower rectangular regions of the map, *k* should be interpreted as time; meanwhile, for $X_a[k]$ falling into the blue shade outside the regions mentioned above, the interpretation of *k* is frequency [6].

b. Multi-component chirp

Given the input signal, a chirp signal with 3 components:

$$x(t) = \sum_{k=1}^{3} e^{j(\omega_k t + c_{r_k} t^2)} = \sum_{k=1}^{3} e^{j(\omega_1 kt + c_{r_1} kt^2)}$$

where the fundamental initial angular frequency is $\omega_1 = 1000 rad/s$, the fundamental angular chirp rate is $c_1 = 15000 rad/s^2$, and still with the sampling frequency to be *Fs*=8000Hz.

Obviously, the components are harmonically related with each other, and this is also why a slant line that will be introduced in the following of this section could solve the resolution problem.

The time-domain plot of the input chirp is shown in Fig. 29:

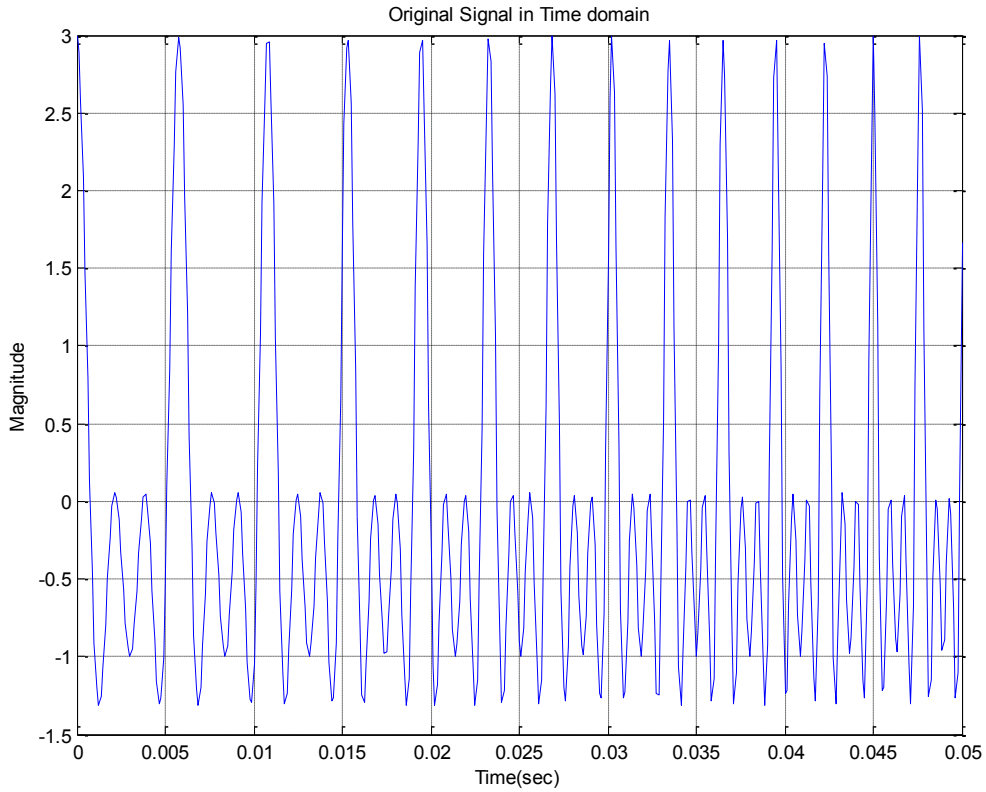

Fig. 29. Plot of a multi-component chirp in time domain.

Merely observed from the plot of this multi-component chirp from Fig. 29, it could be seen that the frequency of the signal is increasing over time, but no further information can be extracted from this time-domain plot.

And the 2-D mapping of the 3-D surface plot of the MA-DFRFT is shown in Fig. 30:

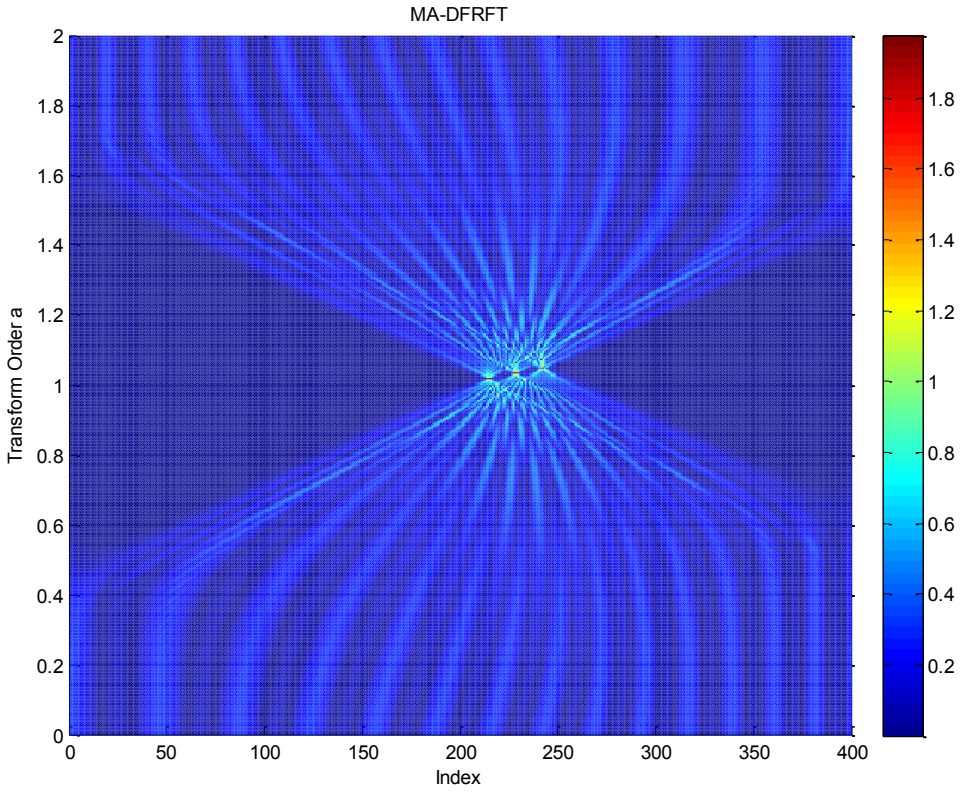

Fig. 30. MA-DFRFT plot of a multi-component chirp.

It could be seen that the 3 components of this complicated chirp signal are distinguished without ambiguity. The 3 different optimum transform orders corresponding to the 3 different components can be obtained directly either from the calculated MA-DFRFT matrix or the empirical formula in (3.3), and the relative positions of the 3 energy-concentration points and the a=1 line is given by Fig. 31.

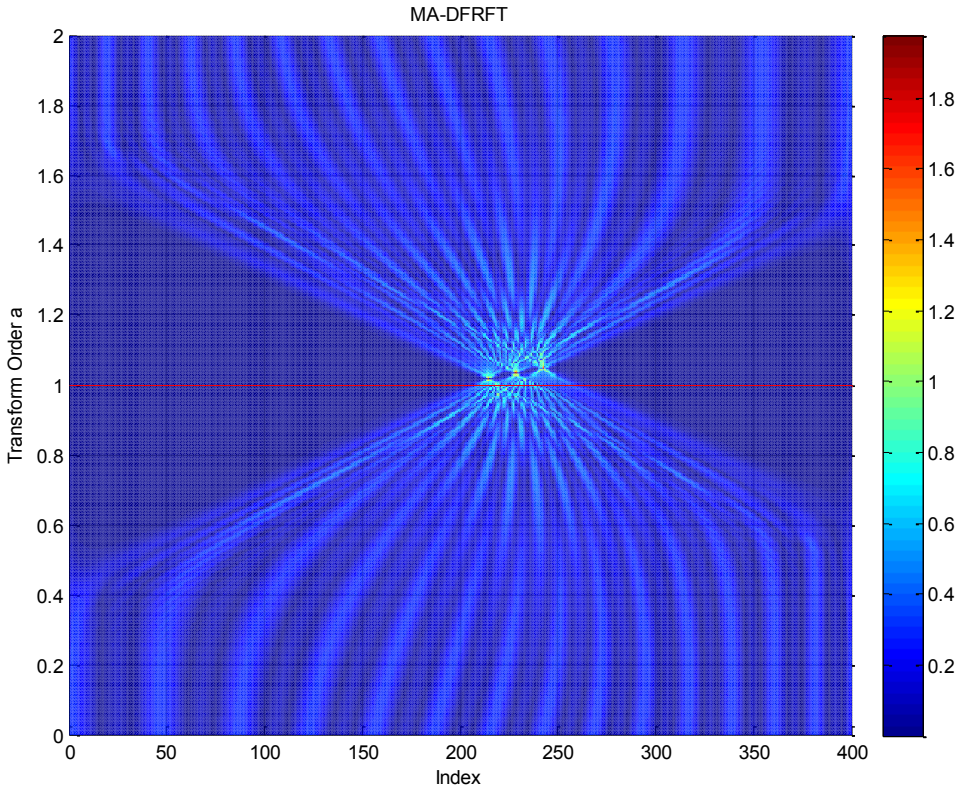

Fig. 31. MA-DFRFT of a multi-component chirp with the *a*=1 line.

The 3 optimum transform orders are:

$a_1 = 1.019$

$a_2 = 1.038$

$a_3 = 1.057$

D. Multi-angle Centered Discrete Fractional Fourier Transform (MA-CDFRFT) & Performance Comparison with MA-DFRFT

1. MA-CDFRFT

Compared with the continuous transform order *a* from 0 to 2 being the *y*-axis of MA-DFRFT, if a discrete set of the rotation angles is given by

$$\alpha = \alpha_r = \frac{2\pi r}{N} \tag{3.5}$$

which is also to say that a discrete set of transform orders is given by

$$a = a_r = \frac{4r}{N} \tag{3.6}$$

where the discrete $r = 0,1,...,N-1$ is employed, the following matrix of $X_r[k]$ will be obtained taking the place of the $X_a[k]$ of MA-DFRFT:

$$X_r[k] = \sum_{p=0}^{N-1} v_{kp} \sum_{n=0}^{N-1} x[n] v_{np} e^{-j\frac{2\pi}{N}pr} \tag{3.7}$$

Defining $z_k[p]$ as

$$z_k[p] = v_{kp} \sum_{n=0}^{N-1} x[n] v_{np} \tag{3.8}$$

Based on the renowned DFT expression, it could be observed that (3.7) can be expressed in the form of DFT of $z_k[p]$:

$$X_k[r] = \sum_{p=0}^{N-1} z_k[p] W_N^{pr} \tag{3.9}$$

where $0 \le r,k \le N-1$, and $W_N^{pr} = e^{-j\frac{2\pi}{N}pr}$.

It may have been noticed that the subscript and index of (3.7) have been interchanged to be shown in (3.9) to highlight the feature of this computation process: each iteration of the DFT computation will induce the *k*-th element of the CDFRFT for the whole set of transform orders α_r as given in (3.5). The resulting transform $X_k[r]$ containing the CDFRFT for these discrete angles is called the *multi-angle* CDFRFT (MA-CDFRFT), just like the *multi-angle* DFRFT.

Expressing this new multi-angle transform as a DFT computation facilitates the use of the regular FFT algorithm to efficiently calculate MA-CDFRFT, a transform with a full set of evenly distributed angles. This step has greatly reduced the computational cost of MA-CDFRFT from $O(N^3)$, i.e., the case for direct computation using N matrix multiplications, to $O(N^2 \log_2 N)$,when using the radix-2 FFT algorithms with $N = 2^v$.

As a high level resemblance of MA-DFRFT, the MA-CDFRFT is also a matrix, as already denoted: $X_k[r]$. Similar with MA-DFRFT, MA-CDFRFT is also a 2D mapping of the 3D demonstration in which time and frequency share the same axis (index *k*), and whether the index *k* should be interpreted as time or frequency depends upon the value of α, or more directly, the parameter *r*.

It can be observed with ease that $X_k[0]$ will be reduced to the original signal $x[n]$ under research if setting $k=n$, and $X_k[N/4]$ will match with the CDFT of $x[n]$ with N being a multiple of 4, since in this case we have $r=N/4$ so $\alpha_{N/4} = \pi/2$.

To better illustrate the regions where the index *k* should be interpreted as time or frequency like Fig. 28 introduced for MA-DFRFT, Fig. 32 will be likewise introduced to show the map of the $X_k[r]$ matrix to illustrate how index *k* has different interpretations based on the variation of the value of the parameter *r*.

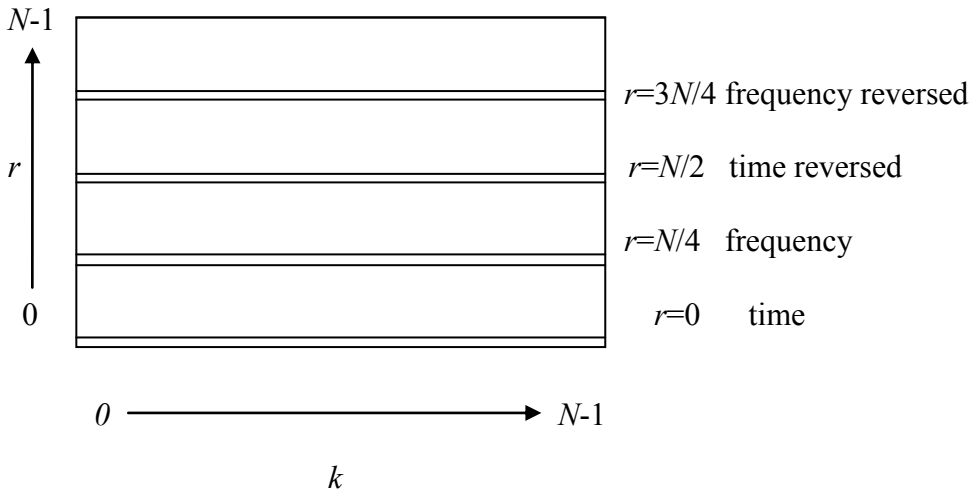

Fig. 32. Map of the *r*=[0,N] region where index *k* should be interpreted as time or frequency in the MA-CDFRFT matrix $X_k[r]$.

As shown in Fig. 32 above, at *r*=0, *k* corresponds to time; and at *r*=*N*/4, *k* should be interpreted as frequency. It could also be deduced from this graphical representation that the upper half of $X_k[r]$ is a reversed version of the lower half, since in this case the region of *r*=[*N*/2,*N*] is a mirror of the region *r*=[0,*N*/2], just like the *a*=[2,4] region is a reversed version of the *a*=[0,2] region in the case of MA-DFRFT.

It will be demonstrated in Fig. 33 of the next section that the MA-CDFRFT of a single-component chirp signal will show two energy-concentration points, located

respectively in the lower half and the upper half of $X_k[r]$. If the signal has no chirp rate, or simply put in this way, the frequency of the input signal is invariable with time, the energy concentration points will be located exactly at the rows of r=N/4, 3N/4 which correspond with the rotation angles at $\alpha = 90°,270°$. And at these two critical angles, CDFRFT will be reduced to the centered DFT (CDFT), and its inverse correspondingly. It should be mentioned that very similar to the case of MA-DFRFT, in a MA-CDFRFT plot, signal with a non-zero chirp rate will yield energy-concentration points at rotation angles of CDFRFT different than $90°$ and $270°$, and whether their locations are above or below those critical values relies on the chirp rate of the signal.

2. Chirp Signal Processed with Both MA-CDFRFT & MA-DFRFT

As a counterpart of MA-DFRFT, a comparison of the performances of both of these two 3-D demonstrations will be made in this section to determine which one provides higher resolution and will be employed in the subsequent research.

The complicated chirp signal with 3 components which are researched on in the previous part of MA-DFRFT is still the main research object:

$$x[n] = \sum_{k=1}^{3} e^{j(\omega_k n + c_{rk}(n-\frac{N-1}{2})^2)} = \sum_{k=1}^{3} e^{j(\omega_1 kn + c_{r1}k(n-\frac{N-1}{2})^2)}$$

where fundamental initial angular frequency is $\omega_1 = 0.5 rad/s$, and the fundamental angular chirp rate $c_{r1} = 0.001 rad/s^2$, and N=128 (the length of the signal is better to be a power of 2 in order to use MA-CDFRFT).

3 different algorithms from the available literatures have been researched on for the computation of MA-CDFRFT, and the main difference among those algorithms lies in that the Grünbaum's tridiagonal commuting matrix takes different expressions. So the 3 different versions of MA-CDFRFT are demonstrated as in the following sections:

a. MA-CDFRFT result based on the algorithm given by [9]:

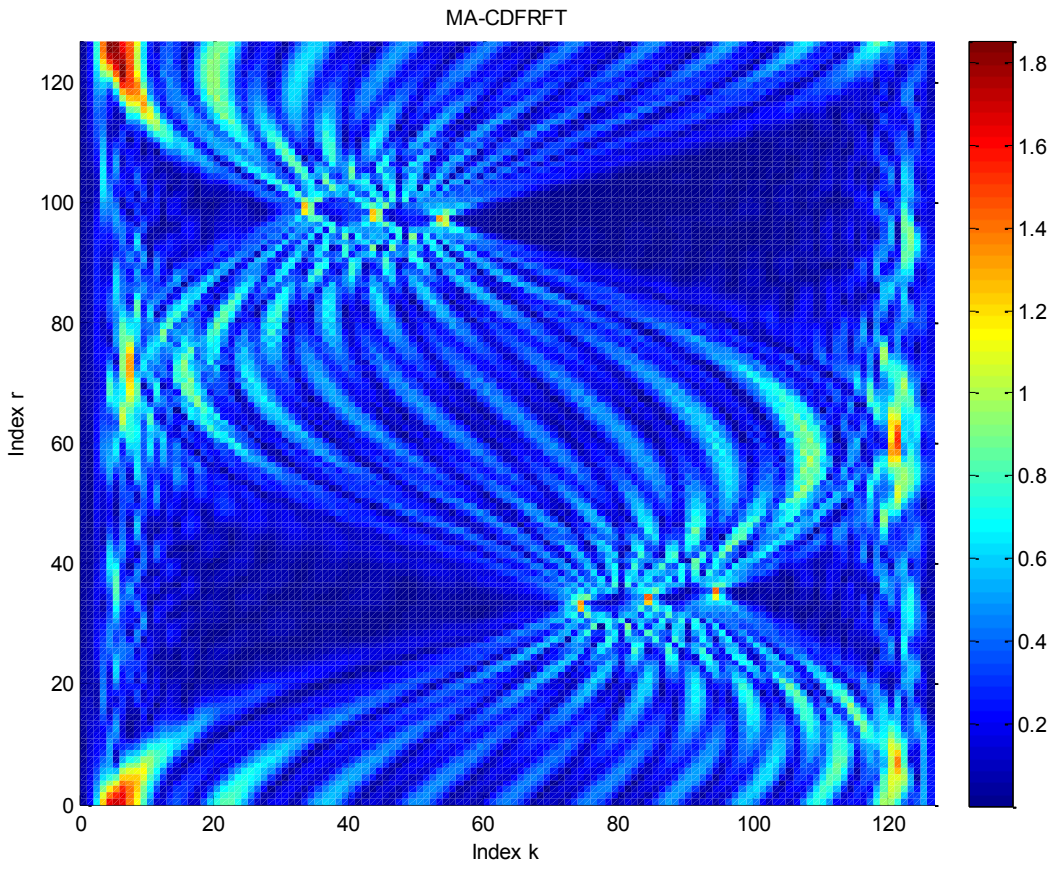

Fig. 33. MA-CDFRFT of a multi-component chirp signal based on [9].

To speak about the overall performance, Fig. 33 above has explicitly demonstrated that the MA-CDFRFT algorithm which is based on the Grünbaum tridiagonal commuting matrix in a form proposed by [9] could provide relatively satisfactory resolution around the energy-concentration points, but when index k is near 0 and N, this MA-CDFRFT algorithm fails to give stabilized continuous high resolution. This kind of failure will bring in huge errors in the subsequent work on the other derivatives, such as Slanted Spectrum and SBSS.

b. MA-CDFRFT result based on the algorithm given by [10]:

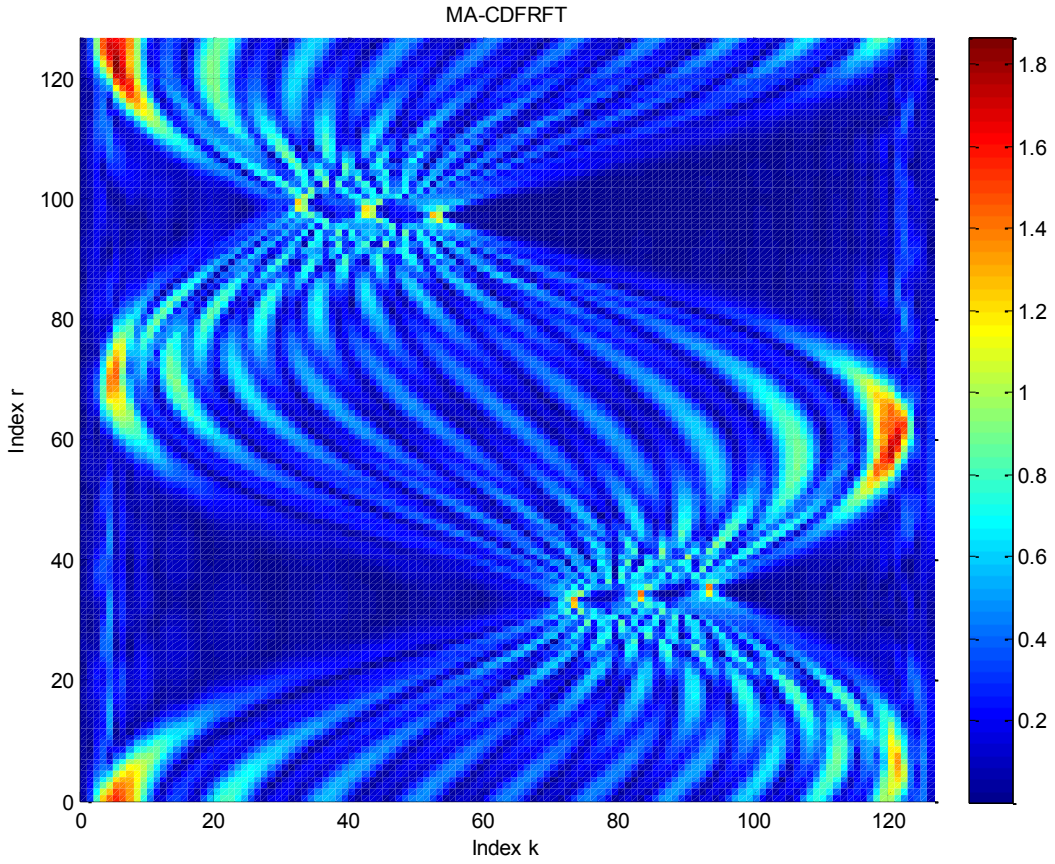

Fig. 34. MA-CDFRFT of a multi-component chirp signal based on [10].

Compared with Fig. 33, Fig. 34 has indicated higher resolution even around the locations near k=0 and N. Actually the Grünbaum's tridiagonal commuting matrix given by [10] is even simpler than that given by [9]:

$$G = \begin{bmatrix} a_0 & b_0 & & & & \\ b_0 & a_1 & b_1 & & & \\ & b_1 & \cdots & \cdots & & \\ & & \cdots & \cdots & b_{N-1} & \\ & & & b_{N-1} & a_{N-2} & b_{N-2} \\ & & & & b_{N-2} & a_{N-1} \end{bmatrix} \tag{3.10}$$

where $a_n = -2\cos(\pi n\tau)\sin(\pi n\tau)\sin(\pi(N-n-1)\tau)$, $b_n = \sin(\pi n\tau)\sin(\pi(N-n)\tau)$ and $\tau = 1/(Nd^2)$. Normally the dilation parameter *d* is set to 1.

And slightly different from (3.10), the Grünbaum's tridiagonal commuting matrix given by [10] offers higher resolution in the MA-CDFRFT plot:

$$G = \begin{bmatrix} a_1 & b_1 & & & & \\ b_1 & a_2 & b_2 & & & \\ & b_2 & \cdots & \cdots & & \\ & & \cdots & \cdots & b_{N-2} & \\ & & & b_{N-2} & a_{N-1} & b_{N-1} \\ & & & & b_{N-1} & a_N \end{bmatrix} \tag{3.11}$$

where $a_n = \cos(\pi / N) - \cos(2\pi(n + \frac{1}{2}) / N), 1 \le n \le N$, $b_n = \sin^2(\pi n / N), 1 \le n \le N-1$.

Both forms of *G* are real symmetric matrices, and their eigenvectors are real and orthogonal.

So it could be concluded that a simpler form of the Grünbaum's tridiagonal commuting matrix could even bring forth higher resolution in MA-CDFRFT plot.

c. MA-CDFRFT result based on [24]

The MA-CDFRFT result based on [24] is shown in Fig. 35 below:

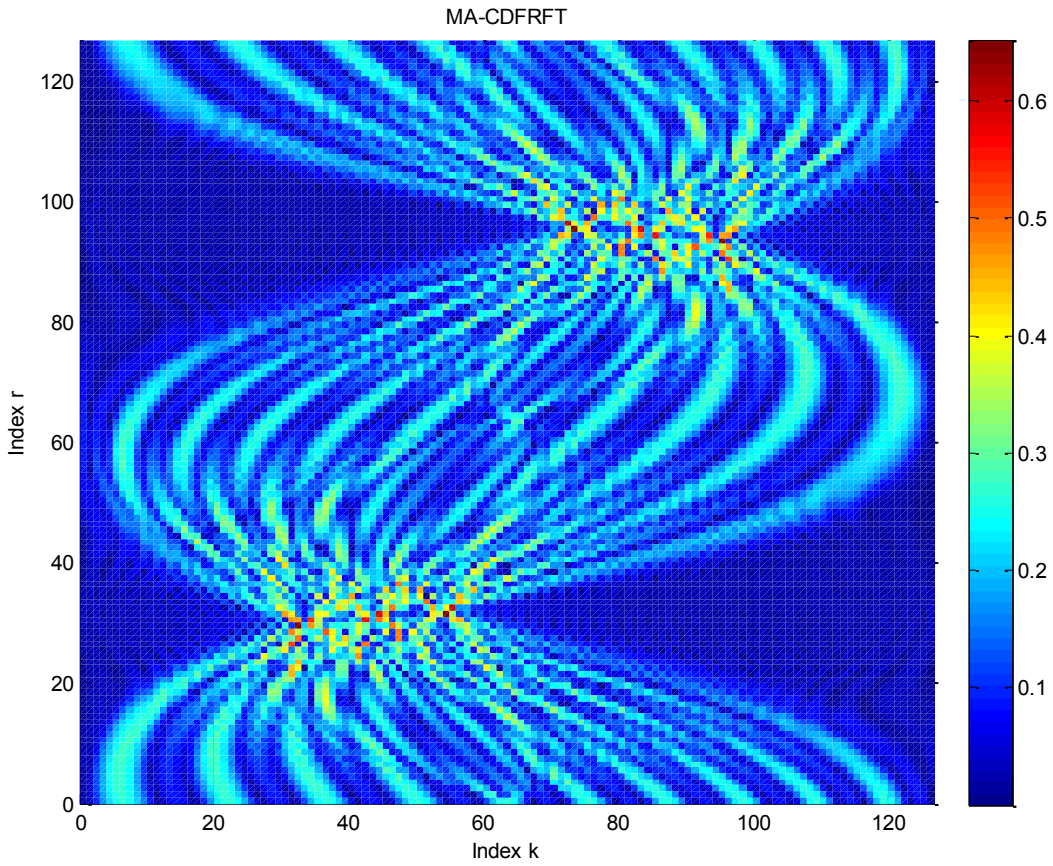

Fig. 35. MA-CDFRFT of a multi-component chirp signal based on [24].

So this demonstration shows that the algorithm of MA-CDFRFT based on [24] fails to provide satisfactory resolution even at the locations of the energy-concentration points, and the plot has a reversed alignment compared with the previous two figures derived from the MA-CDFRFT algorithms based on [9] and [10].

d. As a comparison, the MA-DFRFT based on [3]:

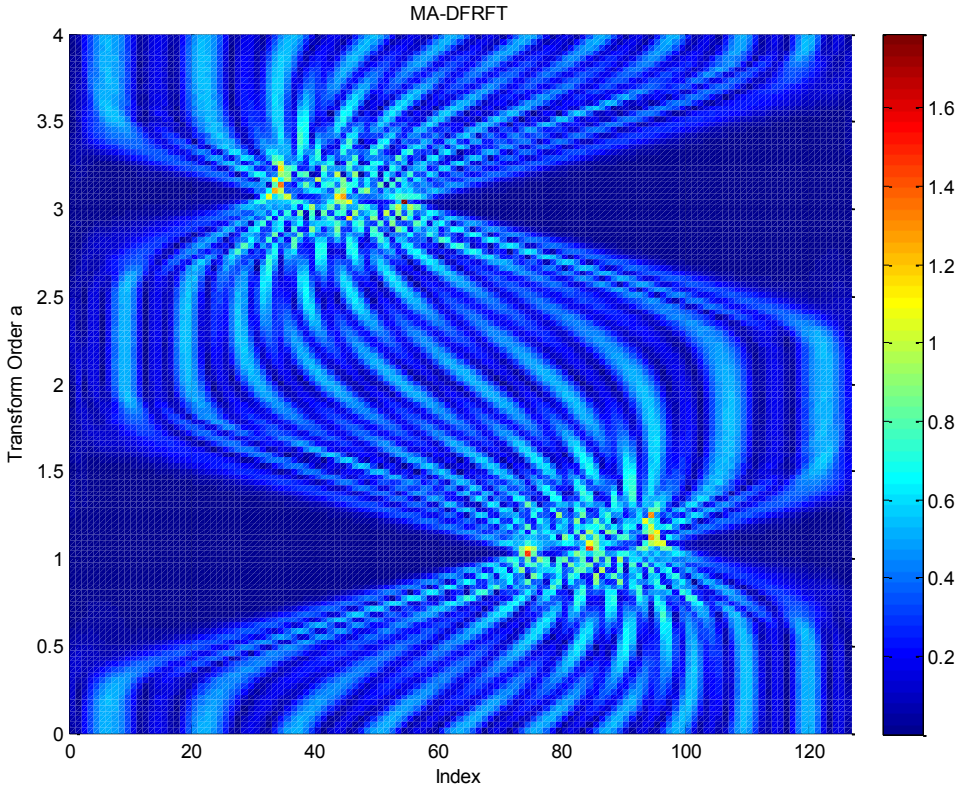

Fig. 36. MA-DFRFT of a multi-component chirp signal based on [3].

It can be easily observed from Fig. 36 that MA-DFRFT has outperformed all the 3 versions of MA-CDFRFT above in that the energy-concentration points are easier to spot from the demonstration, and there is no high energy regions shown in the red color like in Fig. 33 - Fig. 34 around the critical locations of k=0 and N. So these positive features of MA-DFRFT and the unsatisfactory performances of all the 3 versions of MA-

CDFRFT are the strong support for the final decision of picking MA-DFRFT as the basis for further development on the other DFRFT derivatives.

E. Slanted Spectrum

1. Introduction to Slanted Spectrum

A much more complicated case mentioned in the previous section is that when the chirp signal under research is a multi-component one, using the single-dimension DFRFT is not enough for the best processing quality, because different components that comprise the chirp signal may have respectively various chirp rates which require different transform orders to concentrate each of them to a single independent pulse signal in the DFRFT plot.

And Slanted Spectrum is an innovative tool generalized from both DFRFT and MA-DFRFT, and it is best for multi-component signal processing.

The line going through the energy-concentration points in the MA-DFRFT plot of an unknown multi-component signal also has to pass the central point of the MA-DFRFT plot. By calculating the coordinates of one specific energy-concentration point, and wrapping up with the coordinate information of the central point: $[k, a] = [N/2, 1]$, an equation of a line could be obtained. And this line is exactly the slant line to seek for to calculate the Slanted Spectrum.

In succession, there will actually be slant lines with exactly the same number of the total components comprising the chirp signal appearing in the MA-DFRFT demonstration. If the components of the chirp signal are harmonically related, then the

slight difference in the slopes of the slant lines can be neglected, and MA-DFRFT will be retaken align this artificially determined universal slant line, which is to say, a new MA-DFRFT matrix will be generated within a much more confined range than the original k=[0,N-1] and a=[0,2] range.

Furthermore, it should be noted that Slanted Spectrum is comparable to DFRFT in that they are both a 2-D representation with the index k being the x-axis, and magnitude being the y-axis. So the acquisition of a new MA-DFRFT matrix in a more confined range is just a prerequisite of obtaining the Slanted Spectrum, which actually comes from the diagonal elements of the new MA-DFRFT matrix.

In the following section it is going to elaborate on the generation of Slanted Spectrum with the utilization of the multi-component chirp signal which was employed in the previous section of MA-DFRFT.

2. Slanted Spectrum Applied on a Multi-component Chirp Signal

The 3-component chirp signal model will be exploited in this section again to show the acquisition of Slanted Spectrum:

$$x(t) = \sum_{k=1}^{3} e^{j(\omega_k t + c_{r_k} t^2)} = \sum_{k=1}^{3} e^{j(\omega_1 kt + c_{r1} kt^2)}$$

where the fundamental initial angular frequency is $\omega_1 = 1000 rad/s$, the fundamental angular chirp rate is $c_1 = 15000 rad/s^2$, and still with the sampling frequency to be Fs=8000Hz.

It is simple to understand that Slanted Spectrum taken along the horizontal a=1 line going across the center of the MA-DFRFT plot (the red line shown in Fig. 31), equals with directly taking DFT of the input signal. And the result is shown in Fig. 37:

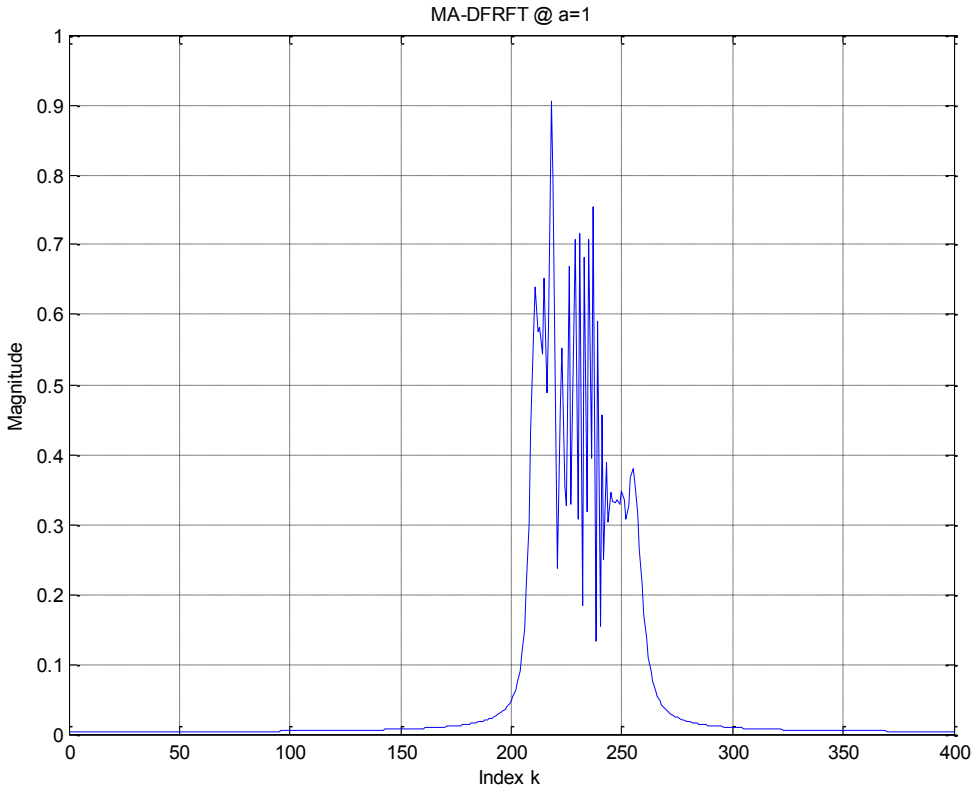

Fig. 37. Slanted Spectrum along the horizontal a=1 line.

Where it is observable that the x-axis of Slanted Spectrum matches with that of the MA-DFRFT plot in Fig. 31, since Slanted Spectrum should be understood as a slice of the MA-DFRFT matrix obtained along a certain line, which in this specific case, is exactly

the a=1 line. But this slice is not sharp enough to provide with the information such as the precise positions of the 3 components of the chirp signal in any domain.

So there is a high demand for introducing the new slant line along which a sharp enough slice will be obtained to give higher resolution to distinguish all the components contained in a complicated chirp signal.

In this case of 3-component chirp signal, the 3 energy-concentration points of the MA-DFRFT matrix will be sought first, and based on the slant line equation inspired by [6], all the 3 slant lines will be obtained with the knowledge of the coordinates of the 3 energy-concentration points with the brightest color in the MA-DFRFT plot: $[k_{opt1}, a_{opt1}]$, $[k_{opt2}, a_{opt2}]$ and $[k_{opt3}, a_{opt3}]$. And it has been discussed above that the slant line shall pass the center point of the MA-DFRFT plot: [k, a] = [N/2, 1], so the equations of all the 3 slant lines where the 3 energy-concentration points and the center point are aligned respectively will be obtained as in (3.12) where k=1,2,3 and corresponds to the number of components in the researched signal:

$$a = \frac{a_{optk} - 1}{k_{optk} - (N-1)/2} * (k - (N-1)/2) + 1 \tag{3.12}$$

and subsequently they will also be presented in the MA-DFRFT demonstration in different colors as in Fig. 38:

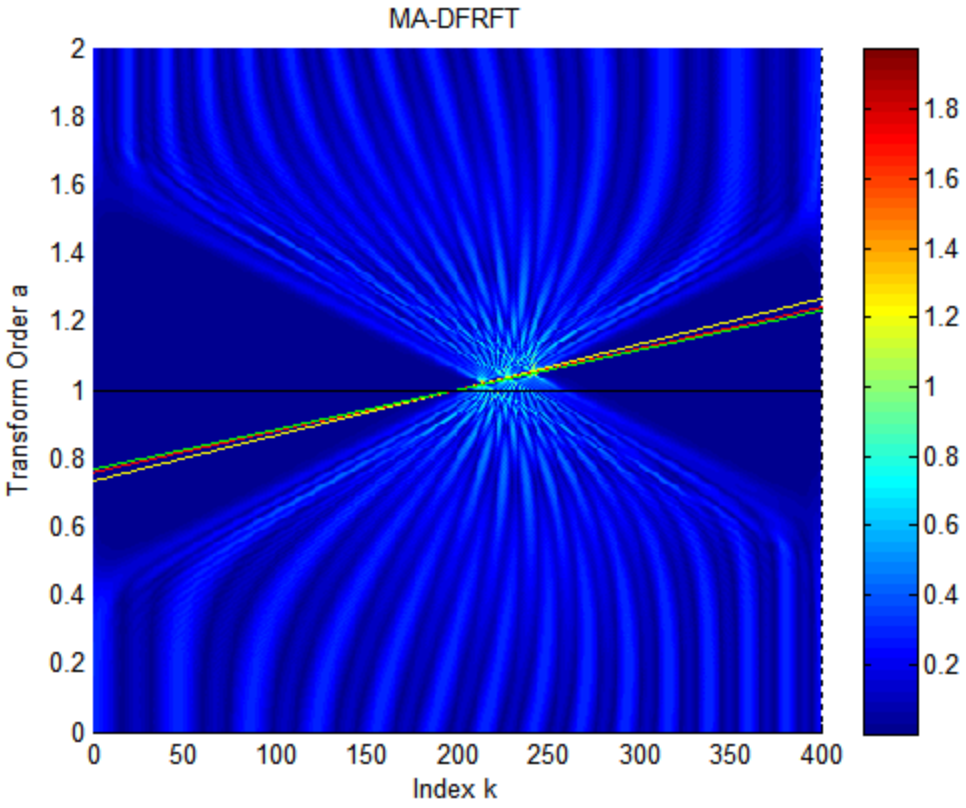

Fig. 38. MA-DFRFT with the 3 slant lines in different colors corresponding to the 3 components of a chirp signal.

In Fig. 38 above, the yellow slant line is in correspondence with the 1st component with the fundamental initial angular frequency of $\omega_1 = 1000 rad/s$, and the fundamental angular chirp rate of $c_1 = 15000 rad/s^2$; the red slant line in between of the yellow and green slant lines is the one which passes the 2nd energy-concentration point which represents the 2nd component of the chirp signal with an initial angular frequency and angular chirp rate twice the value of the 1st component; and the green slant line corresponds to the 3rd component of the chirp signal, with both tripled initial angular frequency and angular chirp rate. It is also worth mentioning that the color of the

horizontal a=1 line has been changed into black to avoid confusion with the red slant line for the 2nd component of the chirp signal.

It is noticeable that the three slant lines are located slightly differently in the MA-DFRFT demonstration given by Fig. due to their different slopes, so here's a question: along which slant line should the Slanted Spectrum of the chirp signal be taken?

As shown in Fig. 38, 3 different Slanted Spectrums have been taken along the 3 slant lines in yellow, red, and green colors respectively. And it is seen that the Slanted Spectrum in yellow has the ability to highlight the leftmost peak to the highest degree, owing to the fact that this Slanted Spectrum is taken along the yellow slant line, which is obtained from the leftmost energy-concentration point, so it is the most appropriate slant line along which the Slanted Spectrum for the 1st component of the chirp signal needs to be taken. It is similar that the Slanted Spectrum for the 2nd component of the chirp signal is best to be taken along the red slant line, and correspondingly, the Slanted Spectrum for the 3rd component should be computed along the green one. So Fig. 39 shows this procedure:

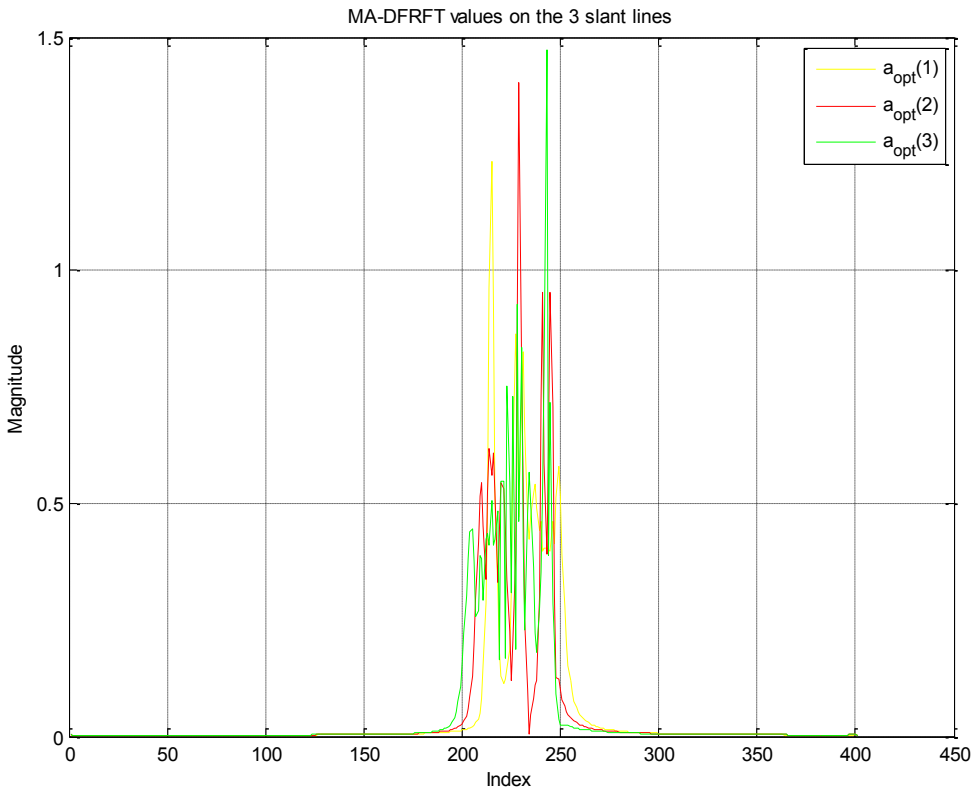

Fig. 39. Slanted Spectrum taken along the 3 different slant lines in 3 colors.

However, this assignment of different slant lines to different components of a complicated chirp signal has not completely and successfully solved the question raised above. When processing a complicated chirp signal with multiple components, if the number of computations of Slanted Spectrum equals with the number of the components, it is understandable that the computational cost will be too high.

The bright side is that the main target objective of this research on chirp signal is limited to types of chirp signals with harmonically related components. So the observation from demonstrated in Fig. that the 3 different slant lines shown in distinct

colors are almost overlapped with one another should be a key factor to take into consideration in order to solve this computation cost issue.

In this 3-component chirp signal case, the slant line in the middle with red color is a good option for taking an overall Slanted Spectrum of the chirp signal as an entirety, as shown in Fig. 40:

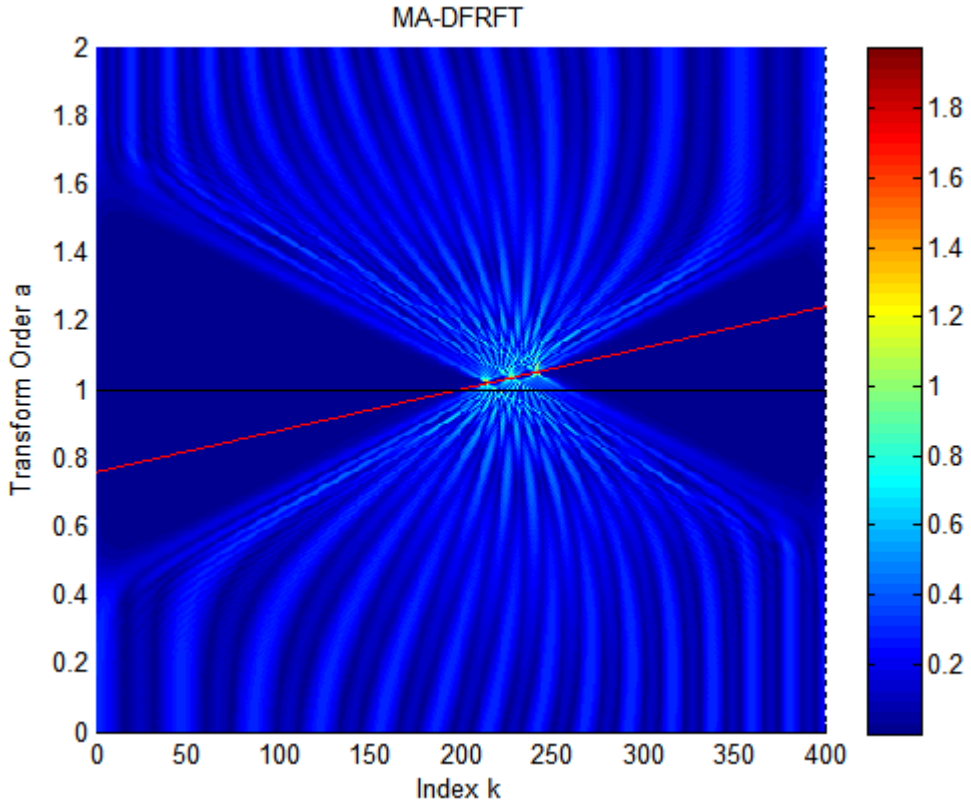

Fig. 40. The slant line in red color along which the Slanted Spectrum of the chirp signal as an entirety needs to be taken.

From Fig. 40 above, it is obvious that the red slant line passes the central point of the whole MA-DFRFT plot, and without any doubt, it has also passed all of the 3 energy-

concentration points. But whether this slant line will apply to the processing of all the 3 components of the chirp still requires a thorough check.

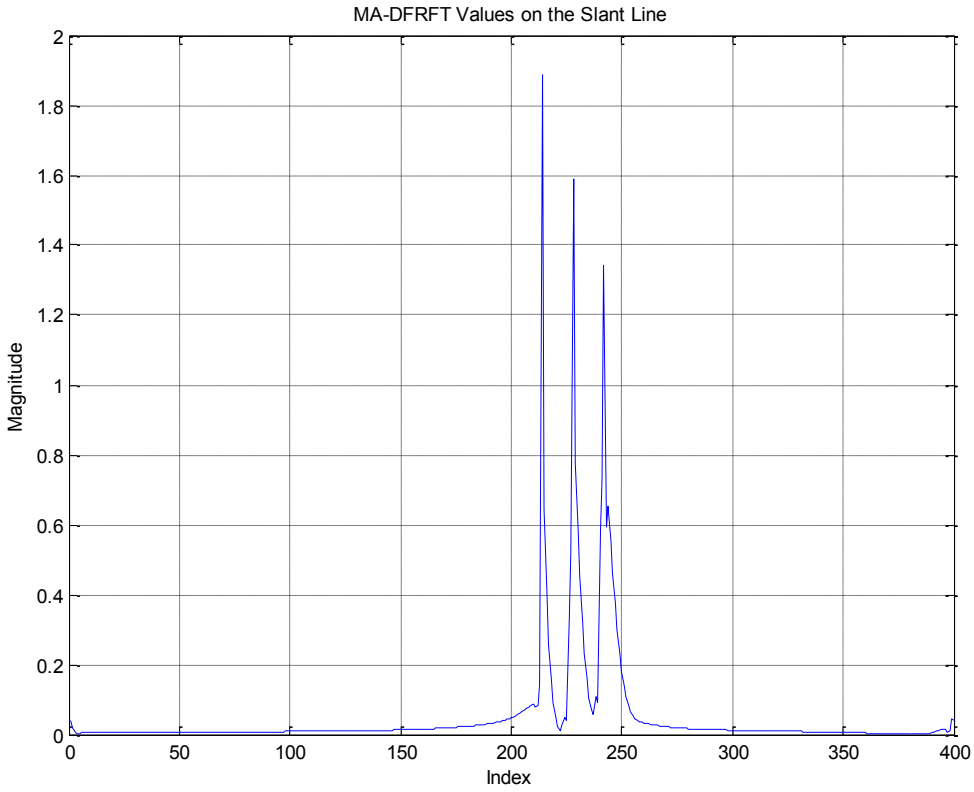

Fig. 41. Slanted Spectrum of the multi-component chirp signal taken along one single slant line.

Fig. 41 above shows much higher resolution when it comes to the distinguishing of the 3 components of the chirp signal, which means that the 3 peaks corresponding with the components could be distinguished without an effort now. And it is finally

demonstrated that the MA-DFRFT could decompose a chirp signal over the analysis frame into multiple energy-concentrated pulses.

Actually this plot shown by Fig. 41 is a successful case of Slanted Spectrum, which is also the basis of the concept of Spectrogram based on Slanted Spectrum (SBSS) introduced in the section in subsequence with the following one.

3. The Analysis of the Advantage of Slanted Spectrum over Traditional FFT

In this section, both FFT and DFRFT have been applied to two different kinds of input signal: a single-component chirp signal and a multi-component chirp signal, with the sampling frequency to be Fs=8000Hz.

a. Single-component chirp signal w/ constant magnitude (FM signal)

$$x(t) = e^{j(1000t+1500t^2)}$$

1) Its FFT result with the 10% plane above the noise floor shown in Fig. 42:

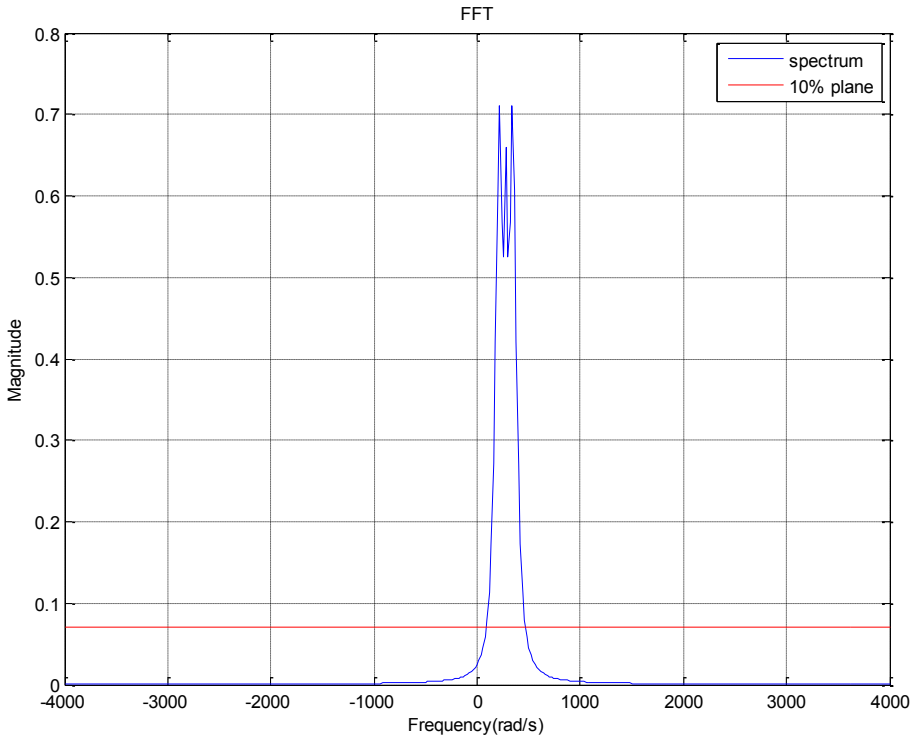

Fig. 42. FFT of a single-component chirp in frequency domain.

2) Slanted Spectrum result with the 10% plane above from the noise floor (based on MA-DFRFT) shown in Fig. 43:

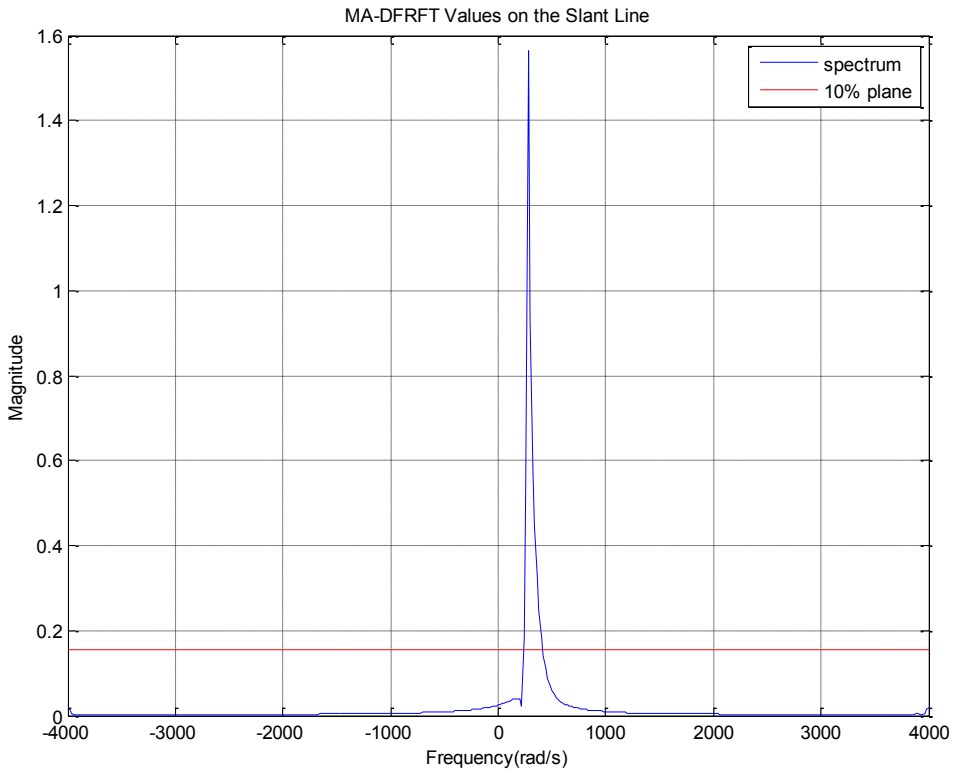

Fig. 43. MA-DFRFT of the single-component chirp in FRFD.

b. Multi-component chirp signal w/ equal constant magnitude (FM signal)

$$x(t) = \sum_{k=0}^{3} e^{j(1000kt+15000kt^2)}$$

1) FFT result with the 10% plane above from the noise floor shown in Fig. 44:

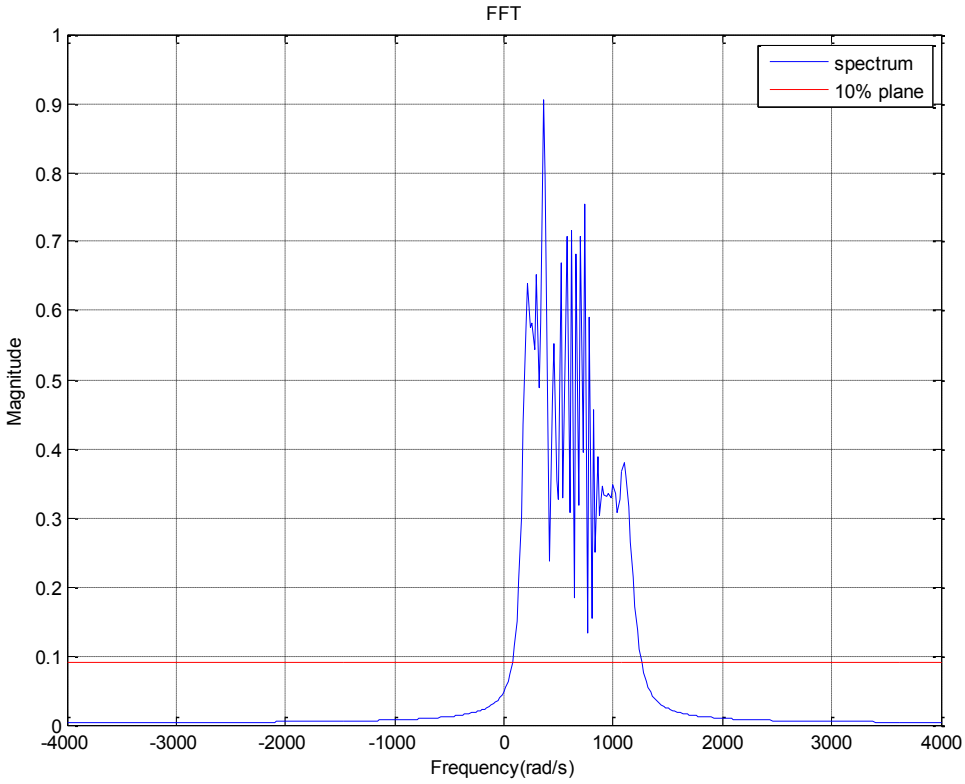

Fig. 44. FFT of the multi-component chirp in frequency domain.

2) Slanted Spectrum result (based on MA-DFRFT) the 10% plane above from the noise floor shown in Fig. 45:

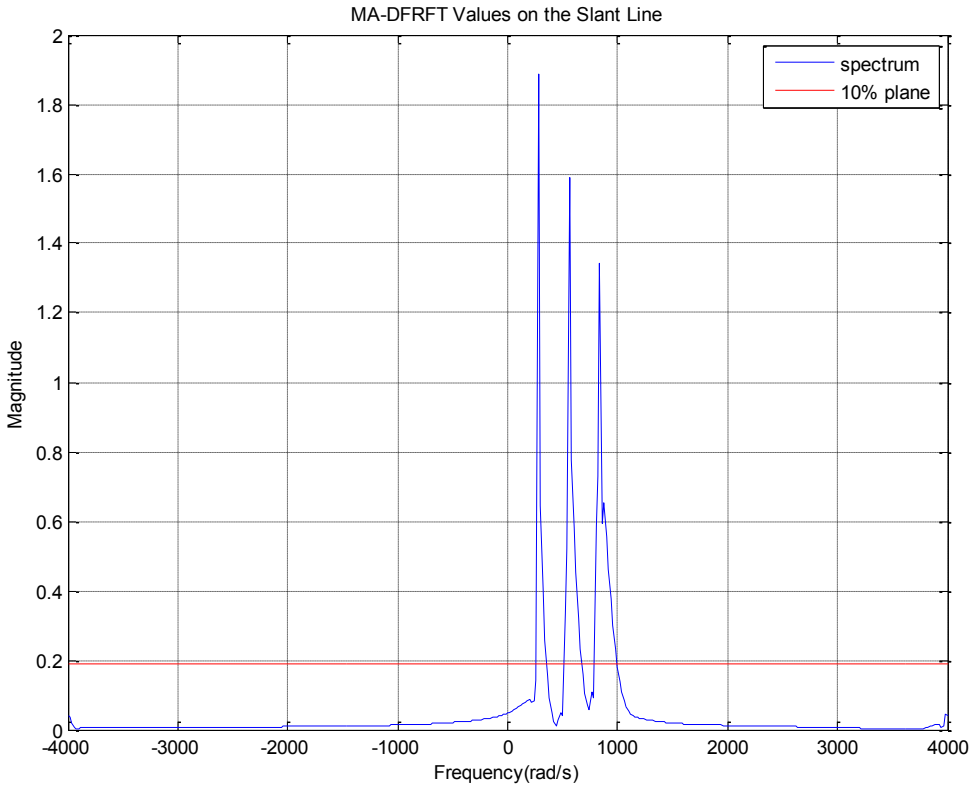

Fig. 45. MA-DFRFT of the multi-component chirp in FRFD.

c. Comparison Table for the 2 different tools applied to both single-component chirp signal and multi-component chirp signal

The performance comparison between the traditional FFT and DFRFT is shown in Table IV:

TABLE IV
FREQUENCY RANGE COMPARISON BETWEEN FFT AND DFRFT

Frequency range at the 10% plane*	Single-component input signal	Multi-component (three-component) input signal
FFT	[100,460]	[80,1260] (cannot distinguish the three components)
DFRFT (Slanted Spectrum)	[240,420]	[260,360], [520,660], [780,1000]

* The 10% plane is measured from the top of noise floor, which is the bottom of the plots in Fig.24 – Fig. 27 (no simulation of noise). The whole range (peak-bottom) of the spectrum is measured, and 10% range is calculated from the bottom of the plot.

So from the comparison table above, we could see the frequency range of the transformed signal is greatly shrunk, which means DFRFT is a better tool to process FM signals.

Because of the participation of the new DOF, transform order *a*, DFRFT provides higher flexibility and resolution especially for research in FM signals.

It has been proved in this section that the energy of the FM signals will be more concentrated with DFRFT analysis than with simply employment of FFT. Because a signal with a chirp rate can only be transformed into a pulse function in an appropriate FRFD, hence DFRFT has an excellent advantage of concentrating the FM signal energy.

F. Spectrogram Based on Slanted Spectrum

1. Comparison between Traditional Spectrogram and Spectrogram Based on Slanted Spectrum

The traditional spectrogram for discrete-time signals is based on the computation of the DFT over a certain number of windowed segments within the whole analysis frame, and is developed with the assumption that the target objective signal is stationary, so in this case the traditional spectrogram has been an effective and reliable time-frequency tool for stationary signal analysis. In other words, as a signal-component decomposition method applied on signals using the DFT, the traditional spectrogram inevitably assumes a multi-component sinusoidal signal model and that the frequency content of the signal is stationary over the analysis frame as the signal model that DFT is mostly employed to deal with. Hence the traditional spectrogram is not an appropriate option for the more complicated case that the frequency content of a signal is chirping over the analysis frame, such as bat echolocation signals, and human speech signals, where the fundamental frequency and its harmonics have chirp rates, i.e., the signals being FM.

The traditional spectrogram is calculated by dividing the whole analysis frame of the input signal into multiple segment frames, by applying different mathematical windows such as Hanning window, Hamming window and Gaussian window to the analysis frame. In each window, the DFT of each input signal segment will be calculated, so there is actually the same number of TFRs for segments of truncated data points of the input signal with the number of frames, and this is also why the spectrogram is also named as the Short Time Fourier Transform.

And then for the SBSS, it is the MA-DFRFT, rather than DFT, has been exploited to define this advanced spectrogram that is able to provide with higher resolution. The most essential attribute of this advanced spectrogram is that it is based on the multi-component chirp model rather than a multi-component sinusoidal model and it will be confirmed to be more efficacious at processing chirp signals in the subsequent section. And SBSS is implemented in a similar technique as the traditional spectrogram: dividing the input signal into different analysis frames, where there may be overlaps between one another frame as input in the presetting procedure.

However, as an innovative spectrogram, SBSS has some tremendous difference from the traditional spectrogram. According to [6], the essence of generating SBSS lies in the selection of transform order within each analysis frame: “With the equation of the line we can select the values of the MA-CDFRFT to obtain the *slanted spectrum*. Repeating this process of finding the largest peak and computing the equation of the line over each frame at different positions in time, we can construct a spectrogram that is sharper than the one based on the DFT.” Moreover, there is further hint obtained from [6] that as DFT needs to be computed to get a regular spectrogram, MA-CDFRFT along the slant line defined by the largest peak also needs to be computed to get the SBSS, where it is worth mentioning that the slope of the slant line changes at every sample (analysis frame).

So to provide more concrete details about the fact of generating SBSS, within every analysis frame, MA-DFRFT will be taken to process each of the segments of the chirp signal and there will be a procedure to seek for the energy-concentration point under the confinement of each single analysis frame which is also followed by generating slant

line in each frame. Therefore the technique of generating Slanted Spectrum which has been elaborately discussed on will be utilized within the range of every analysis frame, and then as the traditional spectrogram, PSD (Power Spectral Density) will be taken upon the Slanted Spectrum matrix of the input signal. Hereto this innovative TFR tool has reached its completion of development.

So to wrap up, which has made SBSS more advanced than the traditional spectrogram is that this algorithm has congregated all the tools that have already been introduced in the previous chapter and sections: DFRFT, MA-DFRFT and Slanted Spectrum, so it has the capability of decomposing the complicated signal into multiple separated components.

2. Traditional Spectrogram Applied on the Multi-component Chirp Signal

As in the previous several sections, the 3-component chirp signal model is put to use in this section and the next section once again to demonstrate the difference between the efficaciousness of the traditional spectrogram and SBSS:

$$x(t)=\sum_{k=1}^{3}e^{j(\omega_k t+c_{r_k}t^2)}=\sum_{k=1}^{3}e^{j(\omega_1 kt+c_{r_1}kt^2)}$$

where the fundamental initial angular frequency is $\omega_1=1000rad/s$, the fundamental angular chirp rate is $c_1=15000rad/s^2$, and still with the sampling frequency to be *Fs*=8000Hz.

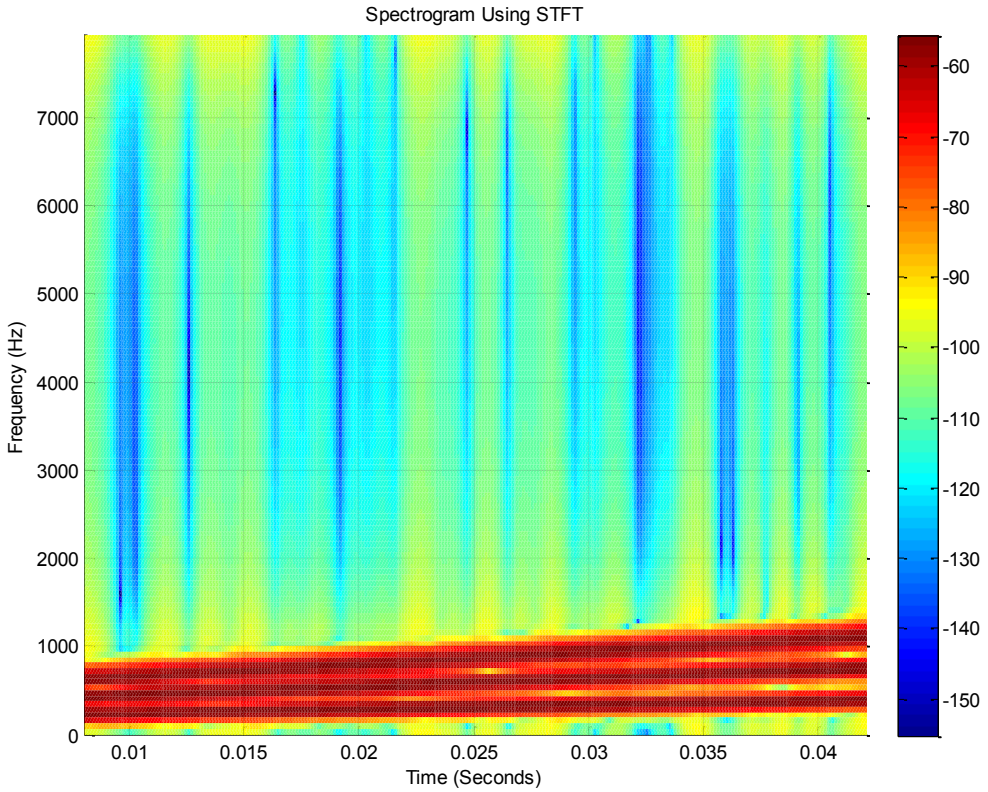

Fig. 46. The traditional spectrogram applied on a 3-component chirp signal.

So from Fig. 46, following information could be obtained by mere observation:

1) The initial frequencies of the 3 components are resided within the range of [0, 1000] *Hz*, matching with the given information of the input signal: the fundamental initial angular frequency is $\omega_1 = 1000 rad/s$, so the fundamental initial frequency is $f_1 = \omega_1/(2\pi) \approx 159.15 Hz$; the 2nd harmonic has a doubled initial angular frequency of $\omega_2 = 2000 rad/s$, so its corresponding initial frequency is $f_2 = \omega_2/(2\pi) \approx 318.31 Hz$; and the initial angular frequency of the

3^{rd} harmonic is $\omega_3 = 3000 rad/s$, so the 3^{rd} initial frequency should be $f_3 = \omega_3/(2\pi) \approx 477.46 Hz$.

2) All the 3 TFRs have positive slopes, because the 3 components have increasing frequencies, i.e. the fundamental angular chirp rate is $c_{r1} = 1{,}5000 rad/s^2$, which means that the gradient should be $c_{r1}/(2\pi) \approx 2{,}387.32 Hz/s^2$. However, the analysis frame has only been confined to a range almost could be called infinitesimal, so the large frequency variation rate has not been shown to a best degree;
3) The drawback of employing the traditional spectrogram is also obvious: The 3 bars with the darkest color in the demonstration fail to provide with high resolution, so there is relative difficulty distinguishing them. If the bars could be turned into crisp lines, which are the ideal shapes to examine, then there will be no trouble with the distinguishing work.

3. SBSS Applied on the Multi-component Chirp Signal

As a specific case, if I set the transform order to be *a*=1, the SBSS of the multi-component chirp signal is as shown in Fig. 47.

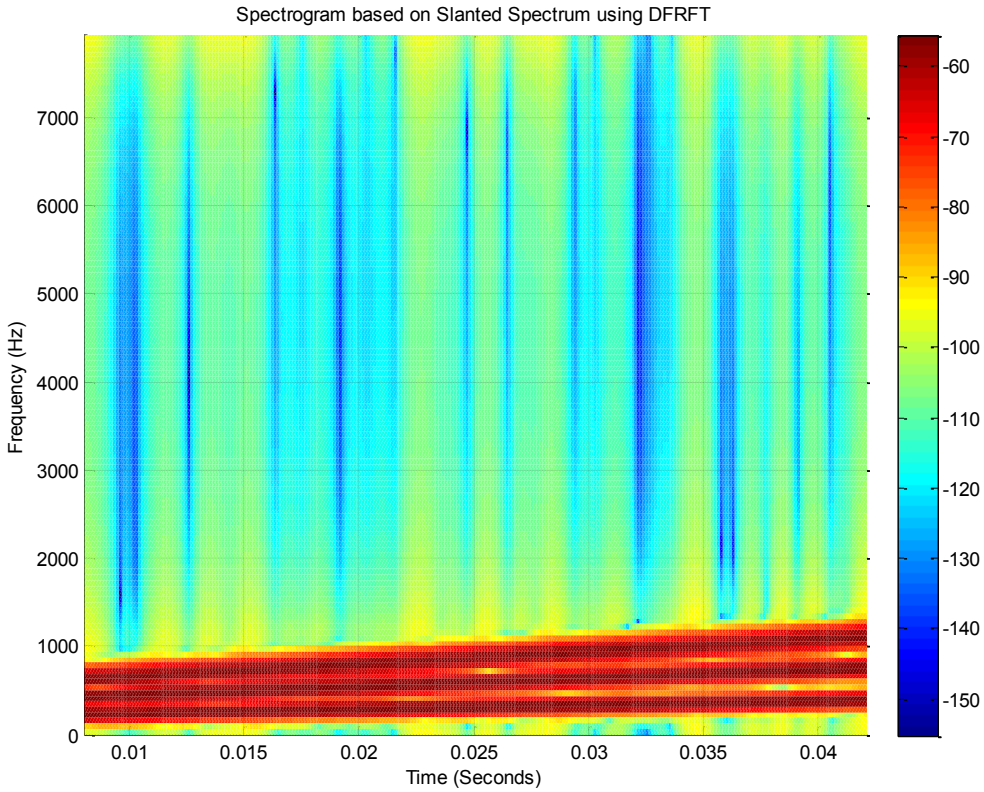

Fig. 47. SBSS applied on a multi-component chirp signal with a=1 being the slant line to compute Slanted Spectrum within every frame.

There shows no difference between Fig. 47 above and Fig. 46 of the traditional spectrogram using traditional DFT, since Fig. 47 is obtained via taking Slanted Spectrum along the a=1 line in every single analysis frame, which equals with the effect of taking DFT of each segment of signal data points.

And if SBSS is taken with respect to the 1st optimum transform order which corresponds to the leftmost energy-concentration point in Fig. 38, i.e., $a = a_1 = 1.019$, then the TFR presented by SBSS will be like demonstrated in Fig. 48:

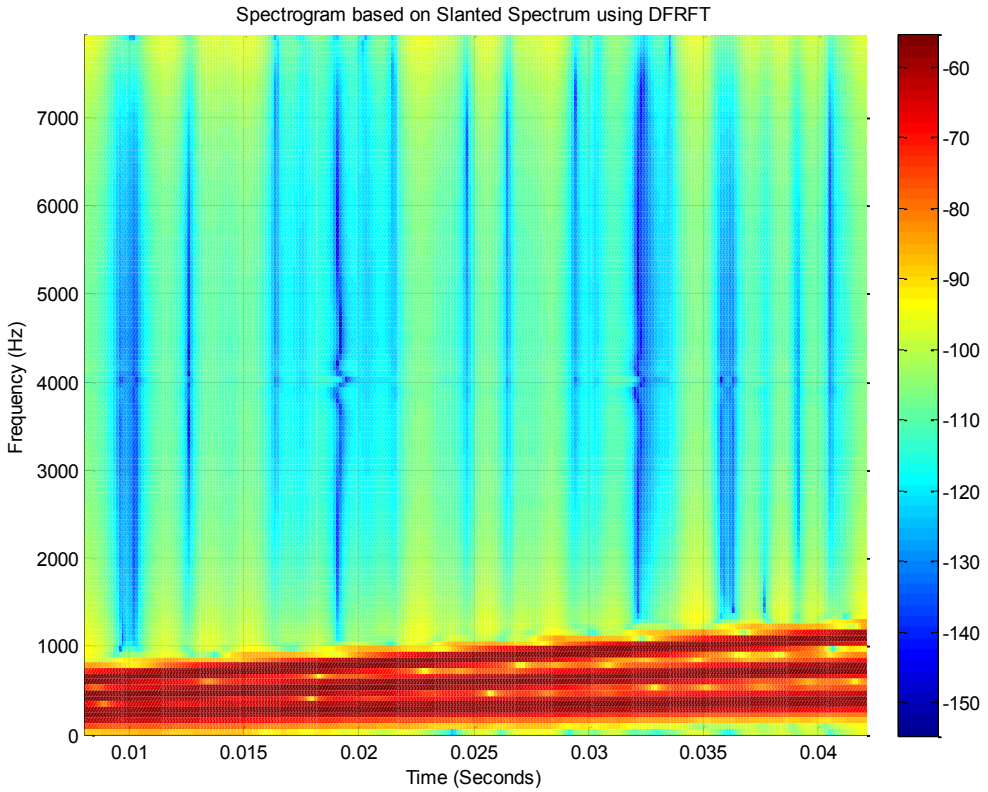

Fig. 48. SBSS applied on a multi-component chirp signal with a=1.019 being the slant line to compute Slanted Spectrum within every frame.

It could be observed that the SBSS corresponding to the slant line with respect to the 1st component of the original chirp signal has obtained a better resolution, because the widths of the red bars have been decreased if compared with Fig. 46 and Fig. 47.

The result acquired by observing all the rules of generating a standard SBSS is given by the following Fig. 49:

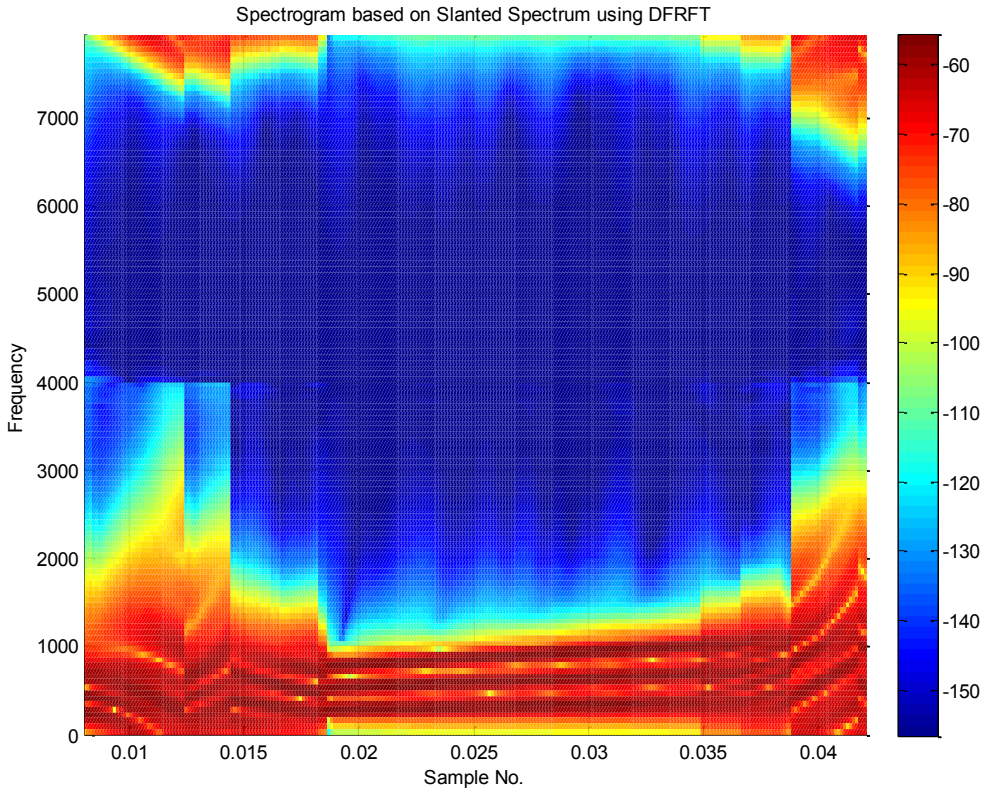

Fig. 49. SBSS applied on a multi-component chirp signal by taking different slant lines to compute Slanted Spectrum within every frame.

Fig. 49 above shows the SBSS result of the 3-component chirp signal, with a series of specification settings: a Hanning window with the length of 128 is applied to obtain each of the analysis frames with the length of 128; the number of data points in overlap between each two successive frames is 127; $F_s = 8{,}000Hz$ still being the sampling frequency; and the frequency axis is set to the *y*-axis.

A particular problem concerned with utilizing SBSS is the selection of the window. By default, a Hamming window with a length equal to that of the FFT computed within each analysis frame is applied. But by recommendation, a Hanning window with a

length of 128 or 256 should be selected to do the traditional spectrogram, and for SBSS, a Hanning window with the length of 256 is proposed to get a higher resolution of the TFR. A single-component chirp signal will be employed to illustrate the difference of specifying the window type and not.

The chirp signal has an expression of $x[n] = e^{j(0.5n+0.001(n-127/2)^2)}$, where n=0,1,…,N-1, and N=500.

1) SBSS with a defaulted Hamming window with the length of 256, number of overlap of 255:

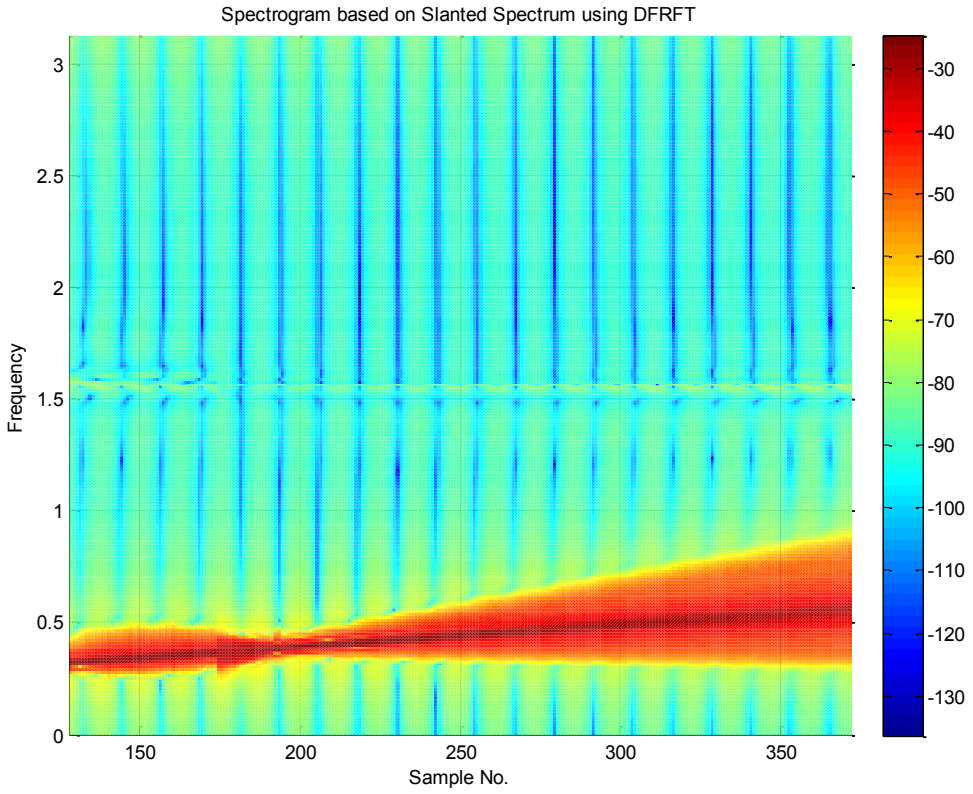

Fig. 50. SBSS applied on a single-component chirp signal with a defaulted Hamming window of the length of 256.

The line with the darkest red color which lies in the middle of the spectrum shown in Fig. 50 has actually provided higher resolution compared with the traditional spectrogram in Fig. 51 below, because there is doubt that the SBSS result has a better concentration.

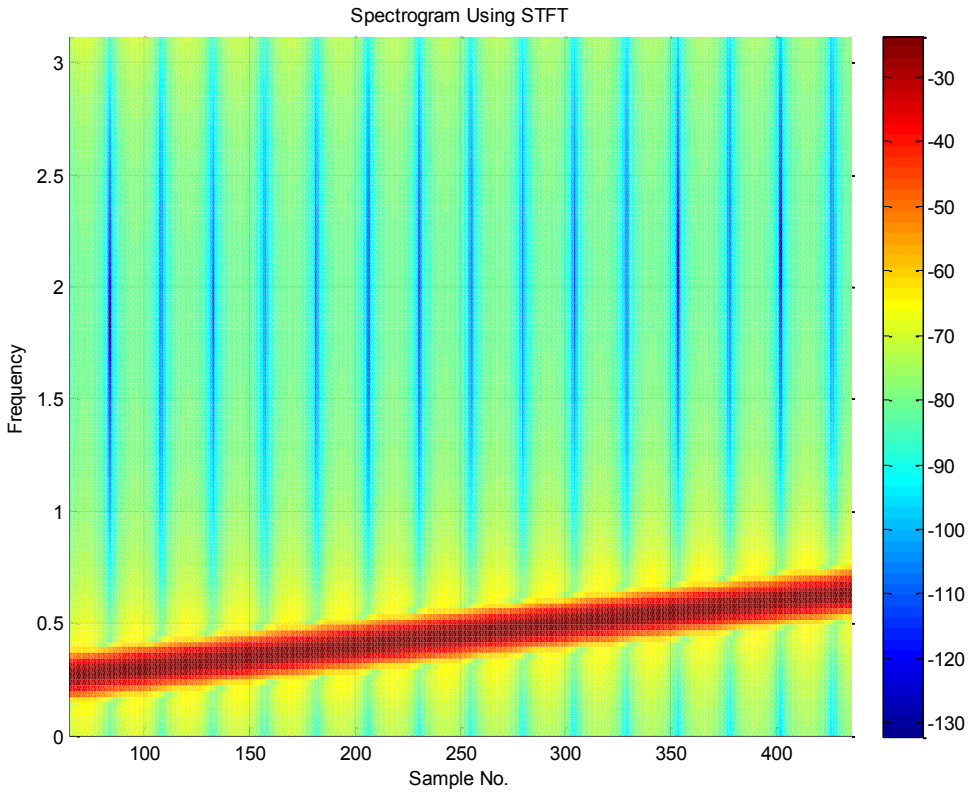

Fig. 51. Traditional spectrogram of a single-component chirp signal.

2) SBSS with a specified Hanning window with the length of 256, number of overlap of 255:

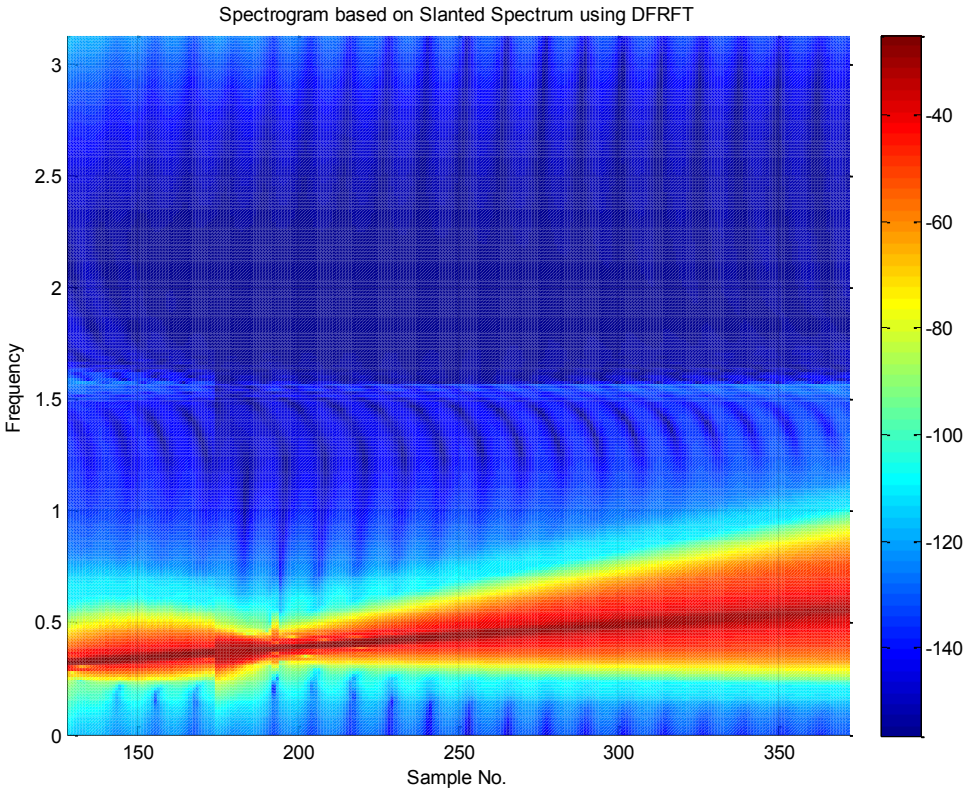

Fig. 52. SBSS applied on a single-component chirp signal with a specified Hanning window of the length of 256.

So based on the Fig. 52, SBSS with a Hanning window of length 256 is suggested to specify when in utilization.

G. Summary for the Method Comprised of Tools from the DFRFT Family

First of all, DFRFT is the cornerstone for all the other derivative tools: MA-DFRFT, Slanted Spectrum and SBSS. It has expanded the traditional FT with another new DOF, which is the very factor which brings in the flexibility and effectiveness for processing

FM signals. It needs to be mentioned that DFRFT alone is best for single-component FM signal, and when it comes to multi-component FM signal, only employing this tool is not enough. That's why the development of other derivative tools is highly demanded.

One of the most essential derivative tools, MA-DFRFT, is a multi-angle version of DFRFT, and it is a demonstration show at first hand at which values of the optimum transform order *a*, the signal under research could get the energy of its different components concentrated to distinct single points. So MA-DFRFT helps to get rid of the scanning process seeking for the optimum transform order a_{opt} and could directly show that information in its plot.

Besides, Slanted Spectrum is generated based on MA-DFRFT, and it is best for multi-component signal analysis, because its algorithm would firstly figure out exactly the slant line which is comprised of the points at which the signal components could get their energy concentrated, and then calculate a new matrix of the MA-DFRFT of the researched signal strictly along this slant line. So this is also why it is named as Slanted Spectrum.

The last but not the least, SBSS, as its name, is an innovative Spectrogram which is based on Slanted Spectrum. It has not yet attracted much attention compared with DFRFT and MA-DFRFT in the community, but it has great potential to give more specific time-frequency information of a FM signal.

CHAPTER IV

MOTOR CURRENT SIGNAL ANALYSIS USING PROPOSED METHODS

A. The Motor Current Signal and Its Importance in Fault Detection

The main practical signal from industry employed to apply DFRFT and its derivatives is the shaft current signal of a 7.5HP, 3 Phase, 208V induction motor 3KX07G manufactured by DAYTON. And the experiment aiming at obtaining necessary current signal data comprises of the following 9 steps:

1) The test-bed was run for 232.58Hrs in a healthy mode, and healthy current signal data is acquired.
2) Inject current for the 1st time to the motor bearing so that damage leading to generalized-roughness fault on the bearing occurs for the first time, and this current injection period last for 25.38Hrs.
3) Stop the current injection and keep the motor running for 44.07Hrs, and track down the current signal data in this faulty status.
4) Repeat step 2) with the 2nd current injection which last for 8Hrs.
5) Repeat step 3) with the motor running for another 89.05Hrs with the 2nd state of faulty signal data recorded.
6) Repeat step 2) with the 3rd current injection which last for 2.47Hrs.
7) Repeat step 3) with the motor running for another 49.53Hrs with the 3rd stage of faulty signal data recorded.
8) Repeat step 2) with the 4th current injection which last for 24.38Hrs.

9) Repeat step 3) with the motor running for another 283.22Hrs with the 4th stage of faulty signal data recorded.

Among these steps, 2), 4), 6) and 8) are the current injection stages and the signal data acquired in these are not the research objective, since these are only records of abnormal current artificially injected to an originally healthy motor bearing. What matters in this research on motor current signal is the subsequent status of the motor current after the current injection, because that was exactly the simulation of a faulty motor bearing which could give valuable information about generalized-roughness fault on motor bearings. Thus the signal data files obtained from steps 1), 3), 5), 7) and 9) are the research objectives here, that is, in order to achieve a thorough examination of the current signal, it is required that both healthy and faulty signal data should be analyzed.

1. Pre-treatment of the Motor Current Signal Data

Each data file obtained from the experiment introduced above contains a 30 Sec-length of motor current signal, with every single data point to be sampled at a sampling frequency of 8kHz. However, using all the sampled data to testify the generated algorithms of DFRFT, MA-DFRFT, Slanted Spectrum and SBSS is overwhelmingly time-consuming, so a new sampling rate of 1.92 kHz is used to resample the data, so the length of an original data file has been reduced to its 24%.

And then MA-DFRFT is firstly applied on the ante-pretreatment signal data files in healthy status to determine its signal type as shown in Fig. 53.

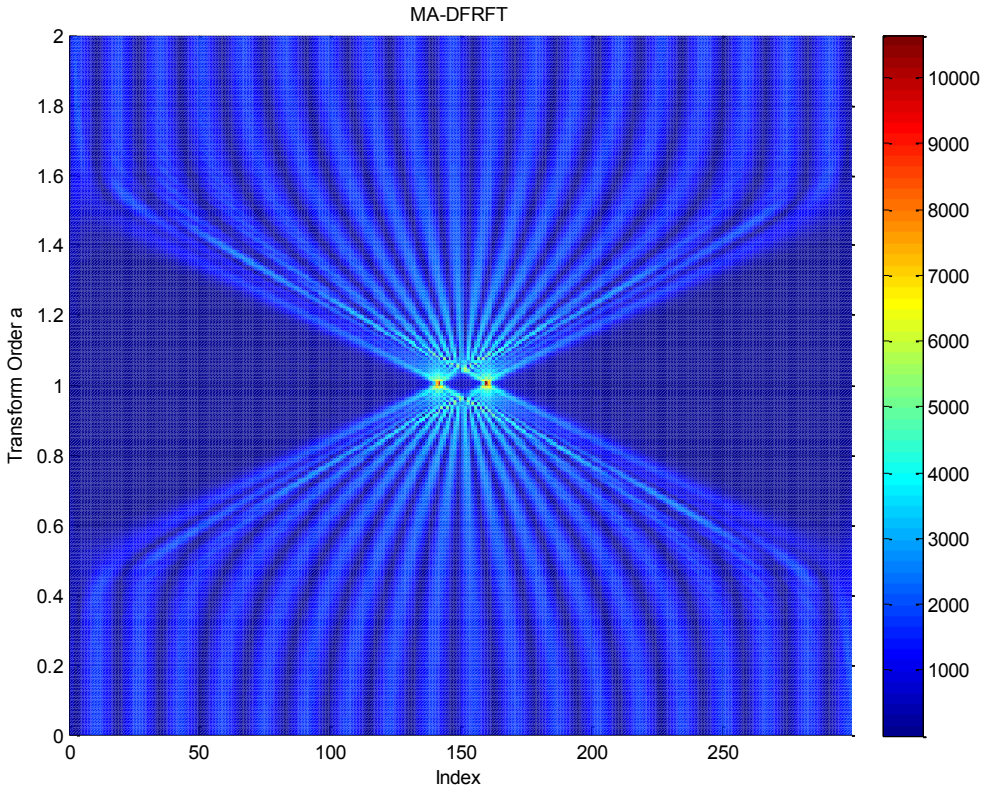

Fig. 53. MA-DFRFT applied on the healthy motor current signal

Both of the chirp rate c_r and optimum transform order a_{opt} are able to be calculated from the peak coordinates of the MA-DFRFT demonstration: $c_r = 0$ and $a_{opt} = 1$.

So by using MA-DFRFT, the procedure of identification of the original signal is achieved. From the plot and the digital computation result, we get to know the signal type of the ante-pretreatment signal might be mainly amplitude modulated.

And then based on the MA-DFRFT result, DFRFT (a=1) was taken on a random file from the healthy state, and the result is shown as in Fig. 54:

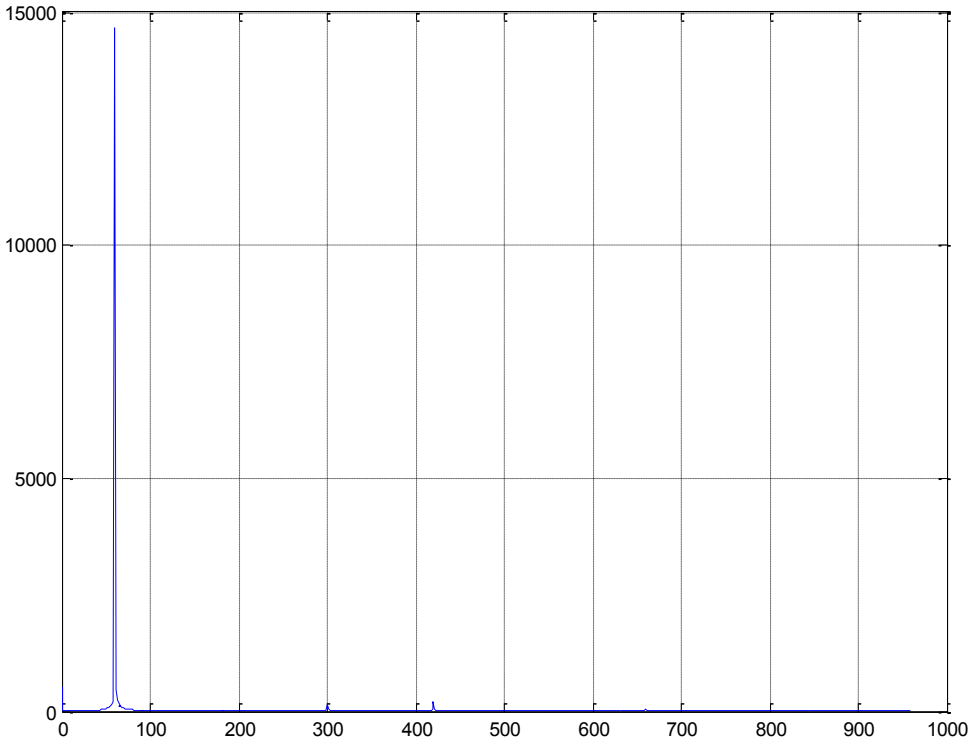

Fig. 54. DFRFT applied on the healthy motor current signal.

A main frequency component with very large amplitude appears at 60Hz, and there are also its harmonics along the frequency axis, so there is a need to filter out all these components with a reliable filtering technique. Following shows the whole procedure of the pre-treatment of the raw data:

Firstly, the DC component is removed by simply subtracting the mean average of all the data.

And then a notch filter based on FFT is applied to remove all the harmonics of the 60Hz component generated from the electrical power supply, where it should be noted

that in order not to have an impact for filtering the other harmonics of the 60Hz component, the stopband width adopted for removing the 60Hz component with the highest magnitude among all the harmonics should not be overlarge and needs to be limited to 80Hz. This subtle but important move is due to the fact that the higher magnitude one component has, the larger energy leakage will occur when trying to remove this component with a not large enough filtering stopband width. So setting the stopband width to be 10Hz for other harmonics would be enough, but the successful removal of the 60Hz component with the highest magnitude requires a relatively high stopband, because it has the most significant energy as shown in Fig. 54.

2. DFRFT and Other Tools Applied on Motor Current Signal Data

Based on the information collected from the last section of data pre-processing, the motor current signal is mainly AM, and the FM exists but is not obvious, since it may take a very long time for an observer to see that FM phenomenon. So DFRFT with a transform order a=1 is the first tool applied here.

a. DFRFT (a=1) results of the 5 states

In this section, DFRFT (a=1) has been taken again on the data of all the five states: healthy state, 1^{st} – 4^{th} faulty states.

1) Healthy State

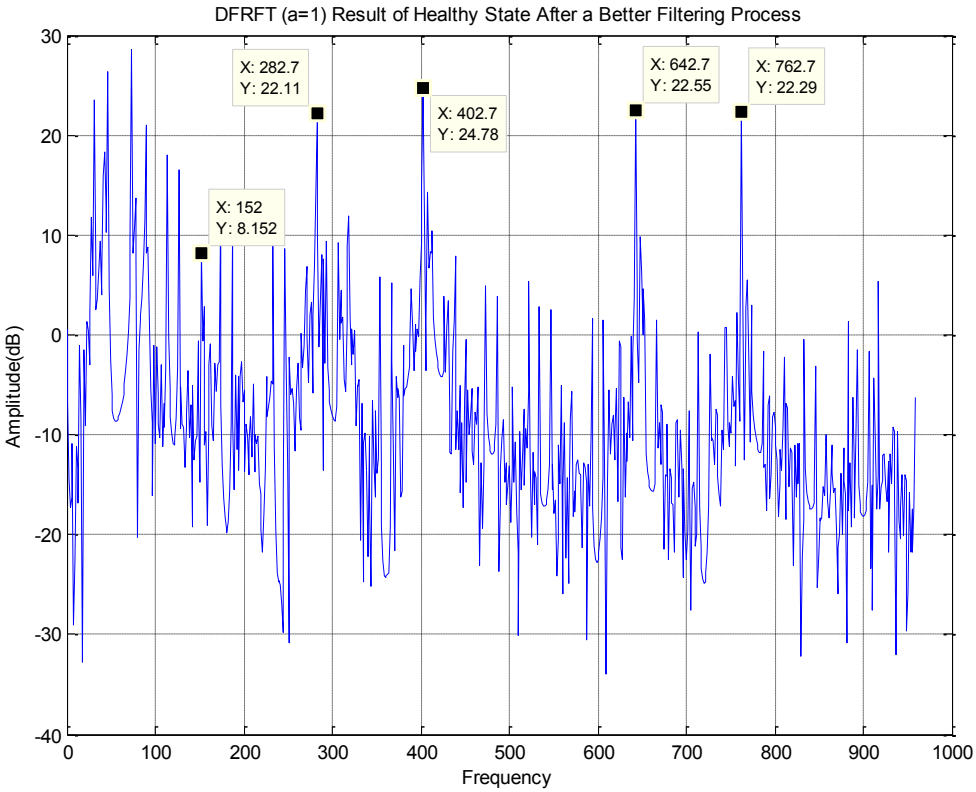

Fig. 55. DFRFT (a=1) taken on data from the healthy state.

2) 1st Faulty State

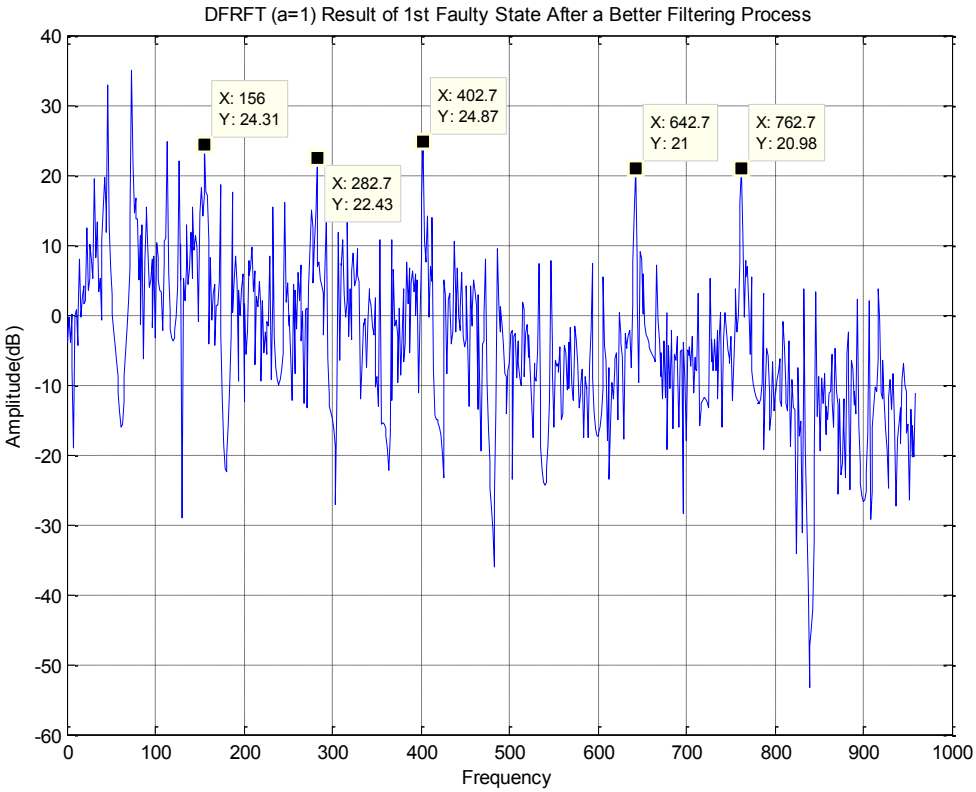

Fig. 56. DFRFT (a=1) taken on data from the 1st faulty state.

3) 2nd Faulty State

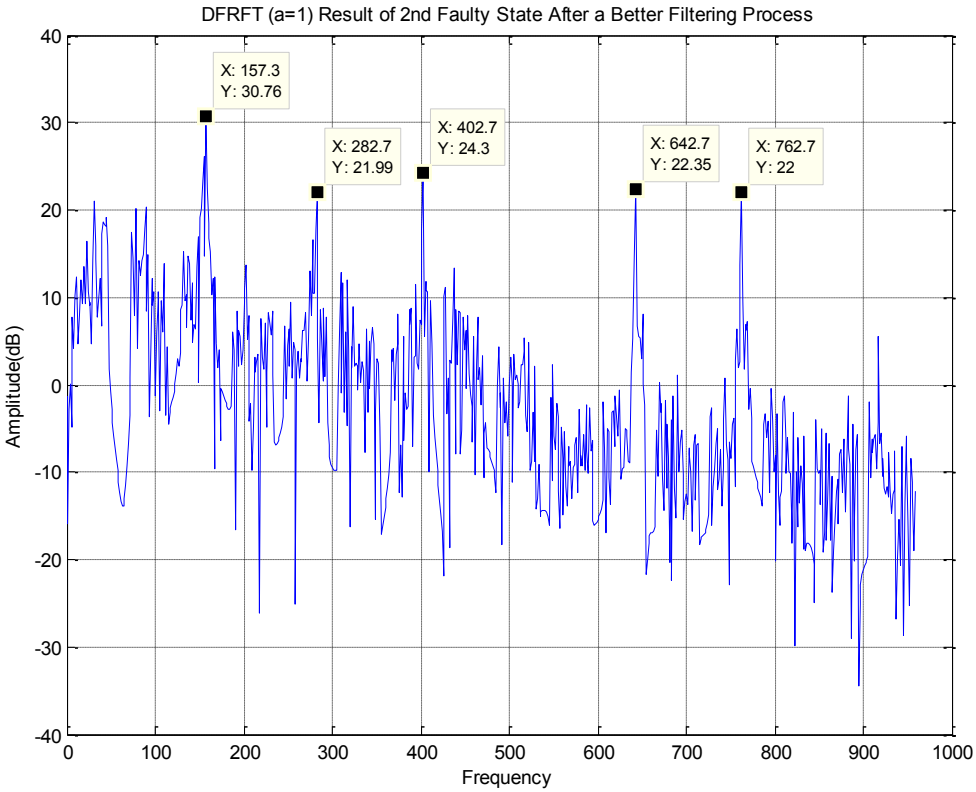

Fig. 57. DFRFT (a=1) taken on data from the 2nd faulty state.

4) 3rd Faulty State

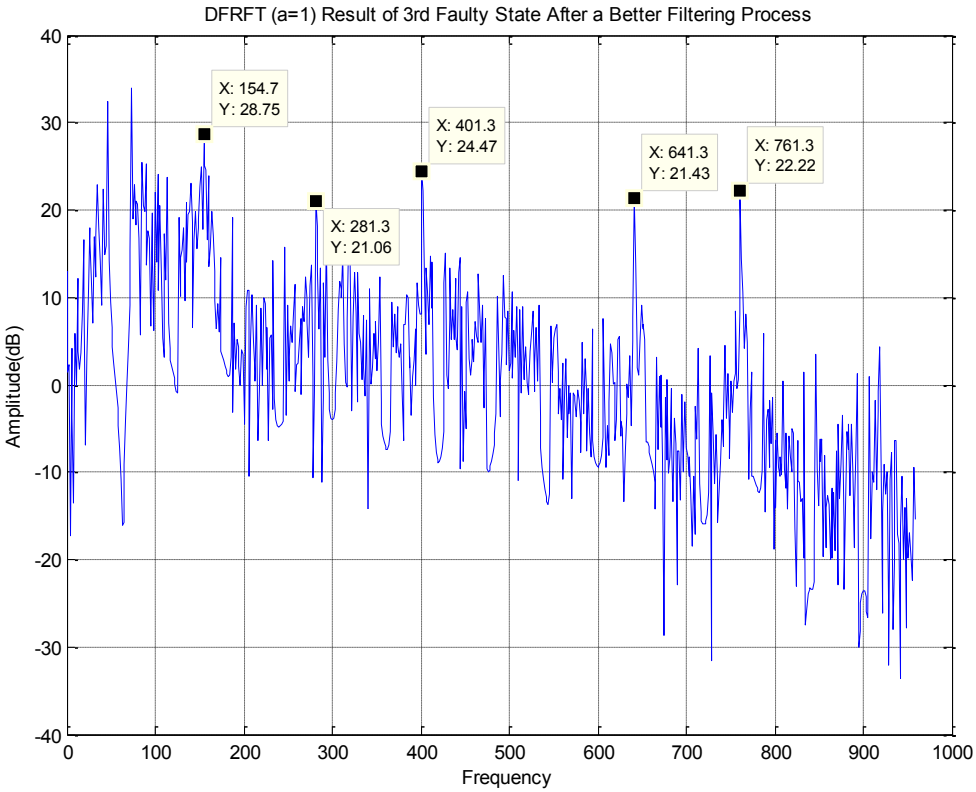

Fig. 58. DFRFT (a=1) taken on data from the 3rd faulty state.

5) 4th Faulty State

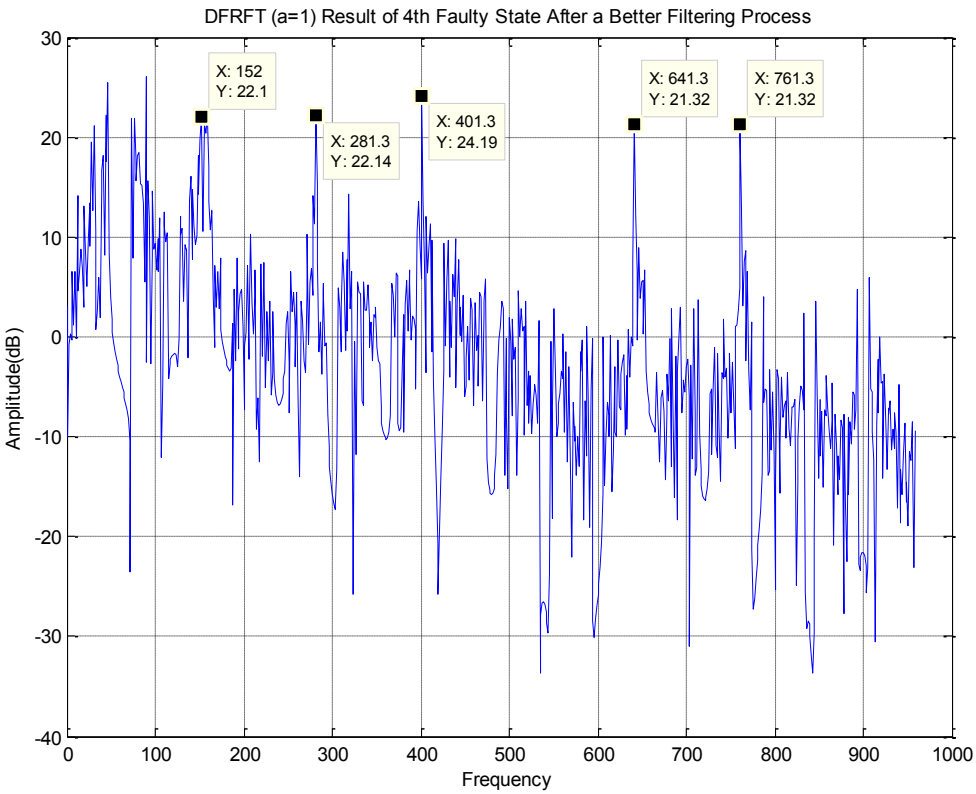

Fig. 59. DFRFT (a=1) taken on data from the 4th faulty state.

6) Conclusion of applying DFRFT on the motor current signal

From observing the DFRFT results shown in Fig. 55 – Fig. 59, the band in between of 152Hz – 157Hz is speculated to be the signature frequency of the fault, since their amplitude has a dramatic rise since the 2nd faulty state; the other 4 frequency components: 282Hz, 402Hz, 642Hz and 762Hz have a relatively stable variation since the healthy state, so they should be the characteristic frequencies of the motor bearing.

b. Moving average results of AM of the speculated signature frequency of the fault and the other 4 characteristic frequency components

In this section, the amplitude change which quantitatively shows the AM phenomenon of the speculated signature frequency of the fault at 152Hz – 157 Hz, and also the other 4 characteristic frequency components at 282Hz, 402Hz, 642Hz and 762Hz will be shown with their moving average plot.

1) Speculated signature frequency of the fault at 152Hz – 157 Hz

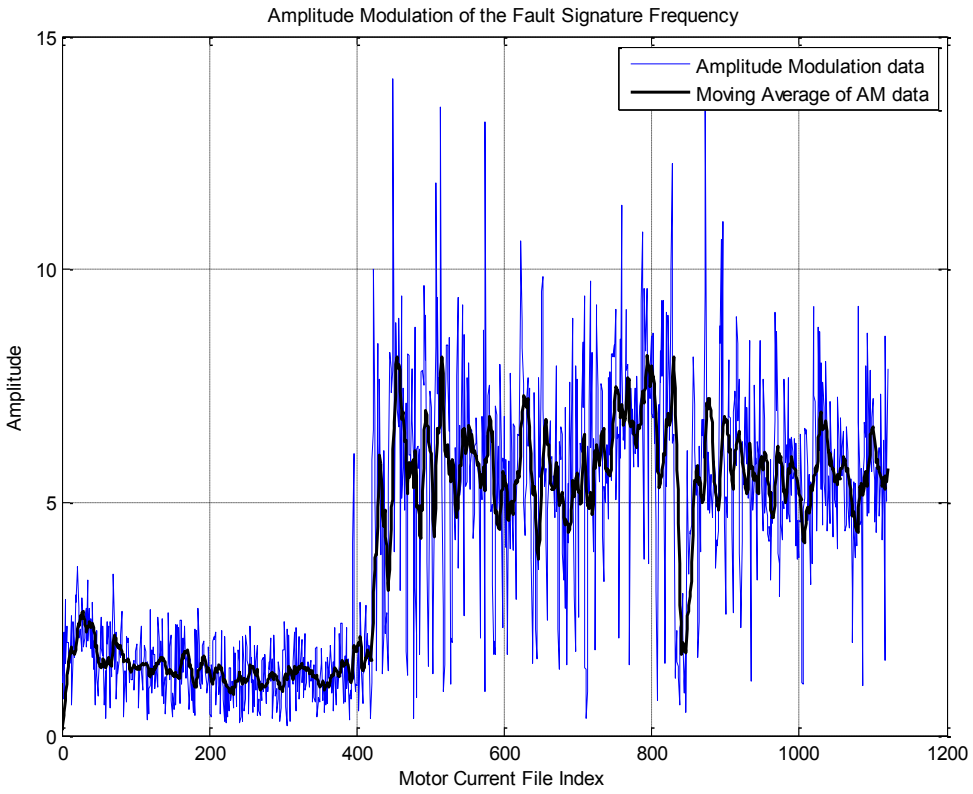

Fig. 60. Amplitude change with moving average result of the speculated signature frequency of the fault.

2) The characteristic frequency component at 282Hz

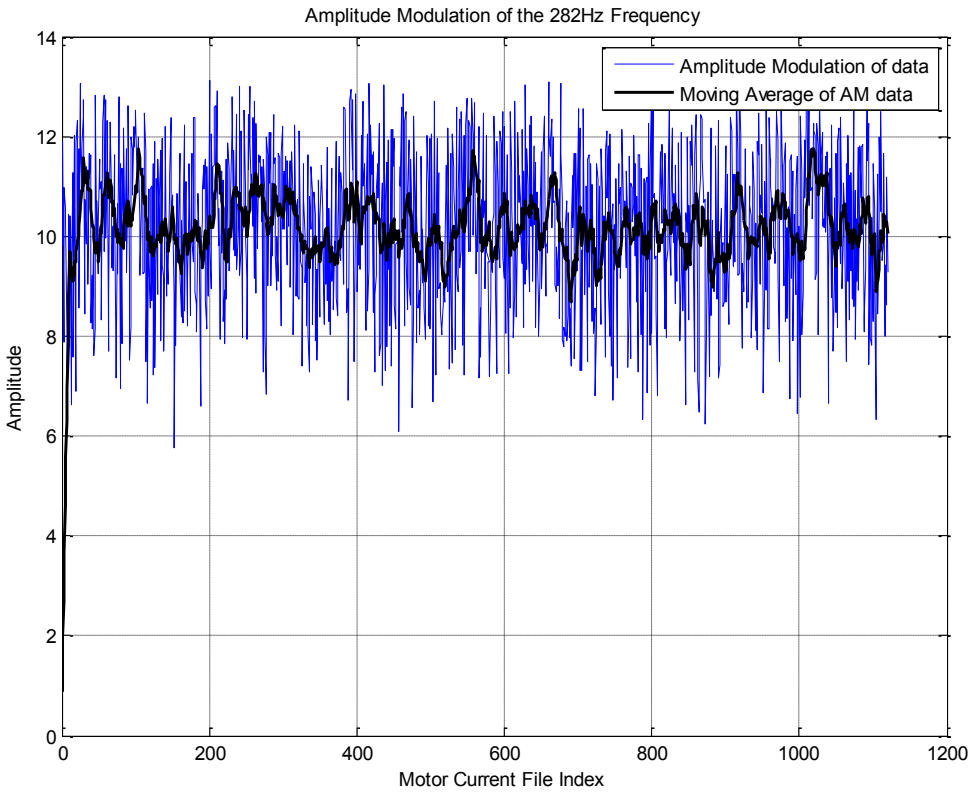

Fig. 61. Amplitude change with moving average result of the characteristic frequency component at 282Hz.

3) The characteristic frequency component at 402Hz

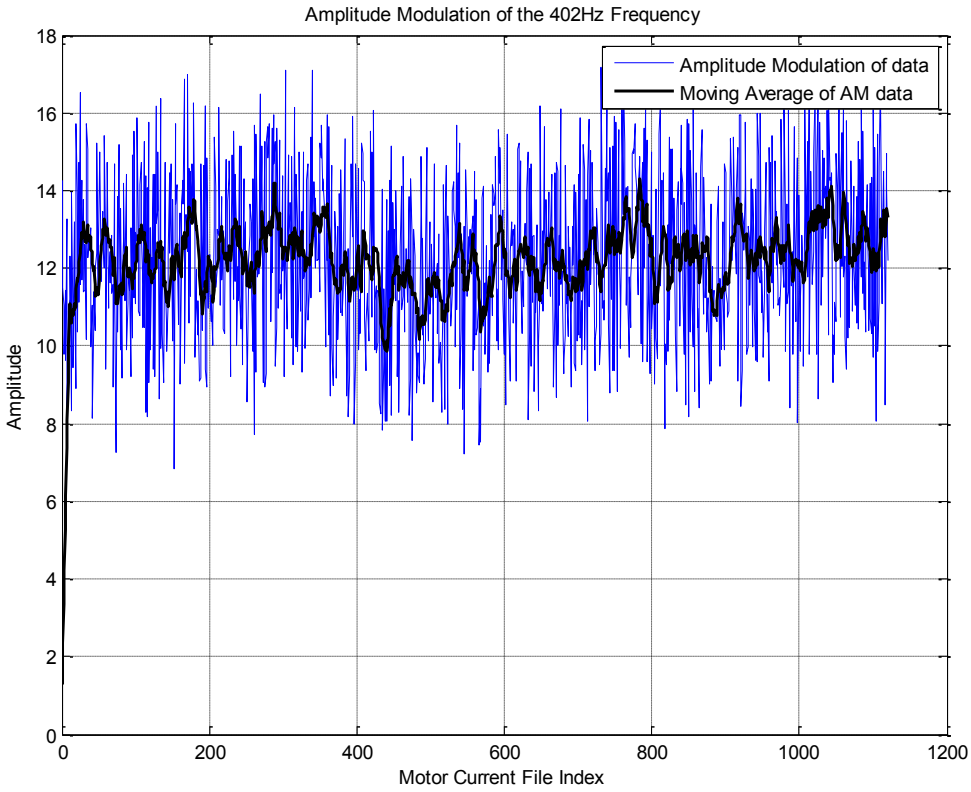

Fig. 62. Amplitude change with moving average result of the characteristic frequency component at 402Hz.

4) The characteristic frequency component at 642Hz

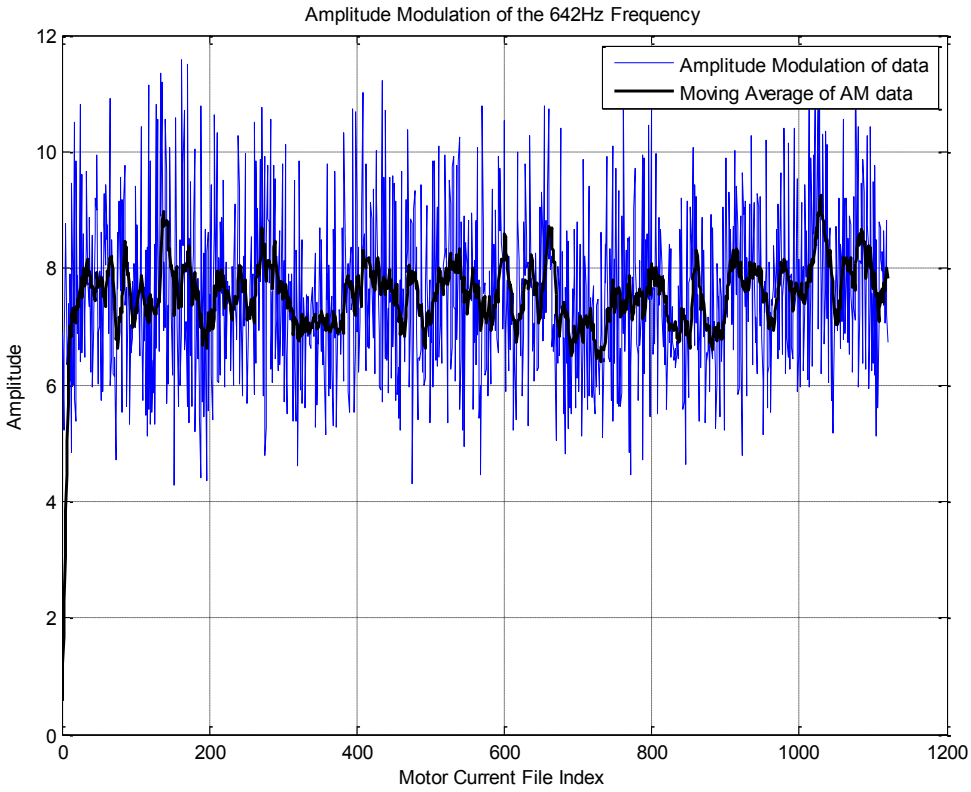

Fig. 63. Amplitude change with moving average result of the characteristic frequency component at 642Hz.

5) The characteristic frequency component at 762Hz

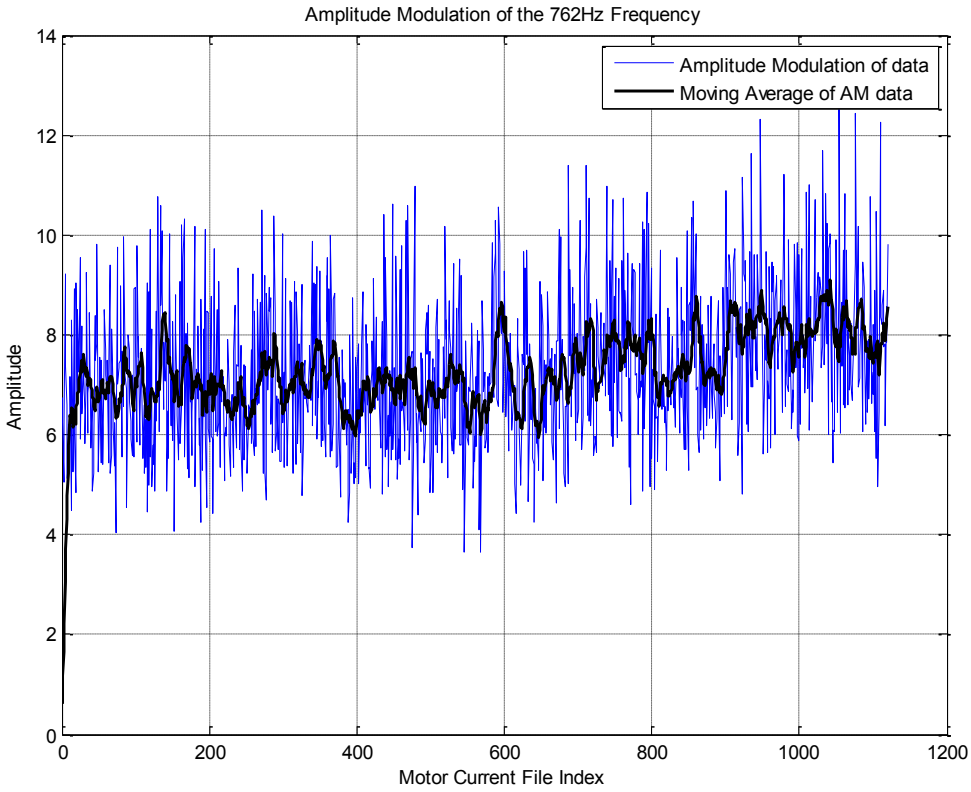

Fig. 64. Amplitude change with moving average result of the characteristic frequency component at 762Hz.

6) Conclusion of the moving average results of AM of the speculated signature frequency of the fault and the other 4 characteristic frequency components

The moving average results of AM has confirmed the speculation drawn in section a, since there was also a dramatic rise in Fig. 60, and the amplitude change in Fig. 61 – Fig. 64 are all relatively stable. So there is no doubt that the current injection has brought in a fault with the signature frequency at 152Hz – 157Hz, the other 4 characteristic frequencies at 282Hz, 402Hz, 642Hz and 762Hz almost remained intact.

3. Traditional Methods Applied on Motor Current Signal Data

a. Traditional spectrogram applied on motor current signal data

7 random data files from each of the states have been taken to do the traditional spectrogram.

1) Healthy state

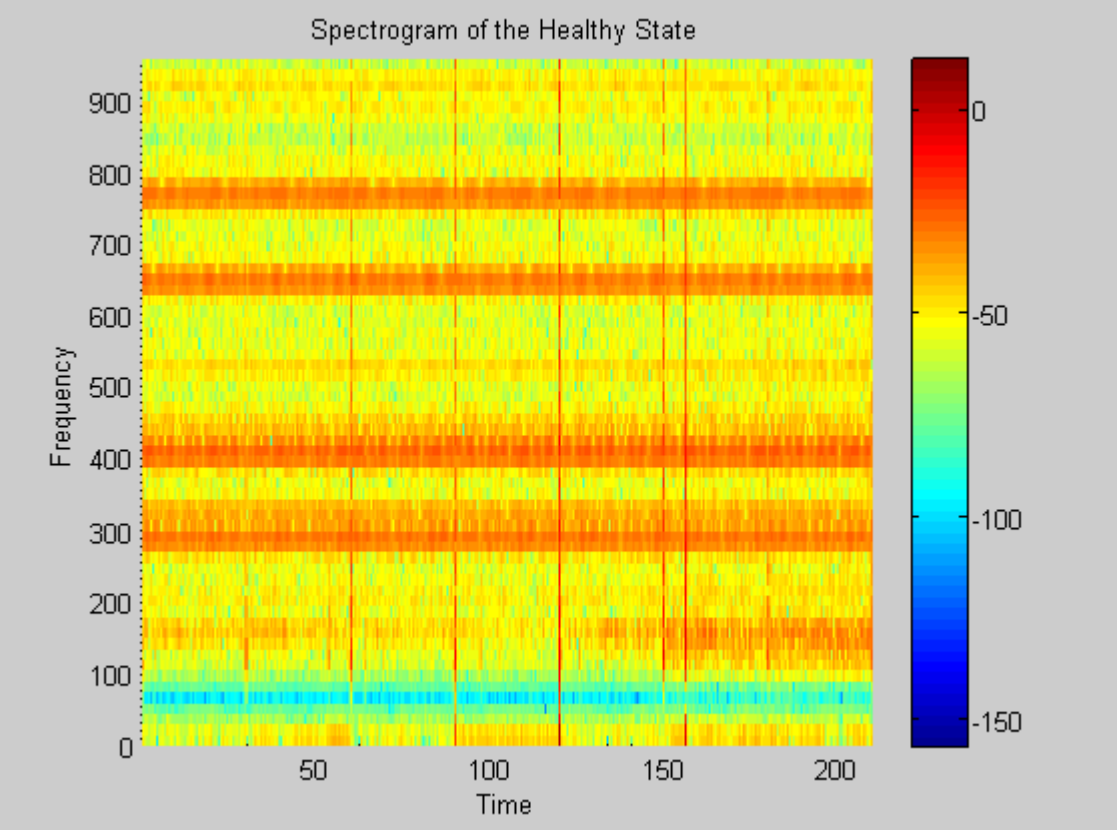

Fig. 65. Traditional spectrogram taken on 7 random motor current data files of the healthy state.

2) 1st faulty state

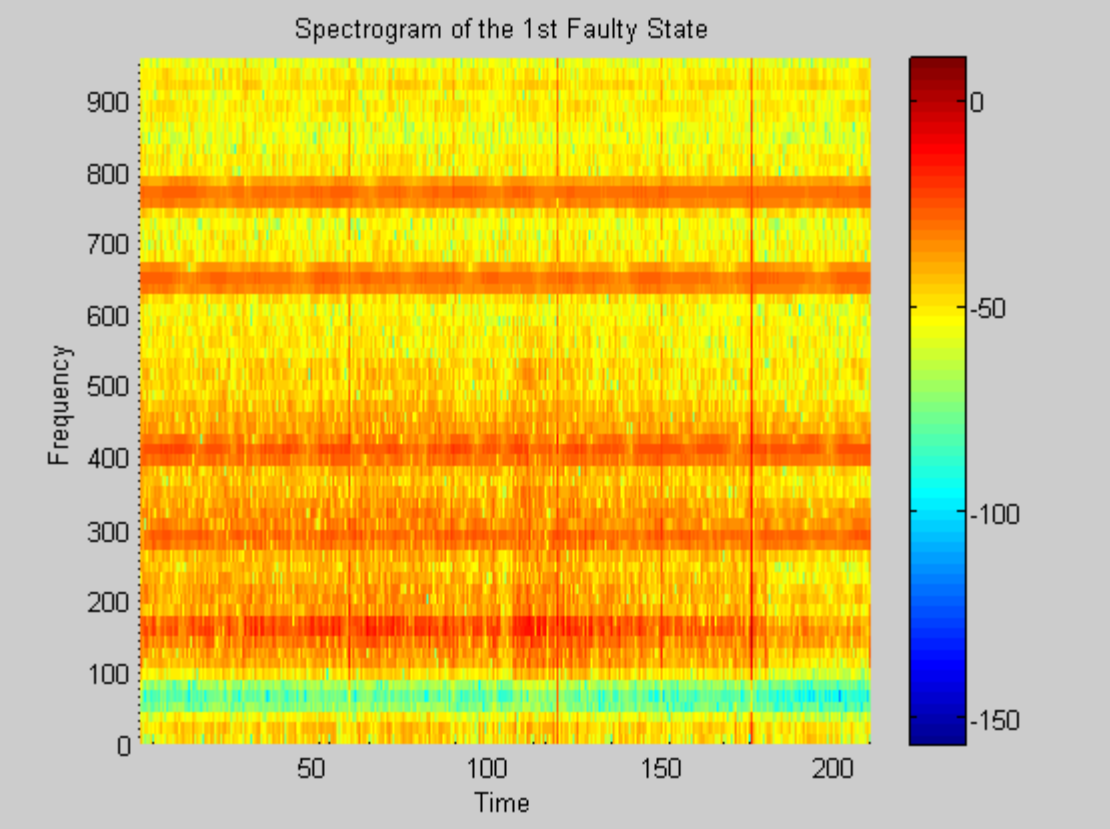

Fig. 66. Traditional spectrogram taken on 7 random motor current data files of the 1st faulty state.

3) 2nd faulty state

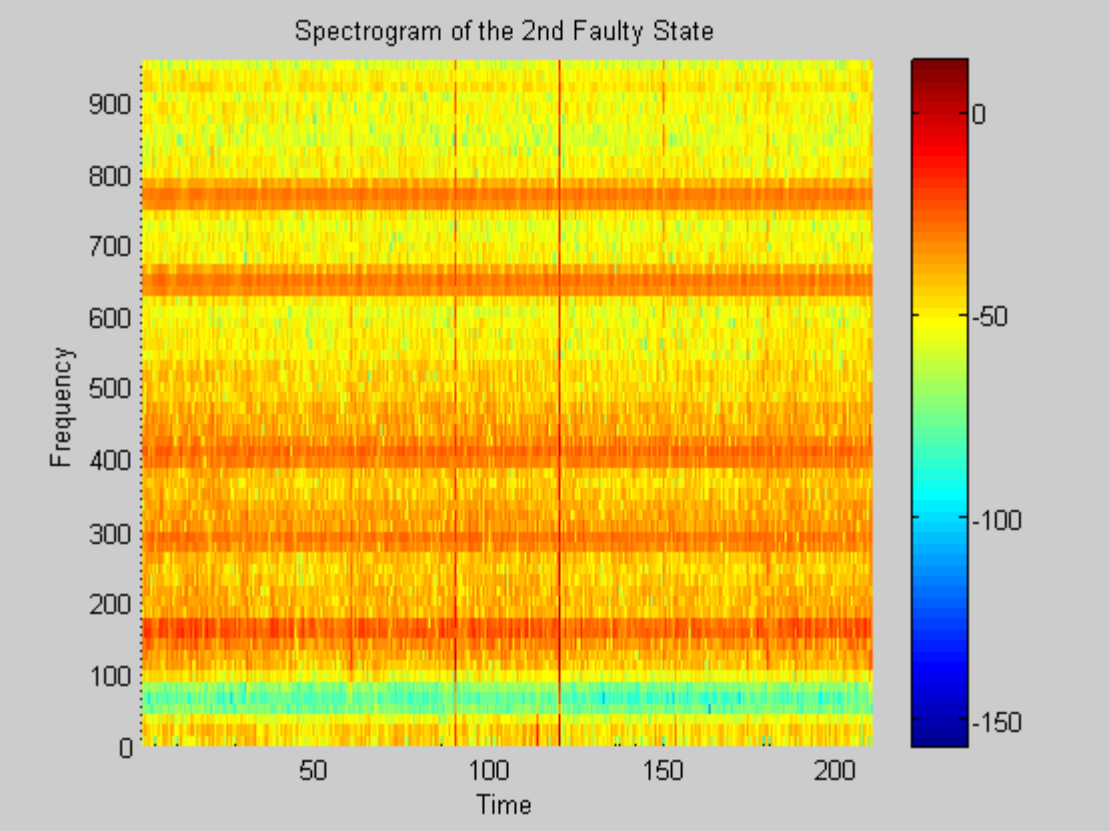

Fig. 67. Traditional spectrogram taken on 7 random motor current data files of the 2nd faulty state.

4) 3rd faulty state

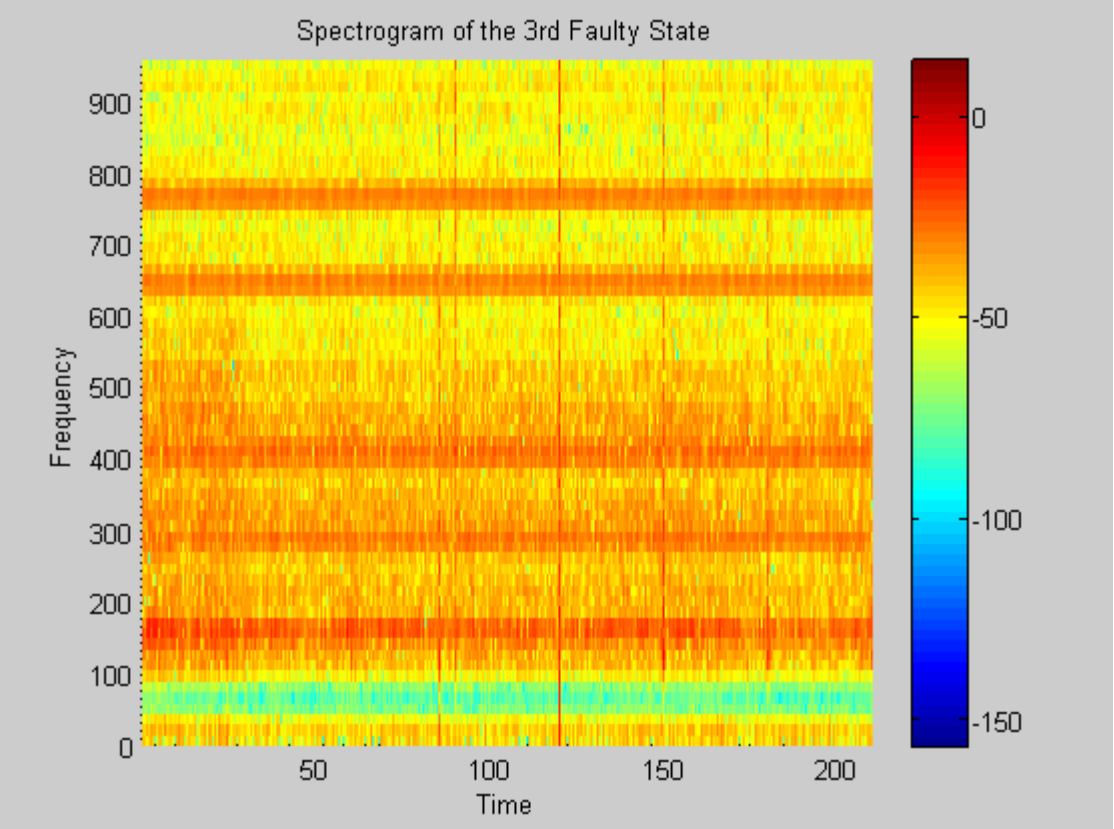

Fig. 68. Traditional spectrogram taken on 7 random motor current data files of the 3rd faulty state.

5) 4th faulty state

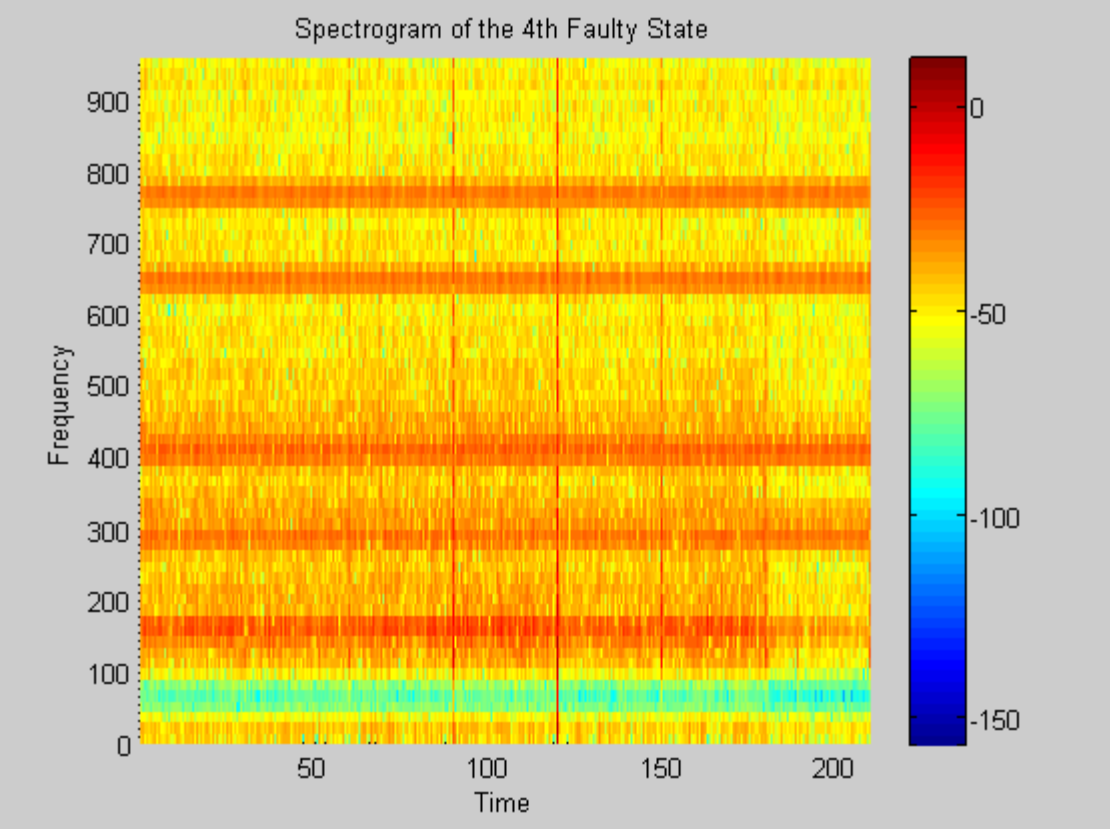

Fig. 69. Traditional spectrogram taken on 7 random motor current data files of the 4th faulty state.

6) Conclusion of the traditional spectrogram results

As shown from Fig. 65, the 4 intrinsic characteristic frequencies are obvious, and the spectrum corresponding to the fault signature frequency around 152Hz - 157Hz is not very distinguishable but still could be seen, because there might be some crack on the bearing before the current injection. However, the current injection has worsened the crack in the following states as shown in Fig. 66 – Fig. 69. To strengthen this conclusion,

another traditional spectrogram demonstration will be shown in the following Fig. 70 in which the 5 states are plotted in one figure to illustrate the AM phenomenon better:

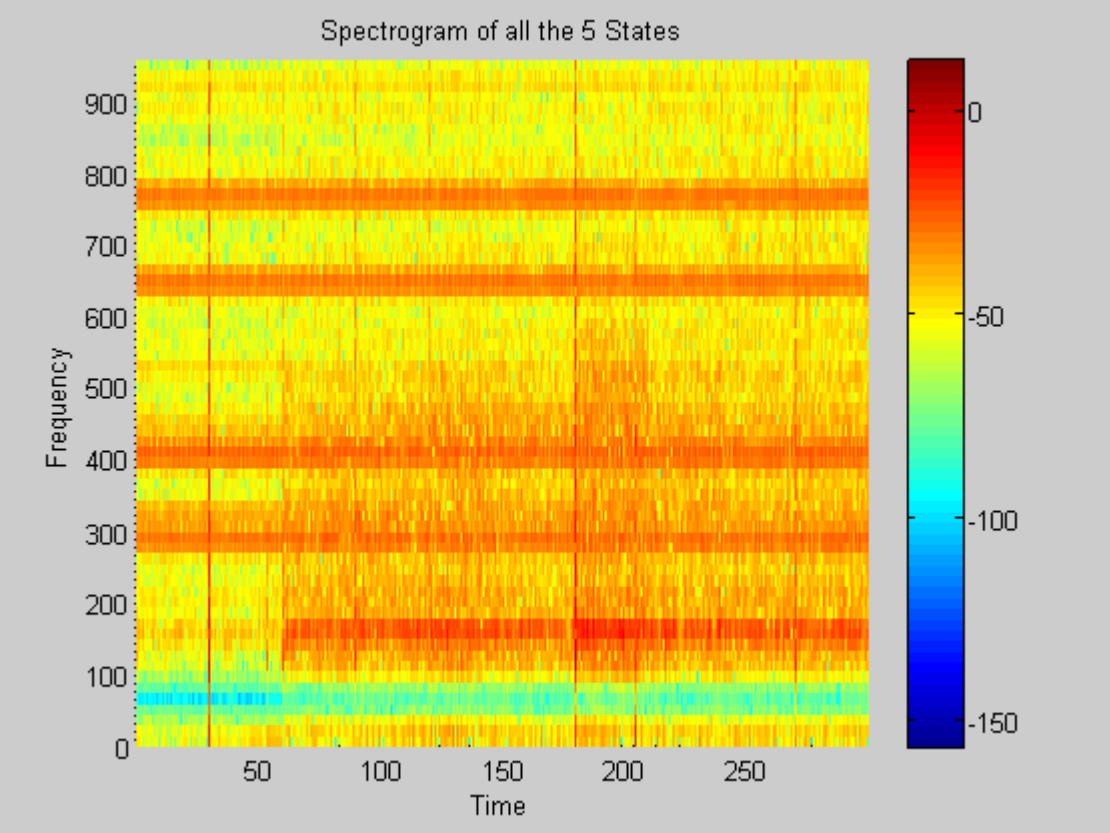

Fig. 70. Traditional spectrogram taken on 2 random motor current data files from each of the 5 states.

To generate Fig. 70, traditional spectrogram is applied on 2 random data files from each of the 5 states, so every 60secs represents one single state. It could be seen that during the first 60secs, the lower red spectrum does not exist until the advent of the 1st faulty state. So the current injection has introduced in the signature frequency of the fault at 152Hz – 157Hz.

b. RMS of the DFRFT (a=1, a=0.5) results of the motor current signal data

In this section, DFRFT with different transform orders at a=1 and a=0.5 are taken on 7 random data files from each of the 5 states first, and then the Root Mean Square (RMS) and its own moving average will be plotted. Every 280 time indices represent one state.

1) RMS and moving average based on DFRFT at a=1

The RMS change trend and its moving average result based on DFRFT (a=1) of the motor bearing destruction experiment is given by Fig. 71:

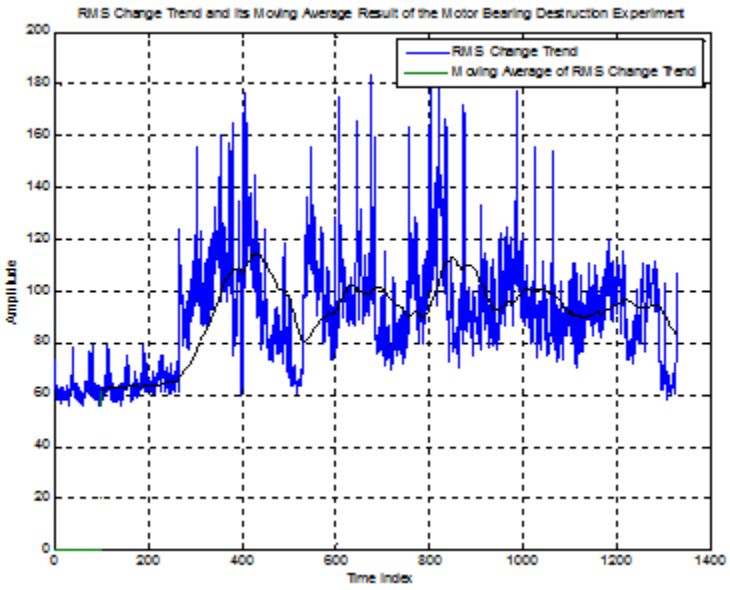

Fig. 71. RMS change trend and its moving average result based on DFRFT (a=1) of the motor bearing destruction experiment.

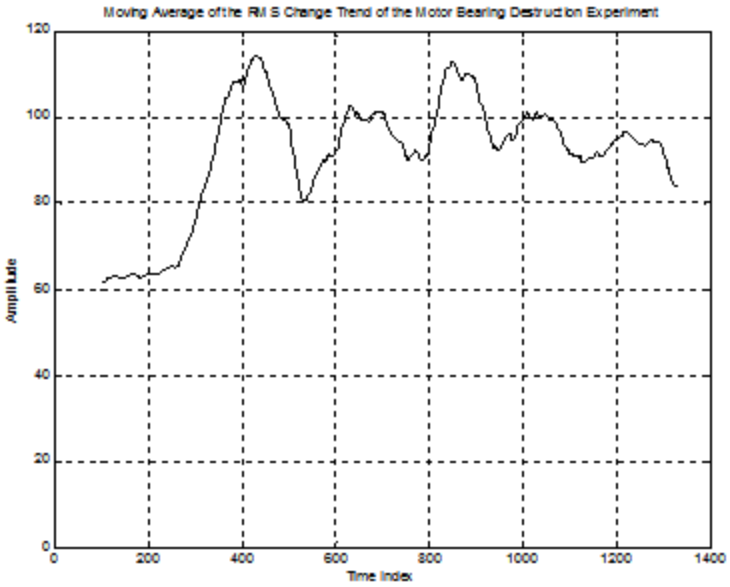

Fig. 72. Moving average result based on DFRFT (a=1) of the motor bearing destruction experiment.

Fig. 72 shows the pure moving average result based on DFRFT (a=1) of the motor bearing destruction experiment, and Fig. 73 gives the relative RMS change curve of the same data:

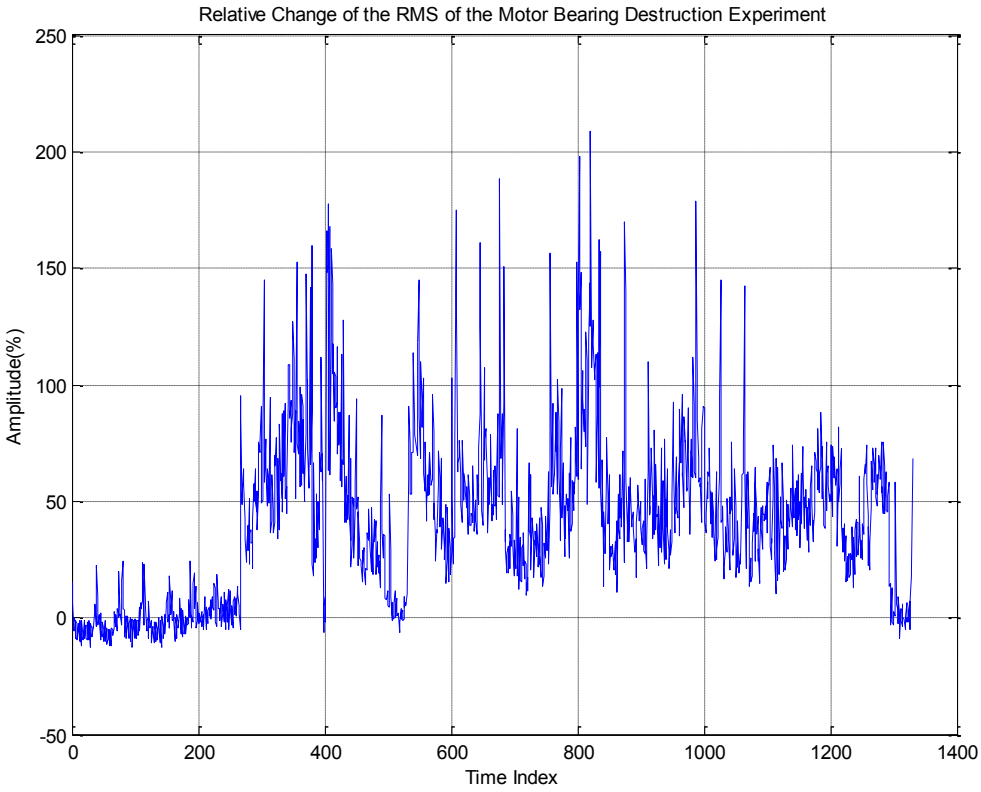

Fig. 73. Relative RMS change curve based on DFRFT (a=1) of the motor bearing destruction experiment.

2) RMS and moving average based on DFRFT at a=0.5

The RMS change trend and its moving average result based on DFRFT (a=0.5) of the motor bearing destruction experiment is given by Fig. 74:

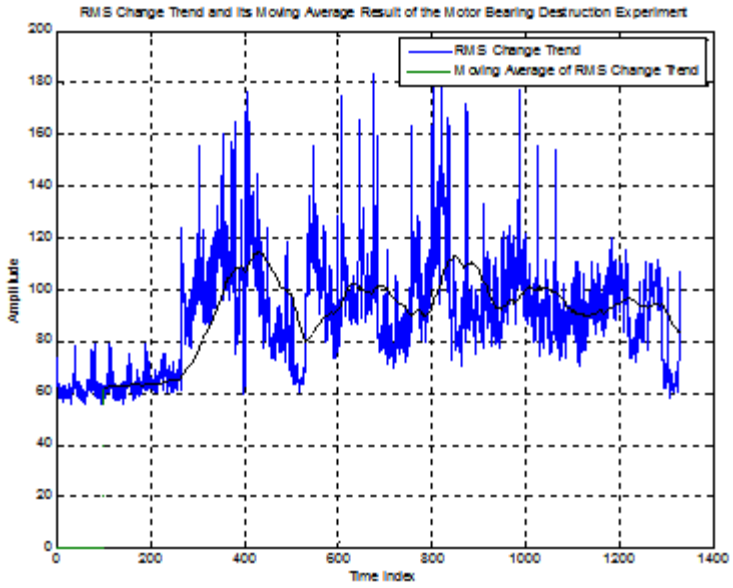

Fig. 74. RMS change trend and its moving average result based on DFRFT (a=0.5) of the motor bearing destruction experiment.

Fig. 75 shows the pure moving average result based on DFRFT (a=0.5) of the motor bearing destruction experiment, and Fig. 76 gives the relative RMS change curve of the same data:

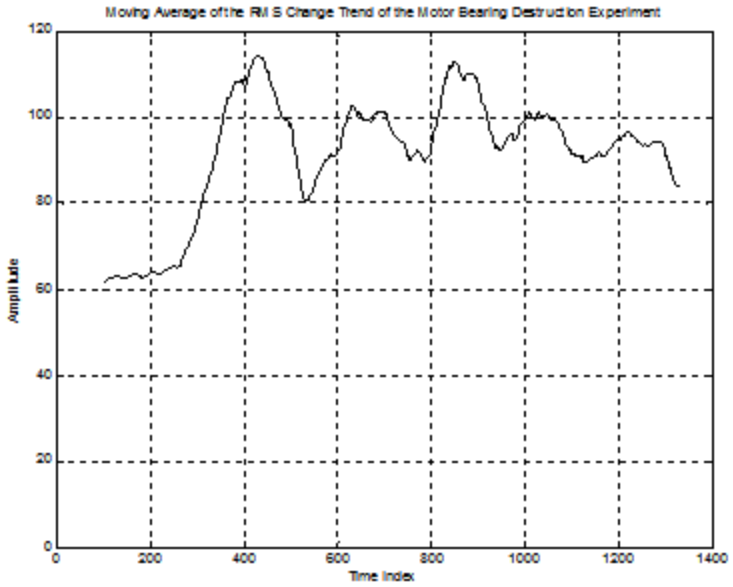

Fig. 75. Moving average result based on DFRFT (a=0.5) of the motor bearing destruction experiment.

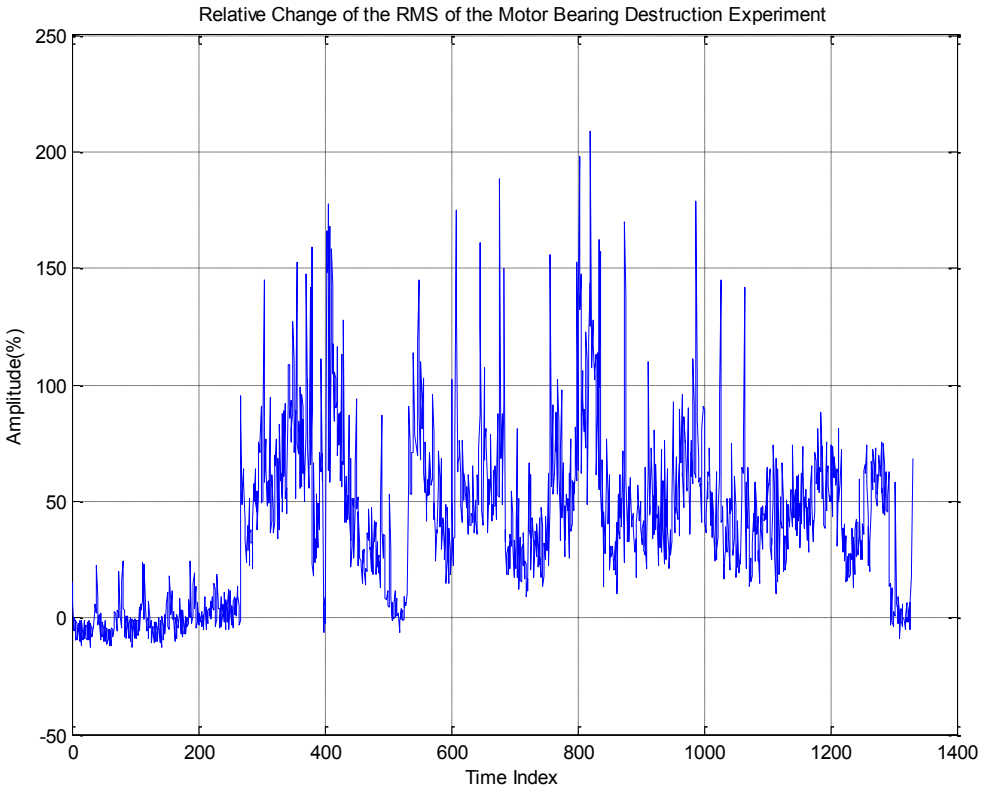

Fig. 76. Relative RMS change curve based on DFRFT (a=0.5) of the motor bearing destruction experiment.

3) Conclusion on the RMS of the DFRFT (a=1, a=0.5) results

The RMS change and its moving average plots have also shown that the motor bearing destruction procedure has introduced in the amplitude increase to some frequency components of the motor current signal after the healthy state.

Plus, from Fig. 71 – Fig. 76, the RMS, its moving average or the relative RMS show no difference between applying DFRFT at different transform order a, so the traditional FFT, which resembles DFRFT at a=1 will be enough for the research on motor current

signal because all these traditional methods could offer less computational cost and higher efficiency compared with the innovative tools of the DFRFT family.

CHAPTER V

SUMMARY AND CONCLUSIONS

In this chapter, all the research work involved in accomplishing this thesis will get summarized. The main objective of this thesis was to generate a systematic methodology with a main motivation of unknown signal identification and fault analysis. And the results of application of this method are fully discussed and suggestions for future work are given.

A. Summary of Research

The Fractional Fourier Transform (FRFT) is a generalization of the traditional Fourier Transform (FT) due to the introduction of a brand new parameter: the transform order a. So this parameter offers the transform an extra DOF, which has expanded the traditional time-frequency domain into a new continuum of FRFD. An FRFD could be at any location between the time and frequency axes, which furnishes an angle α with the time-axis. This angle is also an essential parameter in FRFT and it is denoted as the rotation angle which gives an explicit illustration of the Physics meaning of FRFT based on the existent knowledge of the conventional FT.

There are two lucid expressions for the continuous-time FRFT (CFRFT), which facilitate a comprehensive understanding of this transform. However, discrete-time FRFT (DFRFT) works as a substitution for CFRFT when it comes to the diversified applications of this transform, such as in Optics and DSP.

The spectral expansion form of the definition of FRFT also dominates in the defining process of DFRFT, and the Harper matrix S functioning as the commuting matrix of the DFT matrix F also plays an important role in seeking the orthogonal common eigenvector set of S and F. Admittedly, there are tedious theoretical and mathematical basics to cover for a thorough understanding of the DFRFT algorithm, but it is the fundamental algorithm for all the other derivative tools in this family.

For instance, the tool developed directly following the successful development of DFRFT: Multi-angle DFRFT (MA-DFRFT) gives a 2D mapping of a 3D plot with multiple selections of the transform orders. It provides a more comprehensive view of DFRFT, because by taking MA-DFRFT, the exact point where the signal energy gets concentrated will stand vividly revealed from the computer screen. So it is a recommended tool for processing unknown signals, for the corresponding optimum transform order for the researched signal and its chirp rate can be calculated directly. And then the identification purpose can be achieved with ease and reliability.

As a tool perfect for processing multi-component complicated signals with different chirp rates, Slanted Spectrum is another tool in this family which has maximized DFRFT's advantageous feature of dealing with multi-component FM signals. Slanted Spectrum has the ability of taking DFRFT of a complicated chirp signal with respect to multiple transform orders, so that every component contained in the input signal will be separated and distinguished from each other, under which circumstance the traditional FT will definitely fail to provide with highly distinguished components.

The most promising tool in FRFT family is the Spectrogram Based on Slanted Spectrum (SBSS), which is an innovative version of the traditional spectrogram. It offers a more concentrated presentation for each single spectrum of the signal components, compared with the performance of the traditional spectrogram. Since SBSS is based upon DFRFT, MA-DFRFT and Slanted Spectrum, and the traditional spectrogram merely takes advantage over the conventional STFT, SBSS processes multi-component FM signals with higher resolution and more concentrated spectrum.

And with the development of all these tools in a new domain: FRFD, it has incurred great curiosity about the results when they are applied on a real-world problem. A huge number of motor current signal data files in different states, healthy state and 4 faulty states with increasingly severe bearing damages, have been thoroughly examined with the available tools of FRFT family. And then the applicability of DFRFT and other tools from FRFT family has been discussed and concluded with prudence.

B. Conclusions

The conclusions drawn from the research work are listed below:

1. Both of DFRFT and Slanted Spectrum have the capability of offering much higher concentration of signal energy than FFT in processing complicated linear frequency modulated (LFM) signals.
2. MA-DFRFT and the relative formulas for calculating the optimum transform orders and chirp rates of the different components which compose the researched signal are proved effective in the identification of unknown signal.

3. SBSS is not maturely developed yet, but it has also been proved that it can be utilized for a higher-resolution TFR, compared with the traditional spectrogram when processing LFM signals.
4. The motor current signal has AM phenomenon but very slowly varying FM phenomenon, so its chirp rate is not large enough, which makes all the tools from the FRFT family not highly applicable, and the processing work is better carried out with the traditional tools for the sake of reducing computational cost and computer memory saving. The traditional tools, such as FFT and the traditional spectrogram (STFT) are enough to detect the generalized-roughness fault and successfully distinguish it from the intrinsic frequencies of the motor bearing.

C. Suggestions for Future Work

All the tools developed in this research work have been proved to be viable at processing FM signals: DFRFT is the fundamental algorithm which renders itself best to simple single-component chirp signal, MA-DFRFT processes multi-component chirp signal with great distinguishability and parameters of the optimum transform orders and the chirp rates can be obtained with ease, Slanted Spectrum has solved the problem of presenting a complicated chirp signal with different components which require different optimum transform orders, and SBSS has increased the concentration degree of different spectrums in a TFR.

However, there is still room for development for subsequent research, and the problems that require more research are listed as follows:

1. A better version of SBSS – SBSS has demonstrated its advantage during the presentation of processing single-component chirp signal, but its performance in processing multi-component chirp signal is unsatisfactory, because only the central area in the SBSS plot shows better energy concentration for each component and higher distinguishability between the adjacent spectrums.
2. Other types of signals in nature should be researched with tools from FRFT family – To further support the proposal that DFRFT and its derivatives are a wise option processing complicated signals with large chirp rates, or phenomenal FM.

REFERENCES

[1] K. Singh and S. A. S. Al Kazzaz, "Induction machine drive condition monitoring and diagnostic research – a survey", *Electric Power Systems Research*, vol. 64, no. 2, pp. 145-158, Feb. 2003.

[2] Manuel Duarte Ortigueira and J.A. Tenreiro Machado, "Fractional Signal Processing and Applications", *Signal processing*, 83 (2003) 2285-2286.

[3] Cagatay Candan, Alper Kutay, and Haldun M. Ozaktas, "The Discrete Fractional Fourier Transform", *IEEE Transactions on Signal Processing*, vol. 48, no. 5, May 2000.

[4] Soo-Chang Pei, Min-Hung Yeh and Chien-Cheng Tsang, "Discrete Fractional Fourier Transform Based on Orthogonal Projections", *IEEE Transactions on Signal Processing*, vol. 47, no. 5, May 1999.

[5] Juan G. Vargas-Rubio and Balu Santhanam, "The Centered Discrete Fractional Fourier Transform And Linear Chirp Signals", *IEEE 11th Digital Signal Processing Workshop & IEEE Signal Processing Education Workshop*, 2004.

[6] Juan G. Vargas-Rubio and Balu Santhanam, "An Improved Spectrogram Using The Multiangle Centered Discrete Fractional Fourier Transform", *Acoustics, Speech and Signal Processing Proceedings,* 2005.

[7] F. Alberto Grunbaum, "The Eigenvectors of the Discrete Fourier Transform: A Version of the Hermite Functions", *Journal of Mathematical Analysis and Applications*, 88, 355-363, 1982.

[8] Cagatay Candan, Student Member IEEE, M. Alper Kutay, Member IEEE, and Haldun M. Ozaktas, "The Discrete Fractional Fourier Transform", *IEEE transactions on Signal Processing*, vol. 48, no. 5, May 2000

[9] Peng Chen, Chao-Huan Hou and Xiao-Chuan Ma, "The Modification of MA-CDFRFT Algorithm Used in Computing Discrete Fractional Fourier Transform", *Journal of the Graduate School of the Chinese Academy of Science*, vol. 24, no. 2, March, 2007.

[10] Zhen-Kai Zhang, Lan Xu, and Yu-Bo Tian, "A Novel Method for LFM Signal Parameter Estimation Based on Centered Discrete Fractional Fourier Transform", *Space Electronic Technology*, no. 3, 2009.

[11] Juan G. Vargas-Rubio and Balu Santhanam, "On the Multiangle Centered Discrete Fractional Fourier Transform", *IEEE Signal Processing Letters*, vol. 12, no. 4, April, 2005.

[12] Ran Tao, Bing Deng, Wei-Qiang Zhang and Yue Wang, "Sampling and Sampling Rate Conversion of Band Limited Signals in the Fractional Fourier Transform Domain", *IEEE Transactions on Signal Processing*, vol. 56, no. 1, Jan, 2008.

[13] Luis B. Almeida, "The Fractional Fourier Transform and Time-Frequency Representations", *IEEE Transactions on Signal Processing*, vol. 42, no. 11, November 1994.

[14] N. Wiener, "Hermitian polynomials and Fourier analysis", *Journal of Mathematical Physics (MIT)*, 8 (1929) 70-73

[15] V. Namias, "The fractional order Fourier transform and its application to quantum mechanics", *IMA Journal of Applied Mathematics*, 25 (3) (1980) 241-265

[16] A. McBride and F. Kerr, "On Namias' Fractional Fourier Transforms", *IMA Journal of Applied Mathematics*, vol. 39, pp. 159-175, 1987

[17] Michael Bennett, Steve McLaughlin, Tom Anderson, and Norman McDicken, "Filtering of Chirped Ultrasound Echo Signals with the Fractional Fourier Transform", *IEEE International Ultrasonics, Ferroelectrics, and Frequency Control Joint 50th Anniversary Conference*, 2004

[18] C. Capus, Y. Rzhanov, and L. Linnett, "The analysis of multiple linear chirp signals", *IEEE Seminar on Time-Scale and Time-Frequency Analysis and Applications (Ref. No. 2000/019)*, 2000

[19] Qi Lin, Tao Ran, Zhou Siyong, Wang Yue, "Adaptive Time-Varying Filter for Linear FM Signal in Fractional Fourier Domain", *6th International Conference on Signal Processing*, 2002

[20] Michael J. Bennett, Steve McLaughlin, Tom Anderson, and Norman McDicken, "The Use of the Fractional Fourier Transform with Coded Excitation in Ultrasound Imaging", *IEEE Transactions on Biomedical Engineering*, vol. 53, no. 4, April, 2006

[21] R. Tao, B. Deng, W. Q. Zhang, Y. Wang, “Sampling and sampling rate conversion of band limited signals in the fractional Fourier transform domain”, *IEEE Transactions on Signal Processing*, 56 (1) (2008) 158-171

[22] S. C. Pei, J. J. Ding, “Closed-form discrete fractional and affine Fourier transforms”, *IEEE Transactions on Signal Processing*, 48 (5) (2000) 1338-1353

[23] Tao Ran, Ping Xianjun, Zhao Xinghao, Wang Yue, “Detection and Estimation of Moving Targets Based on Fractional Fourier Transform”, *6th International Conference on Signal Processing*, 2002

[24] Juan Gaspar Vargas-Rubio, “The Centered Discrete Fractional Fourier Transform, properties, computation, and application to linear chirp signals”, Ph.D Dissertation, The University of New Mexico, 2004

VITA

Name:	Xiao Duan
Address:	Department of Mechanical Engineering 3123 TAMU College Station TX 77843-3123
Email Address:	oasis4margaret@gmail.com
Education:	B.S., Mechanical Engineering, Xi'an JiaoTong University, Xi'an, P. R. China, 2007 M.S., Mechanical Engineering, Texas A&M University, College Station, U.S.A., 2012